89 Diversity of Heme Proteins in Sulfate Reducing Bacteria

Célia V. Romão, Margarida Archer, Susana A. Lobo, Ricardo O. Louro, Inês A. C. Pereira, Lígia M. Saraiva, Miguel Teixeira and Pedro M. Matias

Instituto de Tecnologia Química e Biológica, Universidade Nova de Lisboa, Apartado 127, 2781-901 Oeiras, Portugal

List of Abbreviations

Ahb	Alternative heme biosynthetic proteins
ALA	Aminolevulinic acid
APS	Adenosine phosphosulfate
ATP	Adenosine triphosphate
Bfr	Bacterioferritin
CbiK	Cobalt chelatase
CD	Circular Dichroism
CysG	Siroheme synthase
DFT	Density functional theory
DNA	Deoxyribonucleic acid
Dms and Dor	Dimethyl sulfoxide reductase
Dsr	Dissimilatory sulfite reductase
EPR	Electron paramagnetic resonance
GlcNAc	*N*-Acetyl-D-glucosamine
HCO	Heme-copper oxygen reductases
HDR	Heterodisulfide reductases
HMB	1-Hydroxymethylbilane
Hmc	High-molecular weight cytochrome
HQNO	2-Heptyl-4-hydroxyquinoline-*N*-oxide
$NADH^+$	Nicotinamide adenine dinucleotide

NADPH	Reduced nicotinamide adenine dinucleotide phosphate
Nap	Periplasmic nitrate reductase
Nhc	Nine-heme cytochrome
Nir	Periplasmic cd_1 nitrite reductase
NMR	Nuclear magnetic resonance
Nrf	Nitrite reduction with formate
Ohc	Octaheme cytochrome
ORF	Open reading frame
PBG	Porphobilinogen
PC-2	Precorrin-2
PDB	Protein Data Bank
QFR	Quinol:fumarate oxidoreductases
Qmo	Quinone-interacting membrane oxidoreductase
Qrc	Quinone reductase complex
Rd II	Rubredoxin II
ROS	Reactive Oxygen Species
rRNA	Ribosomal ribonucleic acid
SAM	S-adenosyl methionine
SirB	Sirohydrochlorin ferrochelatase
SH	Siroheme
SHC	Sirohydrochlorin
SQR	Succinate:quinone oxidoreductase
SRB	Sulfate-reducing bacteria
SSC	Split-Soret cytochrome *c*
SUMT	SAM-dependent uroporphyrinogen III methlytransferase
Tmc	Tetraheme membrane cytochrome complex
Tor	Trimethylamine N-oxide reductase
TpI-c_3	Type I cytochrome c_3
TpII-c_3	Type II cytochrome c_3
UV	Ultraviolet

I. Introduction

Sulfate-reducing bacteria (SRB) are a broad group of anaerobic microorganisms widespread in a variety of aquatic and terrestrial environments.[1-3] They have in common the ability to perform dissimilatory sulfate reduction, which is coupled with the oxidation of a wide range of electron donors, such as organic acids (*e.g.* formate, fumarate or lactate), fatty acids, alcohols or hydrogen. Some SRB may also use a variety of distinct electron acceptors (such as sulfite, nitrate, nitrite, fumarate or transition metal ions).

The history of SRB started with Beijerinck in 1895, when he was studying the contamination of Delft city canals during summer time, caused by large amounts of hydrogen sulfide. The levels of "sulfidferment" reached a maximum at that time of the year. This annual phenomenon was considered "eine wahren Screcken" (a true horror). The large production of hydrogen sulfide was then attributed to a microorganism from a muddy canal at Delft, which was isolated by Beijerinck and constituted the first known example of a SRB, which was named *Spirillum desulfuricans* (later called *Desulfovibrio desulfuricans*).[3,4]

The classification of SRB into different genera has changed over the years due to the identification of new strains, and to the need of using more specific taxonomic markers. During the 1950–1960 period, the SRB were classified only in two genera: *Desulfotomaculum* for the sporeforming strains, and *Desulfovibrio* for the non-sporeforming, vibrio-shaped species.[3–5] A later classification of the different types of SRB was made according to taxonomic markers such as the phenotypic characteristics (presence of a green dissimilatory sulfite reductase, desulfoviridin, lipid fatty acids or menaquinones) and the DNA GC content (guanine + cytosine fraction of total DNA bases).

The application of 16S rRNA sequence analysis was important for the elucidation of the genetic relationships at various taxonomic levels.[3–5] Nowadays, the sulfate reducers are distributed into five bacterial and two archaeal lineages according to the analysis of their 16S rRNA sequences: in the deltaproteobacteria class several families of Gram-negative organisms are included, comprising most described genera of SRB (e.g. *Desulfovibrio*); the Clostridia class include the Gram-positive SRB (e.g. *Desulfotomaculum*, *Desulfosporosinus* and *Thermodesulfobium*); and the thermophilic bacteria include members of the Nitrospira class (e.g. *Thermodesulfovibrio*) and the Thermodesulfobacteria phylum (e.g. *Thermodesulfobacterium*). In terms of growth temperature, the large majority of SRB are mesophilic, with the optimum in the range 30–37 °C. Nevertheless, there are examples of thermophilic organisms with growth temperatures of 60–65 °C, and psychrophilic with a growth temperature of 10 °C. There are also two groups of sulfate reducers from the Archaea domain, belonging to the euryarchaeota and crenarchaeota genera.[3,4,6] However, the present chapter concerns only the bacterial sulfate reducers, and it has to be noted that excellent and comprehensive monographic reviews on multiple aspects of sulfate reducers are available in Refs. 7 and 8.

Originally, SRB were considered to be strict anaerobic organisms, in the sense that the growth of the organism was irreversibly inhibited by oxygen. However, several studies in some SRB have demonstrated that these bacteria can tolerate exposure to aerobic conditions, up to atmospheric levels of oxygen.[9–13] In fact, they can use molecular oxygen as a terminal electron acceptor,[13,14] and even

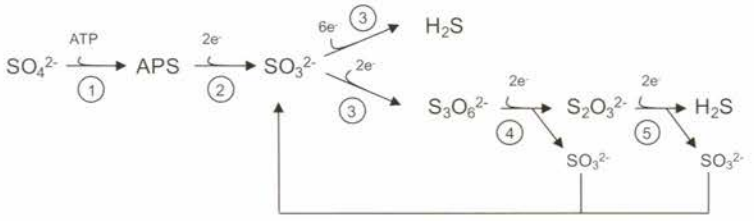

Figure 1. Reduction steps involved in sulfate reduction by SRB. Enzymes involved are: (1) ATP sulfurylase; (2) APS reductase; (3) dissimilatory sulfite reductase; (4) putative trithionate reductase; and (5) putative thiosulfate reductase.

produce ATP under aerobic conditions, at least by substrate level phosphorylation.[15] Furthermore, these organisms have a whole array of different proteins that scavenge oxygen and reactive oxygen species (ROS), such as superoxide dismutases and reductases, catalases and rubrerythrins (reviewed in Ref. 16).

The common physiological activity of all SRB is the reduction of sulfate to sulfide by an eight-electron process that occurs in the cytoplasm (Figure 1).[17] After transport inside the cell, sulfate is first activated by reaction with ATP by the ATP sulfurylase (Figure 1, step 1)[18] to produce adenosine phosphosulfate (APS), also known as adenylylsulfate. APS is reduced to sulfite in a two-electron reaction carried out by APS reductase (Figure 1, step 2).[19] Sulfite is then reduced by the dissimilatory sulfite reductase DsrAB (Figure 1, step 3, see Section V), by a still disputed mechanism that may involve either direct reduction to sulfide or the formation of intermediate products like trithionate and thiosulfate (Figure 1, steps 4 and 5) (reviewed in Refs. 1 and 20). These compounds are produced in *in vitro* assays of the dissimilatory sulfite reductase, but their physiological significance is still unclear. There is no convincing evidence for the presence of trithionate reductases (Figure 1, step 4) in SRB, either biochemically or by genome analysis, and thiosulfate reductases (Figure 1, step 5) are present in only a few SRB.[21]

Apart from the enzymes involved in sulfate respiration, all SRB contain multiple hydrogenases, which have a key role in their metabolism. Hydrogenases are enzymes that have the ability either to oxidize hydrogen or generate hydrogen, by reducing protons. These proteins possess iron-sulfur clusters of the $[3Fe4S]^{1+/0}$ and/or $[4Fe4S]^{2+/1+}$ types which are involved in electron transfer to or from the catalytic site, accepting or delivering electrons to their physiological partners. The iron-sulfur cluster further apart from the catalytic site is named distal cluster, and it is also the closest center to the protein surface. The catalytic site is a binuclear metal center, formed by two iron atoms in [FeFe]-hydrogenases, or by a nickel and an iron atom in [NiFe] and [NiFeSe]-hydrogenases; in the latter, one of the cysteine ligands to the nickel atom is a selenocysteine (for reviews, see Refs. 22 and 23). The tetraheme cytochrome c_3 is generally believed to be the physiological

electron acceptor of the periplasmic hydrogenases, subsequently transferring the electrons to a multitude of different redox proteins in the periplasm, as will be amply discussed in Sections IV–VI.

The large production of hydrogen sulfide, which is a molecule with a characteristic foul smell, has been considered an environmental problem due to its corrosive properties and toxicity. Therefore, the environmental presence of these bacteria has a strong economical impact, for instance in the petroleum industry, due to metal biocorrosion, which affects pumping equipment, storage tanks and pipelines, oil and gas souring and worker safety.[3,24] Also, SRB have been implicated in food spoilage due to endospore-producing thermophiles. The SRB effect on the petroleum industry and food spoilage are only two examples of the relationship between the SRB and the environment, which have been one of the driving forces for research on SRB. The SRB are also present in the intestinal tract of humans and animals, but a correlation between these bacteria and diseases has not yet been established.[25]

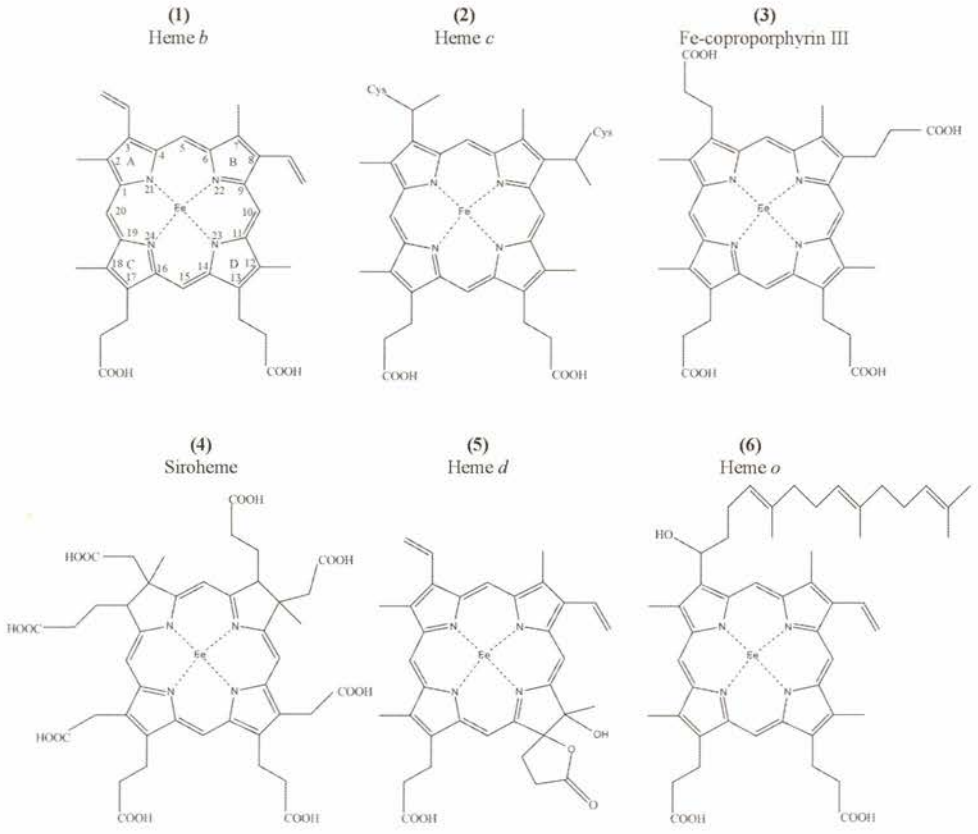

The SRB contain a wide diversity of heme-containing proteins, of which the most common are undoubtedly the single and multi-heme cytochromes *c*. In parallel with this diversity, six different heme types were so far found in those proteins. Heme *b* (**1**), which is not covalently bound to the protein, is present in the membrane subunits of several respiratory complexes and enzymes, usually with a bis-histidine axial coordination. Heme *c* (**2**) is the most common, and is covalently bound to the polypeptide chain by thioether bridges to cysteine residues, which are included in a heme binding motif usually of the form CXXCH; with few exceptions, one of the iron axial ligands is the histidine in the motif, and the other is either histidine or methionine. A more rare heme type, Fe-coproporphyrin III (**3**), occurs in a bacterioferritin, and a siroheme (**4**) is bound to one of the subunits of the dissimilatory sulfite reductases, and to assimilatory sulfite reductases. Finally, the quinol: oxygen reductases of the *bd* family have a *d*-type heme (**5**),[14] and evidence for the existence of an *o*-type heme (**6**), associated with the heme-copper oxygen reductase was reported in 2011.[26]

II. Biosynthesis of Modified Tetrapyrroles

A. From δ-Aminolevulinic Acid to the First Cyclic Intermediate

As in other biological systems SRB rely on a wide range of modified tetrapyrroles such as heme *b*, siroheme and vitamin B_{12} that are cofactors of proteins underpining essential biological processes.[17,27–29] In general, tetrapyrroles are synthesized *via* a complex biosynthetic pathway that branches after the formation of the first macrocyclic intermediate, uroporphyrinogen III (Urogen III) (Figure 2).[30] The precursor of all modified tetrapyrroles, δ-aminolevulinic acid (δ-ALA), is formed by two different routes, namely the Shemin pathway (also known as the C_4-pathway) and the C_5-pathway. Humans, animals and fungi employ the Shemin pathway, in which δ-ALA is synthesized by a one-step enzymatic condensation of succinyl-coenzyme A and glycine. Plants, algae, archaea and bacteria, with the exception of the proteobacteria alpha group, utilize the C_5-route, which involves the incorporation of the intact five-carbon skeleton of glutamate into δ-ALA, via a three-step enzymatic process (Figure 2).[31,32] As in other bacteria, the C_5-pathway of the deltaproteobacterium *D. vulgaris* Hildenborough, the most studied representative of the SRB family, starts with a glutamyl-tRNA molecule derived from a glutamate and a $tRNA^{Glu}$, in a reaction catalyzed by glutamyl-tRNA synthetase, an enzyme encoded by the *gltX* gene. The reactive carboxyl group of glutamyl-$tRNA^{Glu}$ is reduced to a formyl group by an NADPH-dependent glutamyl-tRNA reductase, encoded by the *hemA* gene, to form glutamate-1-semialdehyde, a

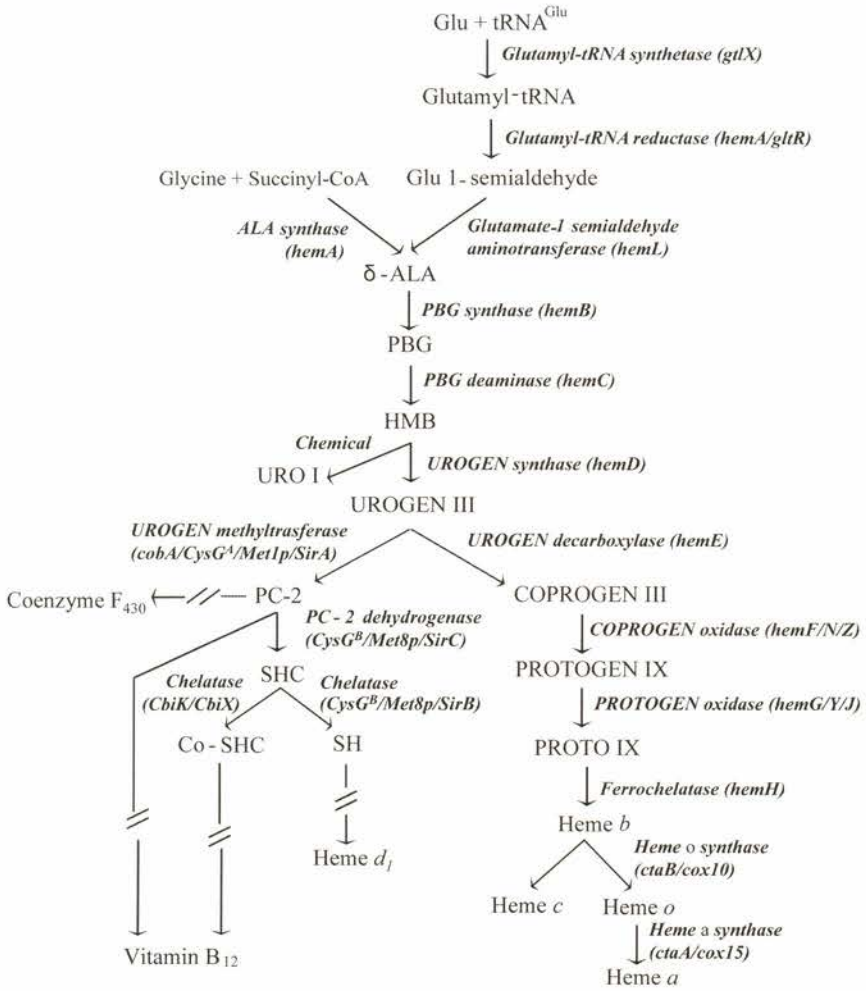

Figure 2. General modified tetrapyrrole biosynthetic pathway: δ-aminolevulinic acid (δ-ALA), porphobilinogen (PBG), hydroxymethylbilane (HMB), uroporphyrinogen III (UROGEN III) uroporphyrin I (URO I), precorrin-2 (PC-2), sirohydrochlorin (SHC), cobalt-sirohydrochlorin (Co-SHC), siroheme (SH), coproporphyrinogen III (COPROGEN III), protoporphyrinogen IX (PROTOGEN IX), protoporphyrin IX (PROTO IX), magnesium-protoporphyrin IX (Mg-PROTO IX). Adapted from Ref. 30.

compound that is further transaminated to δ-ALA by the pyridoxal-5′-phosphate-dependent glutamate-1-semialdehyde aminotransferase (the gene product of *hemL*) (Figure 2).[30,33]

In the first step of tetrapyrrole biosynthesis, two δ-ALA molecules undergo asymmetric condensation generating the monopyrrole porphobilinogen (PBG) *via* the action of porphobilinogen synthase, also known as ALA dehydratase and encoded by the *hemB* gene (Figure 2).[34] The binding of the substrate to PBG

synthase and the reaction mechanism have been extensively analyzed by biochemical and structural studies.[34–36] The enzyme has two distinct binding sites for the δ-ALA molecules, the A-site, which will form the acetic-acid chain of PBG, and the P-site that will give rise to the propionic-acid side chains of PBG.[34] In general, the active site of PBG synthases is highly conserved and, according to the species, the enzyme differs on the requirement for metal ions (such as Mg(II) or Zn(II)).[37] Moreover, different oligomeric assemblies of PBG synthases, the so-called morpheeins, have been described. For example, *Pisum sativum*, human and *Rhodobacter capsulatus* PBG synthases can undergo rearrangements switching between a low activity homodimer and a highly active homohexameric form. In contrast to the *R. capsulatus* PBG synthase, the other two enzymes require metal ions for catalysis.[38–40] In the case of *D. vulgaris*, the active form of PBG synthase is also a homohexamer, and the enzyme catalyzes the condensation reaction only when in the presence of Zn(II). This metal binds to cysteine amino acid residues which, as well as other amino acids involved in the binding of the substrate, are conserved in this family of enzymes.[41]

In the second step, four molecules of PBG are polymerized by the enzyme porphobilinogen deaminase (encoded by the *hemC* gene), to form the linear tetrapyrrole 1-hydroxymethylbilane (HMB) (Figure 2).[42] *Escherichia coli* and *D. vulgaris* PBG deaminases were shown to contain a dipyrromethane cofactor covalently attached to a conserved cysteine residue at the catalytic site.[41–43] This cofactor is derived from two molecules of the enzyme's own substrate PBG and acts as an anchor for the assembly of the sequential linkage of another four PBG molecules, which upon cleavage make the enzyme active site available for the next reaction cycle.[44] HMB is a very unstable molecule that may cyclize chemically to form uroporphyrinogen I, the reduced form of uroporphyrin I (URO I). Although uroporphyrin I is considered to be a non-biologically relevant molecule, its iron-complex was co-purified with *D. gigas* rubredoxin:oxygen oxidoreductase, an enzyme involved in oxygen reduction.[29,45] However, the significance of this observation remains to be established as all other enzymes of this family, the flavo di-iron enzymes, (see e.g. Ref. 46) do not contain a heme moiety. Also, the recombinant enzyme from *D. gigas* lacks it while maintaining its activity.[47]

In the majority of the organisms, HMB is cyclized with simultaneous rearrangement/inversion of the D pyrrole ring to form uroporphyrinogen III, in a reaction catalyzed by uroporphyrinogen III synthase (encoded by the *hemD* gene) (Figure 2).[30,48] Like in other bacteria, such as the obligate anaerobic and fermentative bacteria *Lactobacillus reuteri*, *Selenomonas ruminantium* and *Clostridium josui*, in *Desulfovibrio* sp. the *hemD* gene is fused to the *cobA* gene, which encodes the S-adenosyl methionine (SAM) dependent uroporphyrinogen III methyltransferase (SUMT).[41,49] This gene fusion codes for a bi-functional

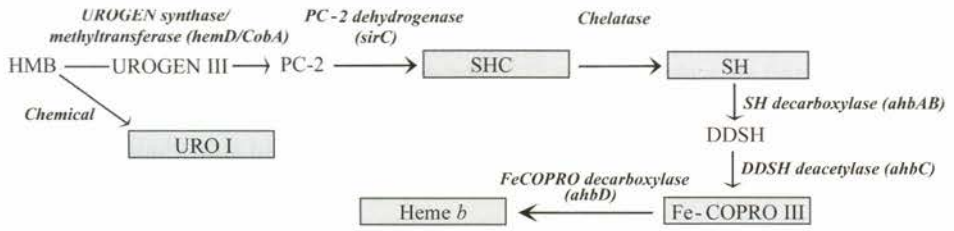

Figure 3. Modified tetrapyrrole biosynthetic pathway operative in *Desulfovibrio* sp. δ-aminolevulinic acid (δ-ALA), the precursor of all modified tetrapyrroles, is formed by the C_5-route. Two molecules of δ-ALA are condensed to form the monopyrrole porphobilinogen (PBG) and four molecules of PBG are subsequently polymerized into the linear tetrapyrrole hydroxymethylbilane (HMB). HMB can chemically cyclize forming uroporphyrin I (URO I) or be enzymatically converted into precorrin-2 (PC-2). PC-2 is oxidized to sirohydrochlorin (SHC) that represents the first branch point of the *Desulfovibrio* tetrapyrrole pathway. SHC can be chelated with cobalt to yield cobalt-sirohydrochlorin (Co-SHC), the first metalated precursor of the anaerobic biosynthetic branch of vitamin B_{12}, or with iron to produce siroheme (SH). SH is converted to heme *b* by the intermediates didecarboxysirohydrochlorin (DDSH) and Fe-coproporphyrin III (Fe-COPRO III). The modified tetrapyrrole cofactors found in several proteins of *Desulfovibrio* sp. are highlighted in grey boxes: URO I is the cofactor of *D. gigas* rubredoxin:oxygen oxidoreductase; SHC and SH are both present in dissimilatory sulfite reductases of the desulfoviridin type, and SH in assimilatory sulfite reductases and desulforubidins (dissimilatory sulfite reductases); Co-SHC and/or related cobalt-isobacteriochlorins are present in several *Desulfovibrio* proteins;[50] Fe-COPRO III is the cofactor of *D. desulfuricans* ATCC 27774 bacterioferritin and hemes are ubiquitously found in multiple proteins of *Desulfovibrio* sp.[27–29,33,51,52] Adapted from Ref. 53.

uroporphyrinogen III synthase/methyltransferase that utilizes HMB to synthesize the tetrapyrrole intermediate precorrin-2 (PC-2) (Figure 3). *In vitro* and *in vivo* studies using the truncated form of the *D. vulgaris* Hildenborough enzyme demonstrated that the N-terminal domain of this bi-functional protein is indeed linked to the SUMT activity whereas the C-terminal region acts upon HMB to form uroporphyrinogen III.[41]

B. Siroheme Branch

Siroheme (SH) is the prosthetic group of many prokaryotic assimilatory sulfite and nitrite reductases and of dissimilatory sulfite reductases, which in SRB are key metabolic enzymes. Sulfite reductases have a unique siroheme/iron-sulfur center involved in the six electron reduction of sulfite to sulfide. The complexity of these enzymes has been unravelled by several crystallographic structures namely those of dissimilatory sulfite reductases from *D. vulgaris*, *D. gigas*, *Archaeoglobus fulgidus* and *Desulfomicrobium norvegicum* (formerly known as *D. desulfuricans* Norway 4),[27,51,54,55] described in Section V. Intriguingly, some of those enzymes, besides siroheme and iron-sulfur clusters, contain also sirohydrochlorin (the

demetalated siroheme), which is the last precursor of the siroheme biosynthesis and the first precursor of the anaerobic biosynthetic pathway that leads to the formation of vitamin B_{12} (Figure 2).[27,54,56,57]

The synthesis of siroheme from urogen III is accomplished in four enzymatic-steps: two SAM-dependent methylations at rings A and B to form PC-2; dehydrogenation of PC-2 to generate sirohydrochlorin (SHC); and ferrochelation of SHC (Figure 2).[58] In some organisms, such as *E. coli* and *Salmonella thyphimurium*, these steps are performed by a single multifunctional enzyme, the siroheme synthase CysG. This enzyme has two functional domains: the N-terminal domain $CysG^B$, which is linked to the PC-2 dehydrogenase activity and iron chelation, and the C-terminal domain $CysG^A$, which has SUMT activity.[58,59] In the case of yeast *Saccharomyces cerevisae* these steps are performed by two distinct enzymes, Met1p that has SUMT activity, and the bifunctional dehydrogenase/ferrochelatase Met8p.[60] In other organisms, as for example *Bacillus megaterium*, siroheme is formed *via* three independent and distinct enzymes: SirA, SirB and SirC, which have SUMT, ferrochelatase and dehydrogenase activities, respectively.[61] As previously mentioned, in the case of *D. vulgaris* the SUMT activity is linked to the bifunctional uroporphyrinogen III synthase/methyltransferase (HemD/CobA). The PC-2 intermediate is next used by the SirC NAD^+-dependent dehydrogenase to form SHC that will subsequently be chelated with iron by a chelatase (Figure 3).[41]

Metal insertion into a tetrapyrrole, catalyzed by the family of metal chelatases, involves distortion of the tetrapyrrole ring to allow deprotonation of two pyrrole nitrogens and formation of the metal-ligand bond.[62] Chelatases are divided into three classes according to their subunit and energy requirements. Class I chelatases are composed of three subunits and are ATP dependent (e.g. protoporphyrin IX:magnesium chelatase BhlH-I-D of the chlorophyll synthesis pathway and hydrogenobyrinic acid *a,c*-diamide cobaltochelatase of aerobic vitamin B_{12} synthesis pathway). Class II chelatases are normally found as monomers or homodimers and do not require ATP (e.g. sirohydrochlorin cobaltochelatases $CbiX^S$, $CbiX^L$ and CbiK, the sirohydrochlorin ferrochelatase SirB and the protoporphyrin IX ferrochelatase HemH). Class III chelatases are ATP-independent multifunctional homodimeric enzymes and include the yeast Met8p and *E. coli* CysG.[63] Although in all *Desulfovibrio* sp. with genomes so far sequenced, an ortholog of a sirohydrochlorin ferrochelatase is absent, in *D. vulgaris* Hildenborough two distinct ATP-independent CbiK sirohydrochlorin cobaltochelatases are present, which were named $CbiK^C$ and $CbiK^P$ in accordance with their predicted cytoplasmic and periplasmic localization in the cell, respectively.[64] Moreover, both $CbiK^P$ and $CbiK^C$ promote the *in vitro* and *in vivo* chelation of iron into SHC, and also the chelation of cobalt yielding Co-SHC, the first metal-chelated intermediate of the

anaerobic (O_2-independent) pathway of vitamin B_{12} synthesis that occurs in *D. vulgaris* Hildenborough (Figure 3). Nevertheless, location of these proteins in distinct cell compartments suggests that the two chelatases may contribute to different processes and, given that the biosynthesis of vitamin B_{12} takes place in the cytoplasm of the cell, $CbiK^C$ rather than $CbiK^P$ is likely to be involved in the vitamin B_{12} pathway.[64]

Biochemical and structural data showed that *D. vulgaris* $CbiK^P$ is a tetramer and, so far, is unique within its class as the protein contains a heme *b* cofactor, with a stoichiometry of one heme *b* per dimer.[52,64] Although the production of a truncated form of $CbiK^P$, obtained by the cleavage of the periplasmic leader signal peptide, yields a recombinant protein that lacks the heme *b* group, the protein still retains its tetrameric structure and the ability to chelate iron or cobalt into SHC. This shows that the heme is not necessary for the tetramer assembly and it does not participate in the metal insertion reaction.[64] In fact, the crystal structure of $CbiK^P$ (Figure 4) reveals that the heme is located in a hydrophobic pocket, in-between two monomers, coordinated by two histidines (His96) related by crystallographic symmetry and distant from the SHC binding site. The two hemes *b* present in the tetramer are quite distant from each other and nearly coplanar, with the propionic acid side chains pointing towards the center.[52] Sequence and structural comparison alignments of *D. vulgaris* Hildenborough $CbiK^P$ with other chelatases whose structures are available, such

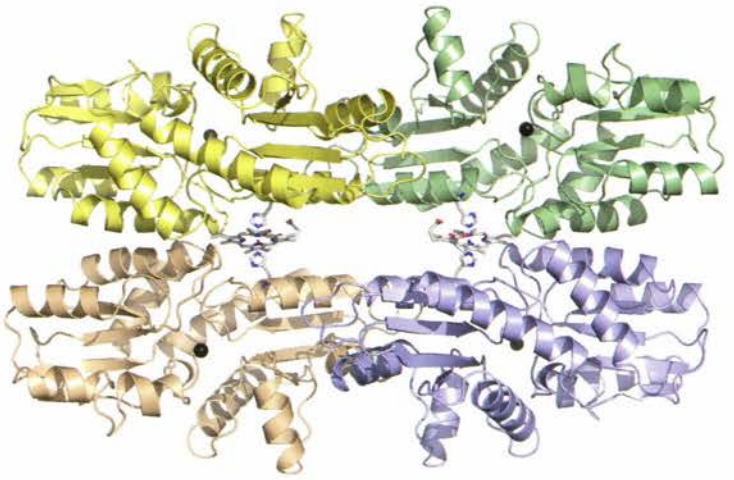

Figure 4. Overall structure of *D. vulgaris* Hildenborough $CbiK^P$ (PDB 2xvz, Ref. 52) The protein chains are represented as ribbons, with each monomer is coloured differently. The cobalt sites are displayed as black spheres in each monomer and the hemes *b* in between subunits are drawn as sticks together with the axial iron ligand His96. Atom colors are blue for nitrogen, light gray for carbon, red for oxygen and brown for iron. Figure made with PyMOL.[68]

as *Salmonella enterica* CbiK, *A. fulgidus* $CbiX^S$ and the human and *Bacillus subtilis* protoporphyrin IX ferrochelatase HemH, show that in general these proteins have a very similar overall topology and that the cobalt ligand residues are conserved.[52,65–67] However, *Desulfovibrio* $CbiK^P$ homologs are, so far, the only ones containing the histidine heme ligand residue.[52] The crystal structures of the metal-complexed sirohydrochlorin $CbiX^S$ and CbiK of *A. fulgidus* and *S. enterica*, respectively, and of the *D. vulgaris* Hildenborough $CbiK^P$ obtained by co-crystallization with cobalt provided new insights into the active site of these proteins and on the cobalt chelation and substrate binding mechanisms. In particular, they show that cobalt binds to the chelatase *via* residues His154, Glu184 and His216 (*D. vulgaris* Hildenborough numbering). Moreover, the binding of cobalt to $CbiK^P$ promotes the rearrangement of the protein ligands, shifting the imidazole ring of His154 in relation to its initial position in the apo-protein.[52] Regardless of the conservation in sirohydrochlorin cobaltochelatases and protoporphyrin IX ferrochelatases of the amino acid residues involved in the chelatase reaction, the porphyrin bound structures exhibit significant differences concerning substrate orientation. Hence, this suggests that these proteins share a common ancestor upon which a structural pressure was imposed by the need of substrate discrimination.[52]

In spite of the questions raised by the presence of a periplasmic heme-containing cobaltochelatase in *D. vulgaris* Hildenborough that can hardly be implicated in the cytoplasmic synthesis of vitamin B_{12}, some insights can be retrieved from its genomic organization. With the exception of *D. desulfuricans* ATCC 27774, in all other genomes from *Desulfovibrio* sp. available in 2011, the gene encoding $CbiK^P$ is located in a putative operon, formed by gene products with sequence similarity to those encoding iron transport proteins, permeases, Fe(III) siderophores and periplasmic iron binding proteins. Therefore, a possible role for $CbiK^P$ in heme/iron transport in *D. vulgaris* Hildenborough is envisaged.[64] Besides *Desulfovibrio* sp., two CbiK encoding genes are also found in the genomes of other prokaryotes being the majority members of the deltaproteobacteria group including *Desulfobulbus*, *Desulfatibacillum* and *Desulfobacterium* and also in some archaeal species such as *Methanospirillum*, *Methanobrevibacter* and *Synthrophobacter*.

C. Alternative Heme *b* Branch

Earlier studies performed on the cytochrome c_3 isolated from cells of *D. vulgaris* Hildenborough grown in the presence of labeled SAM indicated that the heme methyl groups of rings A and B (C2 and C7) were derived from SAM methyl groups rather than from δ-ALA, as it would be expected.[66] Additionally, a novel

intermediate compound, the 12,18-didecarboxysirohydrochlorin, a decarboxylated form of SHC, was identified.[66,67] Subsequent work with recombinant heme biosynthetic enzymes showed that *D. vulgaris* Hildenborough produces precorrin-2 from HMB, also suggesting the bypass of the uroporphyrinogen III release step.[41] Altogether, these results raised the hypothesis of an alternative heme *b* biosynthetic route operative in *D. vulgaris* Hildenborough, where heme *b* was made *via* PC-2 or SHC (Figures 3 and 5). The release of several genomes from *Desulfovibrio* sp. further revealed the absence of genes encoding the canonical enzymes of heme biosynthesis that are involved in the steps downstream to uroporhyrinogen III: uroporphyrinogen III decarboxylase (encoded by *hemE*), protoporphyrinogen IX oxidase (encoded by the genes *hemG*, *hemY or hemJ*) and protoporphyrin IX ferrochelatase (*hemH*) (Figure 2). Studies on the archaeon

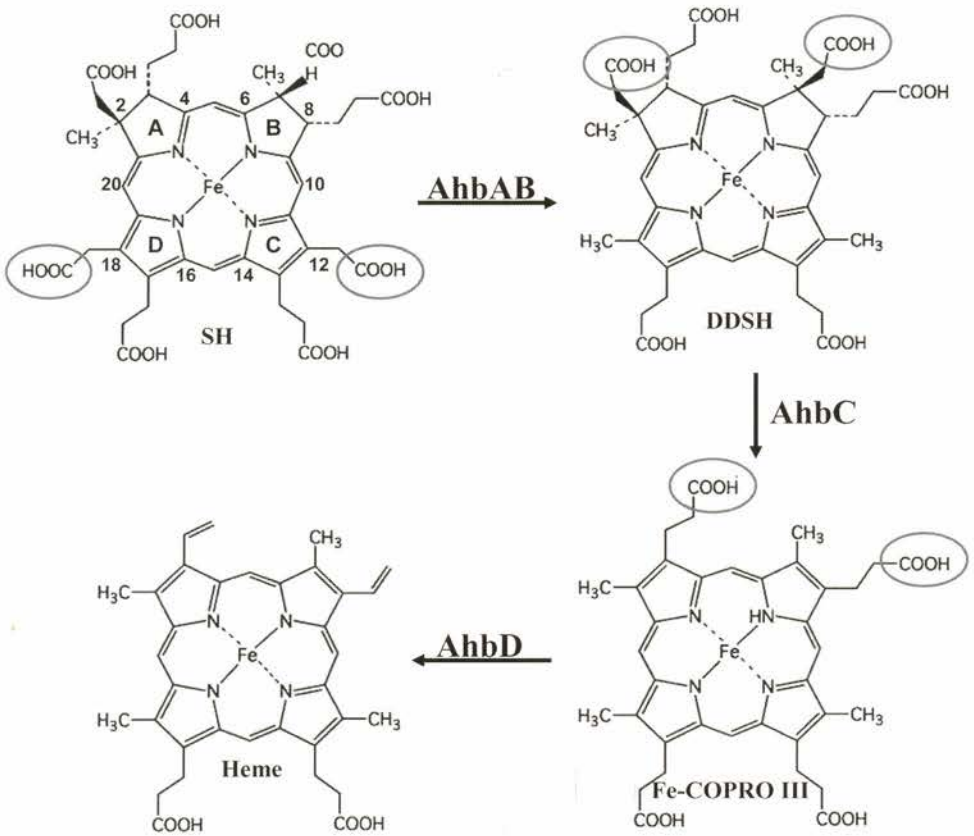

Figure 5. Alternative heme *b* pathway downstream of the synthesis of siroheme (SH) and operative in *Desulfovibrio* sp. Modifications in the peripheral chains of the SH porphyrin lead to the formation of didecarboxysirohydrochlorin (DDSH), Fe-coproporphyrin III (Fe-COPRO III) and ultimately heme *b*. Adapted from Ref. 53.

Methanosarcina barkeri, that also lacks genes coding for enzymes orthologs of the late heme biosynthesis pathway, led to the proposal that heme *b* is formed *via* a pathway that involves two methylation reactions using SAM.[65,69] Alternative intermediates occurring during the latter steps of the pathway were investigated in cell lysates of *D. vulgaris* Hildenborough anaerobically incubated with siroheme. These experiments allowed detection of mono-decarboxysiroheme, didecarboxysiroheme, Fe-coproporphyrin III, mono-vinyl Fe-coproporphyrin III and heme *b*, and the presence of these compounds is consistent with a pathway where the decarboxylation of siroheme, removal of the acetate chains attached to C2 and C7 of didecarboxysiroheme and ultimately sequential decarboxylation of the propionic acid chains attached to C3 and C8 of Fe-coproporphyrin III occur sequentially (Figure 5).[53] While lacking the canonical enzymes of the heme *b* synthesis, the genomes of *Desulfovibrio* sp. encode gene products known to participate in the synthesis of heme d_1, the cofactor of the cd_1 nitrite reductase (*nirD, nirH, nirJ-1* and *nirJ-2*). Since that enzyme is apparently absent in *Desulfovibrio* and Archaea, the presence of the *nir*-like genes led to the hypothesis that these gene products are operative in the alternative heme biosynthesis.[53,69] Further reinforcing this hypothesis was the fact that in *Desulfovibrio* sp. and in some Archaea three of these four *nir*-like genes are clustered together (*nirD, nirJ-1, nirJ-2*) and two of them encode proteins belonging to the radical SAM family of proteins (*nirJ-1*, *nirJ-2*), suggesting that they could be involved in the last steps of this alternative pathway.[33,53]

In fact, experiments done with *D. vulgaris* and *D. desulfuricans* Nir-like recombinant proteins revealed that siroheme (and not sirohydrochlorin or precorrin-2) is the precursor of heme *b* in this route. This metal-chelated tetrapyrrole is acted upon by the two non-radical SAM Nir-like proteins namely NirD and NirH, which were renamed AhbA and AhbB (alternative heme biosynthetic proteins A and B), to remove the carboxyl groups from the acetic acid chains attached to C12 and C18, yielding 12,18-didecarboxysiroheme (Figure 5).[53] The loss of the acetic acid side chains at C2 and C7 of 12,18-didecarboxysiroheme to form Fe-coproporphyrin III was demonstrated to be assisted by the radical SAM dependent protein NirJ-1 from the archaeon *M. barkeri*, which was renamed AhbC. Furthermore, Fe-coproporphyrin III was shown to be the substrate of the NirJ-2 enzymes from *D. vulgaris* and *D. desulfuricans* (now designated AhbD), which catalyzes a SAM-dependent conversion of the two propionate side chains attached to C3 and C8, into vinyl groups (Figure 5).[53] Hence, *Desulfovibrio* sp. were shown to perform heme synthesis *via* an alternative pathway that involves unprecedented reactions for the conversion of siroheme into heme *b* (Figures 3 and 5).

Studies on *Desulfovibrio* sp. which are part of SRB revealed the existence of an alternative heme *b* biosynthetic pathway and demonstrated that the need for

siroheme is not restricted to the production of a single cofactor, as it also serves to generate the tetrapyrrole intermediate that ultimately leads to the formation of hemes *b*. Although some pieces of the puzzle of how heme biosynthesis occurs in SRB are still missing, the studies so far performed on *Desulfovibrio* sp. have been unveiling the existence of a novel pathway for the biosynthesis of tetrapyrroles.

III. Iron Homeostasis — Bacterioferritin

SRB contain a large number of metalloproteins, of which most contain iron centers. Therefore, these bacteria have a high intracellular requirement for iron. As these bacteria are anaerobes, the iron present in the external medium is in the ferrous form and therefore does not represent a problem in terms of solubility. Nevertheless, the transient exposure to oxygen that these bacteria are able to sustain will promote the oxidation of ferrous iron to the insoluble ferric form. Moreover, the sulfide produced by these organisms from sulfate reduction will react with the ferrous iron forming insoluble complexes of iron-sulfides. To sustain iron bioavailability, SRB need to be able to store iron intracellularly. Until 2011, the only SRB iron-storage protein studied was the bacterioferritin (Bfr) from *D. desulfuricans* ATCC 27774, a heme-containing ferritin. However, a BLAST search of the several currently available genome sequences of SRB using the *D. desulfuricans* ATCC 27774 Bfr sequence as query revealed the presence of orthologs in other SRB species (Table 1) which also contain genes coding for putative canonical ferritins (with no heme moiety).

Table 1. Known Bfr orthologues in SRB.

Accession[a]	Organism	Amino acid identity with *D. desulfuricans ATCC 27774* Bfr (%)	Gene name
Q93PP9	*D. desulfuricans* ATCC 27774	100	Ddes_1387
D9YDX6	*Desulfovibrio sp.* 3_1_syn3	75	HMPREF0326_01699
Q72C87	*D. vulgaris* Hildenborough	70	DVU_1397
E3ILW9	*D. vulgaris* RCH1	70	Deval_1286
A1VE26	*D. vulgaris* DP4	70	Dvul_1675
B8DQ60	*D. vulgaris* Miyazaki F	68	DvMF_1981
Q317G2	*D. alaskensis* G20[b]	66	Dde_0831
E6VRB9	*D. aespoeensis*	63	Daes_0831
C7LUY6	*D. baculatum*	66	Dbac_0293
C8WZ93	*Desulfohalobium retbaense*	66	Dret_0066
B5YHI8	*Thermodesulfovibrio yellowstonii*	35	Theye_A0159

[a] Full information on the protein sequences can be retrieved from http://www.uniprot.org using this accession code.

[b] Formerly known as *D. desulfuricans* G20.

A. Biochemical Studies

The Bfr was purified directly from wild type cells of *D. desulfuricans* ATCC 27774, and exhibited an UV-visible spectrum[70] resembling that of the *D. desulfuricans* ATCC 27774 split-Soret cytochrome *c* (described in Section IV.B). In order to identify the protein, a N-terminal sequence analysis was performed, revealing a sequence with 80 amino acid residues that shared similarity with the ferritin protein family. Bfr is an oligomer of 24 subunits of 19 kDa each. The non-heme iron content was determined as two iron atoms per monomer, indicating that the protein was isolated with a di-iron site; moreover, the protein contained one heme per dimer, with a reduction potential of +140 mV,[70] a value much higher than those of other bacterioferritins, (*ca.* −200 mV).[71,72] Since the protein contained a heme group, it was classified as belonging to the branch of bacterioferritins or, more correctly, hemoferritins.

B. Spectroscopic Studies

As isolated, the *D. desulfuricans* ATCC 27774 Bfr exhibits the characteristic spectrum of a low-spin heme, with a Soret absorption band at 410 nm and another broad band around 540 nm (Figure 6). The spectrum also shows a minor contribution from a high-spin ferric heme form, with bands at 390 and 615 nm; a lower intensity absorption band was observed at 715 nm, which is characteristic of a bis-methionine ligation to the heme iron. Upon reduction, the Soret band is split, with maxima at 417 nm and 425 nm, a feature still unexplained, and the α- and β-bands appear at 550 and 520 nm, respectively (Figure 6).[70] The Soret band of the *D. desulfuricans* ATCC 27774 split-Soret cytochrome *c* displays a similar behavior upon reduction, but in this case the splitting of the Soret band was proposed to be due to the interaction between the transition dipole moments of the heme groups that are located within a van der Waals contact distance (Section IV.B).[73] However, the crystallographic structure of *D. desulfuricans* ATCC 27774 Bfr showed this not to be the case,[74] since the distance between the different hemes is quite large (~43 Å). Although each heme is flanked by two di-iron sites, one from each monomer, the distance between the iron atom in the heme and each iron atom of the di-iron center is *ca.* 13–14 Å, i.e., not close enough to disturb the $\pi \rightarrow \pi^*$ transition on the porphyrin ring.[70]

The EPR spectrum of the oxidized protein at 11 K has a major set of resonances at $g = 2.97$, 2.27 and 1.52, typical of low-spin ferric hemes, but no signature was detected for the bi-nuclear iron center. However, upon reduction and addition of NO resonances characteristic of high-spin ferrous iron bound to NO were detected, and a high-intensity signal was observed, due to an $S = 1/2$

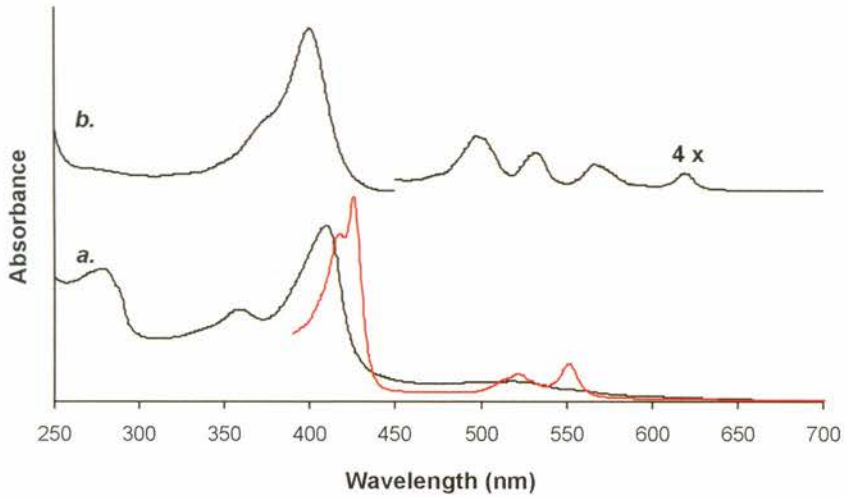

Figure 6. UV-visible spectra of *D. desulfuricans* ATCC 27774 Bfr. *a.* Spectra of the oxidized protein (black line) and reduced with dithionite (red line); *b.* UV-Visible spectrum of the methyl ester of the extracted porphyrin. The Q-band region is magnified 4×. Adapted from Refs. 28 and 70.

spin ground state at $g = 2.05$, 2.02 and 2.01,[70] identical to that assigned to the di-ferrous site in *E. coli* Bfr.[75]

The pyridine hemochrome of the protein showed a α-band at 545 nm, different from heme *c* (550 nm), iron-uroporphyrin I (548 nm) or heme *b*, which is the type generally identified in bacterioferritins.[71] A total molecular mass of 710 Da was determined, by matrix-assisted laser desorption/ionization (MALDI) mass spectrometry, for the extracted heme. The extracted, demetalated and esterified heme yielded a porphyrin with four Q-bands in the visible spectrum at 497.5, 531, 566.5 and 621 nm, identical to those of commercially available coproporphyrin ester (Figure 6),[28] and the identity of the Bfr heme co-factor was finally unequivocally determined by NMR spectroscopy to be Fe-coproporphyrin III (**3**), an unprecedented observation for any heme protein and, in particular, for a bacterioferritin.[28] This assignment was corroborated by its crystallographic structure.[74] Until then, coproporphyrin was regarded only as an intermediate in the heme biosynthetic pathway (Section II). The main difference between this heme and heme *b*, found in all other isolated hemoferritins, is the presence of two extra propionate groups that replace the two vinyl groups of heme *b* (**1**).

C. Functional Studies

A genetic analysis revealed that the gene coding for *D. desulfuricans* ATCC 27774 Bfr forms an operon with the gene encoding the metalloprotein rubredoxin-II (Rd-II),

a small (8 kDa) mononuclear iron protein whose metal is coordinated by four cysteines, and that the transcription level of the two genes is similar in nitrate- and sulfate-grown cells.[76] Interestingly, another open reading frame (ORF) is present upstream and transcribed in the same orientation as the gene encoding Bfr, namely *perR* that encodes a transcriptional repressor that regulates expression of peroxide stress response proteins.[76]

The genetic organization of *D. desulfuricans* ATCC 27774 Bfr and *rd-II* genes suggested a possible interaction between the two proteins. This interaction was confirmed by fluorescence spectroscopy, using the intrinsic fluorescence of tryptophans in rubredoxin.[76] This interaction was further established by observing electron transfer from the reduced Rd-II ($E_0' = +25$ mV) to the Bfr heme moiety ($E_0' = +140$ mV) with a stoichiometry of 2.5 Rd-II per Bfr monomer, thus accounting for the reduction of both the heme and the diiron center.[76]

D. Structural Studies

The crystallographic structure of *D. desulfuricans* ATCC 27774 *bfr* was determined for three different protein states: at 1.95 Å from an 'as isolated' protein sample, anaerobically purified but aerobically crystallized; at 2.05 Å from the same sample, but after crystal reduction with sodium dithionite; and at 2.35 Å from a 'cycled' oxidized sample, i.e. a sample that was crystallized aerobically after being fully reduced and subsequently allowed to re-oxidize by exposure to oxygen.[74] The overall structure of *D. desulfuricans* ATCC 27774 Bfr is similar to that of other ferritins, being composed of 24 subunits arranged in a hollow sphere with 432 point-group symmetry, with external and internal diameters of *ca.* 130 and 85 Å, respectively (Figure 7A).[74] Each monomer is composed of a four α-helix bundle with a fifth shorter helix at the C-terminal. Every subunit contains a di-iron site in the middle of the four-helix bundle (Figure 7B). The Fe-coproporphyrin III heme groups are located in-between two subunits, on a two-fold symmetry axis, and have a bis-methionine axial coordination with each ligand, Met57, belonging to two adjacent monomers (Figure 7B), as predicted from the absorption spectra. The hemes are buried within the Bfr dimer interface in such a way that two of the four propionates are not accessible from the outside of the sphere, while the other two propionates, which are structurally equivalent to those of heme *b*, are exposed to the internal cavity. The *D. desulfuricans* ATCC 27774 Bfr has a C-terminus extension of fourteen amino acid residues after the fifth helix, absent in other bacterioferritins and located inside the sphere cavity, in which Ser168 and Lys169 are involved in the formation of hydrogen bonds with the heme propionates.

The protein was isolated without an iron core, but instead it contained a stable di-iron center. This was the first example of a native bacterioferritin (i.e., not

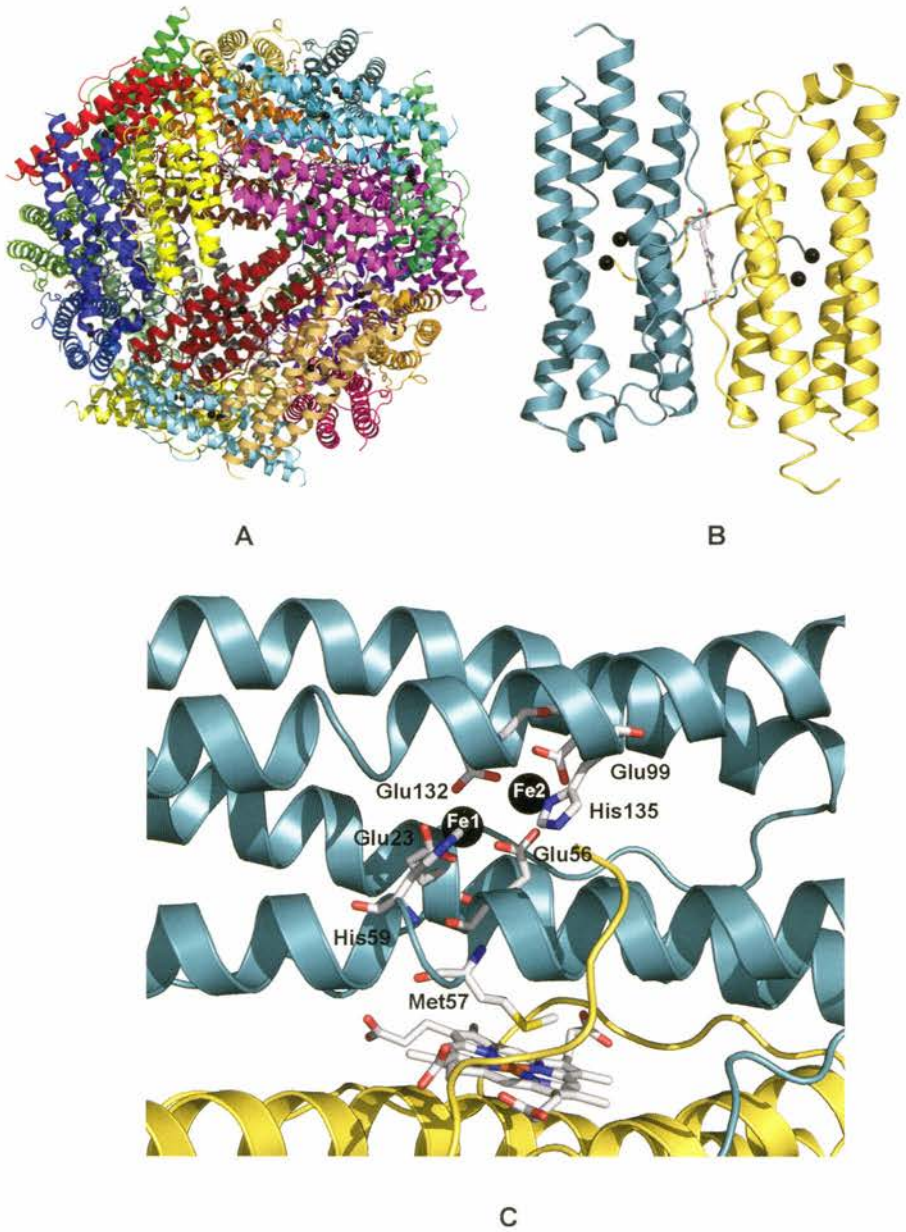

Figure 7. Structure of *D. desulfuricans* ATCC 27774 Bfr (PDB 1nfv, Ref. 74). (A) Overall structure of the Bfr 24-mer viewed from the three-fold axis. The protein chains are displayed as ribbons and each subunit is represented with a different color. (B) Ribbon representation of a Bfr dimer showing the location of the heme group and the di-iron sites. (C) Detail view of the di-iron site in one Bfr monomer, showing the amino acid residues involved in iron binding and heme coordination. The black spheres represent the di-iron sites, and the hemes and selected amino acids are drawn as sticks, with atom colors blue for nitrogen, light grey for carbon, redo for oxygen and yellow for sulfur. Figure made with PyMOL.[68]

reconstituted) isolated with the catalytic site. The di-iron site has the binding motif E23-X_{32}-E56-X_2-H59-X_{39}-E99-X_{32}-E132-X_2-H135, in which Glu23 and His59 are the terminal ligands of Fe1, Glu99 and His135 are the terminal ligands to Fe2, and Glu56 and Glu132 are the bridging ligands between the two irons (Figure 7C).[74] This ferroxidase center is flanked by two tyrosine residues, Tyr30 and Tyr106, which are hydrogen-bonded to the terminal glutamate ligands, Glu99 and Glu23, respectively. The three determined crystallographic structures are in overall similar, but have significant differences at the di-iron site. In the 'as-isolated' protein structure, the distance between the two iron atoms is *ca.* 3.7 Å, and extra electron density lying continuously over the iron site was observed, which however could not be modeled by a single species, suggesting that it results from a mixture of different bridging intermediates.[74] In the crystal aerobically reduced with sodium dithionite, the distance between the two iron atoms increased to 3.99 Å, and no extra electron density was observed above and between the two iron atoms, which is compatible with the reduction of the two ferric ions to the ferrous form. The structure of the reoxidized protein, revealed that the ferroxidase center appeared with one of the iron positions, Fe1, almost depleted, and with both bridging glutamate residues approaching Fe2.

The spherical structure has a 432 point-group symmetry, and contains channels along the three-fold and four-fold axes. In the three-fold channels there is an alternation of positively and negatively charged residues, defined on the outside by Lys111 and Glu115, and by Lys114, Glu126 and Arg123 on the inner surface. However, the four-fold channels are uncharged and defined by four symmetry-related threonine residues, Thr152.[74] Besides these two channel types, two others were identified in the structure: one is the pore leading to the di-iron ferroxidase site, in which the Fe atoms are located *ca.* 6 Å below the pore entrance; the second type consists of the B-pores, which are clusters of negatively charged amino acids at channels located between the three-fold and four-fold axes, which are sufficiently wide to allow the entry of iron atoms and to provide an access route to the protein core.

IV. Electron Transfer and Respiration — Cytochromes

Multiheme cytochromes *c* are particularly abundant proteins in *Desulfovibrio* sp.,[77,78] the most studied genus of SRB. However, it has long been known that not all sulfate reducing organisms contain cytochromes *c*. In 2011, a genomic analysis of 25 available genomes of sulfate reducers showed that these organisms can be divided into two groups concerning their content of cytochrome *c*-encoding genes.[21] The first group formed by the deltaproteobacteria sulfate reducers (which include *Desulfovibrio*) and the single member of *Nitrospira* with a genome

available (*Thermodesulfovibrio yellowstonii*), is characterized by a high number of multiheme cytochromes *c*. The second group is formed by members of Archaea and *Clostridia* that have no or very few cytochromes *c*. For the purpose of this chapter we consider only the deltaproteobacteria organisms, which are the most common and abundant sulfate reducers.

A. Monoheme Cytochrome *c*

Monoheme cytochromes *c* are small periplasmic proteins (*ca.* 100 aa) with a single heme *c* (**2**) group. In addition to the equatorial nitrogen ligands from the porphyrin ring, the heme iron atom is axially coordinated by a histidine and a methionine residue. In SRB, the only studied member of the monoheme cytochrome *c* family is the cytochrome c_{553}, which is characterized by a low reduction potential (*ca.* 20~40 mV) and was proposed to be the physiological partner of formate dehydrogenase[79,80] and [FeFe]-hydrogenase.[81,82] The interaction of *D. vulgaris* Hildenborough cytochrome c_{553} with formate dehydrogenase was studied by molecular biology methods coupled with kinetic experiments. Mutation in the cytochrome c_{553} of residues Lys62–Lys63–Tyr64, located in the C-terminal region of one of the α-helices near the heme group, caused a dramatic reduction of the electron transfer rate between cytochrome c_{553} and formate dehydrogenase.[83,84] Moreover, the analysis of the genomes of *D. vulgaris* Hildenborough and *D. alaskensis* G20 (formerly known as *D. desulfuricans* G20) first suggested that cytochrome c_{553} is involved in aerobic respiration since its gene is the first of a cluster of genes coding for a heme-copper oxygen reductase,[85] and a similar gene organization is observed in several other SRB genomes.[21] The monoheme cytochrome c_{553} was indeed shown to donate electrons to *D. vulgaris* membranes, in a process coupled to oxygen reduction.[86]

Although there are 5 structures of SRB cytochromes c_{553} in the Protein Data Bank (PDB), there are only two independent coordinate sets: from *D. vulgaris* Miyazaki F[87] and *D. vulgaris* Hildenborough.[88] The 3D structure of the *D. vulgaris* Miyazaki F cytochrome c_{553} was determined by X-ray crystallography, whereas that of the *D. vulgaris* Hildenborough ortholog in the reduced state was obtained by NMR spectroscopy. Both structures are very similar (Figure 8), and the NMR study of the *D. vulgaris* Hildenborough molecule revealed a conformationally flexible loop comprising residues 50–53.

Morelli *et al.*[89,90] carried out studies of the interaction between *D. vulgaris* Hildenborough cytochrome c_{553} and the ferredoxin from *D. norvegicum*, using a combination of heteronuclear NMR and soft-docking calculations, aiming to elucidate the electron transfer pathways and the general features of protein recognition between *D. vulgaris* Hildenborough cytochrome c_{553} and its putative

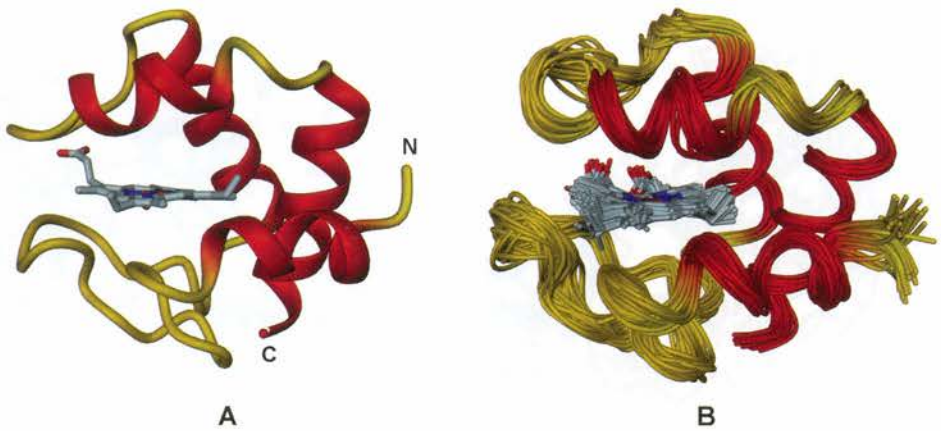

Figure 8. Three-dimensional structures of the cytochromes c_{553} from *D. vulgaris* Miyazaki F (PDB 1c53, Ref. 87) (A) and *D. vulgaris* Hildenborough (PDB 2dvh, Ref. 88) (B). In **A** the protein chain is represented as a ribbon with the α-helices colored red. In **B** the protein chains of the NMR models are represented as thin C^{α} tubes with the α-helical regions colored red. The heme groups are represented as sticks in both structures, with atom colors blue for nitrogen, red for oxygen, light cyan for carbon and brown for iron. Figure prepared with DINO.[91]

physiological partners, formate dehydrogenase and [FeFe]-hydrogenase. At the time, the crystal structure of these two enzymes had not been determined, and a simplified approach to the modeling of the interaction between cytochrome c_{553} and the larger molecules formate dehydrogenase and [FeFe]-hydrogenase was adopted, since both molecules contain a ferredoxin-like domain with 30% identity with *D. norvegicum* ferredoxin I, which was used as a model, constructed from the available coordinates of the ferredoxin II from *D. gigas* (PDB 1fxd).

The combination of these methods allowed the selection of three similar docking solutions between *D. vulgaris* Hildenborough cytochrome c_{553} and *D. norvegicum* ferredoxin I, with shortest metal-to-metal distances between 10.0 and 12.4 Å.[90] The best solution chosen showed a close distance of 4.1 Å between one of the cysteine residues attached to the $[4Fe4S]^{2+/1+}$ cluster of ferredoxin I and another covalently linked to the heme group in cytochrome c_{553}. This was interpreted as the point of electron transfer between the ferredoxin I and cytochrome c_{553} in the complex.

The *D. vulgaris* Hildenborough [FeFe]-hydrogenase is identical to the orthologous enzyme from *D. desulfuricans* ATCC 7757 for which a crystallographic structure was subsequently determined,[92] and the same method was applied to the study of the interaction between cytochrome c_{553} and the [FeFe]-hydrogenase from *D. vulgaris* Hildenborough.[93] *D. vulgaris* Hildenborough [FeFe]-hydrogenase is constituted by two different subunits of 42.5 and 11 kDa, and the large subunit contains a ferredoxin-like domain with three $[4Fe4S]^{2+/1+}$ clusters and a binuclear

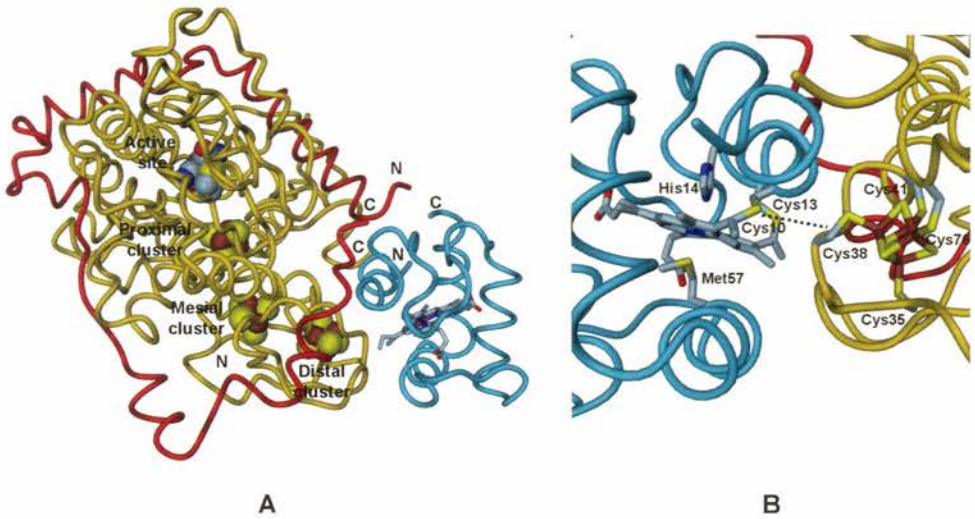

Figure 9. The electron transfer complex between *D. vulgaris* Hildenborough cytochrome c_{553} and [FeFe]-hydrogenase (PDB 1e08, Ref. 93). (A) Model of the complex between *D. vulgaris* Hildenborough cytochrome c_{553} and [FeFe]-hydrogenase. (B) Detail view showing the close contact between Cys10 in cytochrome c_{553} and Cys38 in [FeFe]-hydrogenase (dashed line). The protein chains are represented as C^{α} tubes, colored red and gold for the [FeFe]-hydrogenase small and large chains respectively, and cyan for the cytochrome c_{553}. In (A) the active site and the iron–sulfur clusters of the [FeFe]-hydrogenase are drawn in space-filling mode and the heme group of cytochrome c_{553} is displayed as sticks. In (B) the heme group of of cytochrome c_{553} and the side chains of its linked protein residues, the distal $[4Fe4S]^{2+/1+}$ cluster of [FeFe]-hydrogenase and its linked cysteine residues are shown as sticks. Atom colors are blue for nitrogen, red for oxygen, light cyan for carbon, yellow for sulfur and brown for iron. Figure prepared with DINO.[91]

[FeFe] center. The location and spacing of the $[4Fe4S]^{2+/1+}$ clusters (*ca.* 12 Å apart) suggests that they are part of an electron transfer pathway between the active site and the enzyme surface. Furthermore, the molecular surface in the region of the distal $[4Fe4S]^{2+/1+}$ cluster (see Figure 9), which is the one closest to the surface, is negatively charged, whereas the heme pocket in *D. vulgaris* Hildenborough cytochrome c_{553} is surrounded by positively charged residues, suggesting the possibility of interaction between these two regions. The NMR data allowed the mapping of the interacting site on the cytochrome, which combined with *ab initio* soft-docking methods and metal-to-metal restraints resulted in the selection of two families of optimal docking solutions. In one of them, the heme pocket of cytochrome c_{553} interacts with the distal $[4Fe4S]^{2+/1+}$ cluster of [FeFe]-hydrogenase while in the second it interacts with the mesial $[4Fe4S]^{2+/1+}$ cluster. However, in the second family the heme-cluster distances are markedly larger (16–21 Å) than in the first (12–14 Å) making electron transfer less likely. The best solution chosen from the first family (Figure 9) is remarkably similar to that

obtained for the complex between *D. vulgaris* Hildenborough cytochrome c_{553} and *D. norvegicum* ferredoxin I, with a close contact (3.8 Å) between one of the cysteine residues covalently linked to the heme group in cytochrome c_{553} and another attached to the distal $[4Fe4S]^{2+/1+}$ cluster of *D. vulgaris* Hildenborough [FeFe]-hydrogenase.

B. Multiheme Cytochromes — The Dimeric Diheme Split-Soret Cytochrome *c*

Of the many types of heme proteins present in SRB, the dimeric diheme split-Soret cytochrome *c* (SSC) is probably one of the most intriguing. This cytochrome was first isolated from the SRB *D. desulfuricans* ATCC 27774 (which is also capable of reducing nitrate) and received its name from the observation that upon reduction its UV-visible spectrum presented a Soret band at 424 nm, an unusual value for a cytochrome *c*, with a clear shoulder appearing at 415 nm (Figure 10).[94] The SSC was isolated as a homodimer with a molecular mass of 52.6 kDa, containing two identical subunits of 26.3 kDa. Each subunit binds two heme *c* groups (**2**), with bis-histidinyl axial coordination and distinct reduction potentials.[95] Although SSC is present in both sulfate- and nitrate-grown cells, it is more abundant in cells grown under nitrate-respiring conditions.[94,96] However, SSC has no nitrate or nitrite reductase activities.[94]

The 3D structure of SSC was determined using the anomalous dispersion properties of the iron atoms present in the heme groups and a preliminary structural

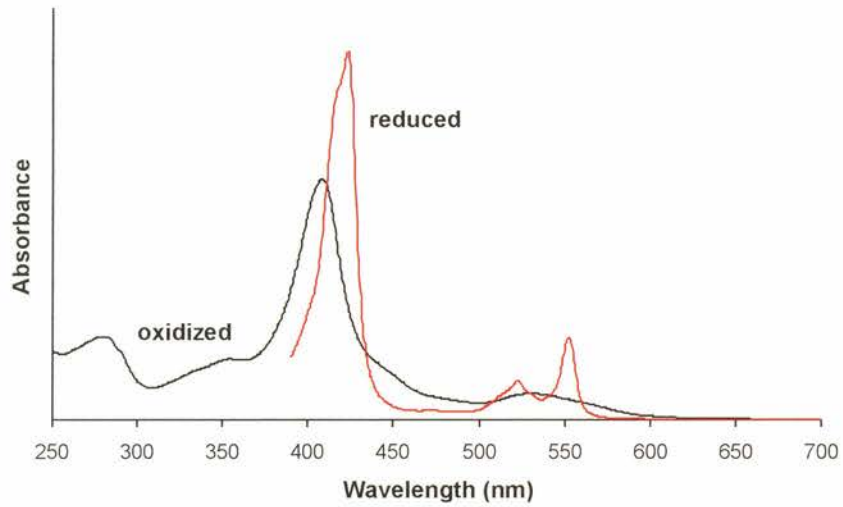

Figure 10. UV-visible spectra of *D. desulfuricans* ATCC 27774 split-Soret cytochrome *c* in the oxidized state (black line) and reduced with dithionite (red line). Adapted from Ref. 94.

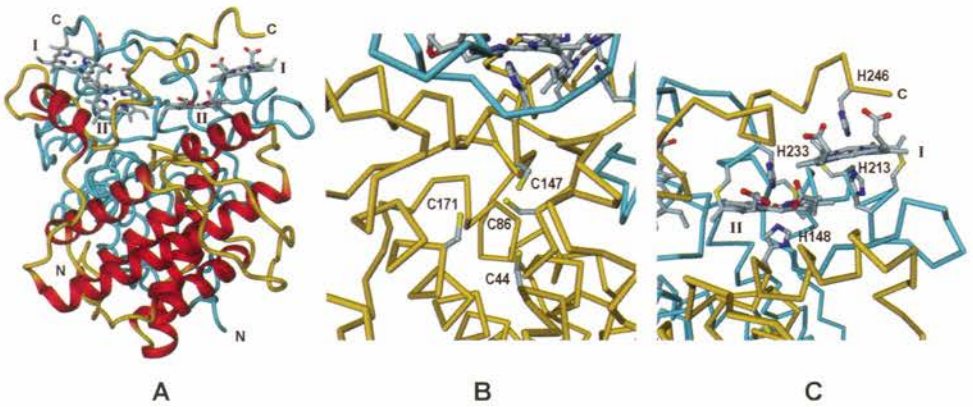

Figure 11. Views of the three-dimensional structure of the split-Soret cytochrome *c* from *D. desulfuricans* ATCC 27774 (PDB 1h21, Ref. 96). (A) Overall view of the homodimer. The foreground monomer is drawn as ribbons highlighting the secondary structure elements, with the α-helices colored red. The background monomer is shown as a C^{α} tube and colored cyan. The heme groups are represented as sticks with atom colors blue for nitrogen, red for oxygen, light cyan for carbon and brown for iron. (B) Detail view showing the four cysteine residues believed to bind a $[2Fe2S]^{+2/+1}$ cluster. Both monomers are drawn as C^{α} traces. The foreground monomer is colored gold and the background monomer is colored cyan. The 4 cysteines, the heme groups and their axial-coordinating histidines are shown in ball-and-stick representation with atom colors as in panel A, and with sulfur atoms in yellow. (C) Detail view showing the heme stacking in the background monomer and their axial coordination. The molecular representation and the atom colors are as in panel B. Figure prepared with DINO.[91]

model was obtained[73] prior to the full sequencing of the protein.[97] Cloning and sequencing of the *ssc* gene in 2003 revealed the presence of a signal peptide, an indication that SSC is a periplasmic protein (as all cytochromes *c*), corrected a few errors in the original protein sequence determination by protein digestion and peptide sequencing, and allowed a full crystallographic model to be built and refined (Figure 11).[96]

The SSC fold is most unusual for a cytochrome *c*, because the heme groups are located at one extreme of the molecule, rather than being enveloped by the polypeptide chain. In addition, the two heme groups in each monomer are stacked, with a closest distance of *ca.* 3.8 Å, and the two heme pairs in the dimer are at an angle of about 45° with a closest distance of *ca.* 3.5 Å. Finally, the axial coordination of each heme group is completed by a histidine residue from the other monomer, showing that the SSC dimer is indeed the biological unit.

Mössbauer and EPR spectroscopic studies[96,97] revealed, in addition to the heme irons, the presence of non-heme iron, most likely in the form of a $[2Fe2S]^{+2/+1}$ cluster. Devreese *et al.*[97] originally proposed this cluster to be bound by Cys29, Cys44, Cys147 and Cys155. However, the 3D structure of SSC shows that Cys29 and Cys155 are located far from each other and from the other two.

The corrected sequence by Abreu *et al.*[96] identified two additional cysteines residues and the 3D structure revealed that they are located near Cys44 and Cys147:Cys 86 (previously Tyr) and Cys171 (previously Ala); these 4 cysteines are located in a surface pocket open to the solvent.

Despite the spectroscopic evidence to attest its presence in SSC, the $[2Fe2S]^{2+/1+}$ cluster was not observed in its 3D structure, very likely because it is very sensitive to oxygen exposure and, although the protein was obtained under anaerobic conditions the crystals were not. Indeed, even when using anaerobic sample preparations, the reduction potential of this center could not be unequivocally determined, and the EPR results showed that this center is present in substoichiometric amounts of cluster iron per monomer.[96]

A simple modeling of a $[2Fe2S]^{2+/1+}$ cluster into the cysteine pocket predicted an unusual binding mode, by only three out of the four cysteine residues present. Abreu *et al.*[96] first proposed the binding residues to be Cys86, Cys147 and Cys171. In 2005, Rodriguez and Abreu proposed a different coordination scheme,[98] involving residues Cys44, Cys86 and Cys147. Either coordinating scheme of the $[2Fe2S]^{2+/1+}$ cluster has the interesting consequence of leaving one of the iron atoms with a vacant binding position and facing the surface pocket entrance. This vacant position could thus function as the binding site for a small molecular species that might be the substrate of SSC. Rodriguez and Abreu[98] investigated the binding of O_2, NO, CO and H_2O to the $[2Fe2S]^{2+/1+}$ cluster of SSC in a fully oxidized $[2Fe2S]^{2+}$ and in partially reduced $[2Fe2S]^{1+}$ states using density functional theory (DFT) calculations. Of the molecules studied, O_2 showed the highest binding energy, followed by NO, CO and H_2O. The calculations predicted that binding of the O_2 molecule causes the destruction of the $[2Fe2S]^{2+/1+}$ cluster, which may explain the experimental difficulties in its characterization. On the other hand, a strong interaction of CO and NO with the $[2Fe2S]^{2+/1+}$ cluster was predicted, but without affecting its structural integrity. The most stable configurations involved binding of C or N to the Fe atom. This study therefore suggests that the substrates of SSC may be CO or NO, or a similar small molecule.

Until 2011, the structure of *D. desulfuricans* ATCC 27774 SSC was the only of its kind present in the PDB. A BLAST search of all published protein sequence databases with the SSC sequence produced a total of 90 hits. However, when the likelihood of structural and functional similarity is further refined by searching for the signatures for heme binding (two CXXCH heme binding motifs and two additional histidines), as well as a $[2Fe2S]^{2+/1+}$ cluster binding (four cysteines) in the sequence alignments, this number is significantly reduced. In addition to SRB, proteins similar to SSC or its domains are encountered e.g., in *Archaeoglobaceae*, *Clostridiales*, *Alteronomonadales* such as *Ferrimonas* and *Shewanella,* and *Desulforomonadales* such as *Geobacter*. Table 2 lists 23 organisms that metabolize

Table 2. SSC in microorganisms capable of metabolizing sulfate and other sulfur compounds.

	Accession[a]	$[2Fe2S]^{2+/1+}$	Heme 1	Heme 2
Sulfate-reducing Archaea		3	2	2
Archaeoglobus veneficus (DSM 11195)	F2KR97	Y	Y	Y
Archaeoglobus fulgidus (ATCC 49558)	O30219	Y[b]	N	N
Sulfate-reducing Bacteria				
Thermodesulfovibrio yellowstonii (ATCC 51303)	B5YFU8	Y	Y	Y
Desulfococcus oleovorans DSM 6200	A8ZZ47	Y	Y	Y
Desulfurivibrio alkaliphilus DSM 19089	D6Z572	Y	Y	N
Desulfobulbus propionicus DSM 2032	E8RIL6	Y	Y	N
Desulfovibrio desulfuricans ATCC 27774	P81040	Y	Y	Y
Desulfovibrio piger ATCC 29098	B6WW99	Y	Y	Y
Desulfovibrio sp. 3_1_syn3	D9Y986	Y	Y	Y
Desulfovibrio alaskensis G20	Q30WE1	Y	Y	Y
Desulfovibrio sp. 3_1_syn3	D9YAW0	Y	Y	Y
Desulfovibrio africanus Walvis Bay	F3YVK9	Y	Y	Y
Desulfovibrio vulgaris Miyazaki F	B8DPH5	Y	Y	Y
Desulfohalobium retbaense DSM	C8X5E6	Y	Y	Y
Desulfonatronospira thiodismutans ASO3-1	D6SSP6	Y[c]	Y	Y
S-reducing Bacteria[d]				
Pelobacter propionicus DSM 2379[e]	A1AP78	Y	N	N
Desulfurobacterium thermolithotrophum DSM 11699	F0S2S6	Y	Y	Y[f]
Desulfurobacterium thermolithotrophum DSM 11699	F0S3I8	Y[g]	N	N
Dethiobacter alkaliphilus AHT 1	C0GEZ5	Y[b]	Y	Y[f]
Dethiobacter alkaliphilus AHT 1	C0GFM4	Y	Y	Y[f]
Desulfitobacterium hafniense Y51	Q24VQ4	Y	Y	Y[f]
Desulfitobacterium hafniense DCB-2	B8G2D7	Y	Y	Y[f]
Bilophila wadsworthia 3_1_6	E5Y9Y7	Y	Y	Y

[a] Full information on the protein sequences can be retrieved from http://www.uniprot.org using this accession code.
[b] Incomplete $[2Fe2S]^{2+/1+}$ binding motif (only three out of four cysteines found).
[c] Motif contains a Se–Cys.
[d] Bacteria that reduce other sulfur compounds.
[e] Assimilative sulfate reduction only.
[f] An exact alignment with SSC was not found, but a nearby His residue may complete the heme axial coordination.
[g] An exact alignment with SSC was not found, but a nearby Cys residue may complete the $[2Fe2S]^{2+/1+}$ binding motif.

sulfur compounds (including and in addition to SRB) for which proteins similar to SSC or its domains have been identified. Eighteen of those protein sequences have both motifs for $[2Fe2S]^{2+/1+}$ cluster and heme binding. In addition to *A. fulgidus* there are two additional sulfur-metabolizing organisms, *Pelobacter propionicus* DSM 2379 (assimilative only) and *Desulfurobacterium thermolithotrophum* DSM

11699, whose homologs lack the heme binding motifs, i.e., have only the $[2Fe2S]^{2+/1+}$ cluster binding motif. However, the latter also contains a full-length SSC homolog. In SRB, the SSC from *Desulfurivibrio alkaliphilus* DSM 19089 and *Desulfobulbus propionicus* DSM 2032 lack the binding motif for the second heme, and in *Desulfonatronospira thiodismutans* ASO3-1 SSC, one of the cysteine residues proposed to bind the $[2Fe2S]^{2+/1+}$ cluster is replaced by a selenocysteine.

The fact that SSC is not exclusively present in SRB or other organisms that metabolize sulfur lends credence to the hypothesis that this class of proteins is not involved in sulfur metabolism. The $[2Fe2S]^{2+/1+}$ cluster appears to be essential to its true function, which remains to be discovered.

C. Multiheme Cytochromes — The Class III Cytochrome Family

The cytochromes of class III, namely cytochromes c_3, are some of the most abundant proteins in the periplasmic space of most SRB, in particular those of the *Desulfovibrio* genus.[77] These organisms also contain other multiheme cytochromes, which up to now have either not been characterized, or characterized only to a lesser level of structural, functional or physiological detail. The cytochromes c_3 include proteins binding from 4 to 16 hemes *c* (**2**), and the basic sequence and structural motifs are represented by the tetraheme cytochrome c_3 also known as Type I cytochrome c_3 (TpI-c_3). Repeats of this motif give rise to more complex structures, such as octaheme (di-tetraheme), nonaheme and hexadecaheme cytochromes c_3. Some of the heme binding motifs in this family of proteins are unusual since they can have three or four residues between the cysteine residues that form thioether bridges with the reduced vinyl groups in the heme, rather than the usual two (CX_nCH with $n = 2, 3, 4$). The tetraheme cores are closely packed together and wrapped by the polypeptide chain. The short heme-to-heme distances enable fast intramolecular electron transfer rates and these proteins are usually involved in electron transfer processes related with the energy metabolism of SRBs. In general, one or more heme groups are incompletely shielded by the protein chain and thus accessible to solvent or to other proteins which function as redox partners of these cytochromes.

1. *Tetraheme Cytochrome c_3*

a. *Introduction*

The tetraheme cytochromes c_3 are proteins isolated from the periplasmic space of sulfate-reducing deltaproteobacteria with molecular masses of 13–15 kDa containing four hemes *c*, with all heme irons axially coordinated by histidines.[99,100]

They were classified as Type I (TpI-c_3) and Type II (TpII-c_3) based on functional, structural and amino acid sequence properties.[101] The physiological function of TpI-c_3 is to accept electrons from the periplasmic hydrogenases, and deliver them to membrane-linked redox complexes that very often include other multiheme cytochromes *c*.[99,100] It has been proposed that TpI-c_3 may act as a proton thruster, in the sense that it would also accept protons from the hydrogenase partner and deliver them to the cytoplasmic membrane with a net energy transfer from the redox to the protonic centers.[102,103] TpI-c_3 from SRB is one of the best characterized electron transfer proteins in terms of structure–function relationships.[103] These studies revealed the presence of two types of phenomena, believed to be relevant to its biological role: positive cooperativity for electron transfer between a pair of hemes, and a pronounced thermodynamic proton/electron coupling, the redox-Bohr effect.[104–107] It should be noted, however, that pH-dependent reduction potentials are observed in a wide range of heme proteins (including monoheme cytochromes) and in many other metalloproteins.

b. *Spectroscopic studies*

The four hemes in cytochromes c_3 provide excellent spectroscopic handles for studying these proteins. Mössbauer spectroscopy of ^{57}Fe labeled cytochromes c_3 showed that the oxidized hemes, which have spin 1/2, are weakly coupled magnetically *via* a dipolar mechanism, as a result of their close proximity. Spectral simulations of data obtained in the presence of an external magnetic field allowed the deconvolution of spectral components that were assigned to four slightly distinct hemes.[108]

UV-visible spectroscopy shows intense absorption bands with characteristic maxima that change considerably from the reduced to the oxidized form (Table 3), as typically observed for low-spin *c*-type cytochromes.

Absorption coefficients for these characteristic bands were reported and are very similar for different cytochromes c_3. These absorption bands are too broad to

Table 3. UV-visible absorption bands for TpI-c_3 from *D. africanus*.

	Oxidized		Reduced	
Band	λ_{max} (nm)	ε ($M^{-1}cm^{-1}$)	λ_{max} (nm)	ε ($M^{-1}cm^{-1}$)
Soret	409	482500	416	711200
alpha	—	—	523	60700
beta	—	—	552	113000

Data taken from Ref. 109.

allow discrimination of the individual hemes but are useful to monitor the degree of oxidation of cytochromes c_3 during redox titrations and in kinetic studies.[106]

High frequency resonance Raman spectroscopy permits the analysis of the heme plane distortions based mainly on the structure-sensitive ν_{10} marker line, which allows for Lorenzian deconvolution of the contributions of the four hemes.[110] Furthermore, in this spectral region some marker bands are also sensitive to the redox state of the protein allowing monitoring of redox transitions.[111] When cytochromes c_3 are adsorbed on electrode surfaces, surface-enhanced resonance Raman spectroscopy shows that the reduction potentials are quite sensitive to the electric field strength.[112]

The cytochromes c_3 were extensively studied by EPR spectroscopy in the oxidized state (the low-spin ferric hemes are paramagnetic) and along redox titrations. If, on one hand, EPR spectroscopy may allow a preliminary assignment of the hemes, based on different rhombicities and reduction potentials, on the other hand this assignment may be hindered due to changes in the signal line widths along the titration (due to the magnetic interactions between the hemes, as shown by Mössbauer spectroscopy), as well as to the changes in g-values and lineshapes of resonances that occur upon partial reduction of several cytochromes c_3. These changes are probably related to redox-linked conformational changes. By correlating the anisotropy of the g tensor with the geometry of the axial ligands of the hemes known from the structure, it was possible to propose a preliminary assignment of the reduction potentials to each specific heme, using either amorphous or single crystal samples.[113,114]

1D ^{1}H NMR spectroscopy performed on the reduced diamagnetic state of cytochromes c_3 does not provide immediate discrimination between the various cytochromes. However, in the oxidized state, signals from the hemes are shifted outside of the protein envelope by paramagnetic effects. The position of these paramagnetically shifted signals is dependent on the geometry of the axial histidines and therefore the 1D ^{1}H NMR spectra of oxidized cytochromes c_3 show a different pattern of paramagnetically shifted signals that is characteristic for each protein and allows its unequivocal identification.[115] Therefore, the hemes are spectroscopically distinct, enabling their discrimination. The signals of individual hemes can also be followed as the oxidation state of the protein is modified. Multidimensional ^{1}H NMR spectroscopy was used to determine the population fraction of all the microscopic redox states that these tetraheme cytochromes can assume during their redox cycling.[116,117] This enabled the determination of the relative reduction potentials and redox interactions among the various hemes.[99] Docking with a Zn-substituted rubredoxin, which is a redox-inactive mimic of the shape and charge of the physiological partner hydrogenase, was shown to occur without major changes in the redox properties of the cytochromes c_3.[118]

Multidimensional ^{1}H NMR spectroscopy was also used to solve the solution structure of several cytochromes c_3 in the reduced diamagnetic state, and in the oxidized paramagnetic state.[119–121] These data are at the core of the detailed functional characterization of cytochromes c_3 described below. Heteronuclear ^{1}H–^{15}N multidimensional NMR spectroscopy performed in reduced samples was used to obtain a solution structure of cytochrome c_3 from *D. vulgaris* Miyazaki F.[122] These experiments also allowed, from relaxation measurements, identification of regions of higher structural mobility that show a good correlation with redox-linked changes in the 3D structure.[122] These spectroscopic methods were also used to map the interaction surface of TpI-c_3 from *D. vulgaris* Hildenborough with TpII-c_3,[123] and with the [FeFe]-hydrogenase.[124] ^{1}H–^{13}C paramagnetic NMR studies performed in natural abundance samples were used to determine the orientation of the axial ligands of the hemes using a semi-empirical model of the heme molecular orbitals.[125] These data were utilized to place the magnetic axes relative to the structural heme frame, an important step to refine solution structures in the paramagnetic state of cytochromes c_3 and low-spin heme proteins in general.[126,127]

c. *Functional studies*

(i) Thermodynamic studies

The spectral discrimination afforded by NMR spectroscopy together with redox titrations followed by NMR and visible spectroscopies provide the detailed determination of the intrinsic reduction potentials of the four hemes of cytochromes c_3. This analysis also enables the determination of the redox interactions between the hemes and the pH dependence of the reduction potentials, i.e., the redox-Bohr effect.[99] This wealth of data can be obtained because of several favorable characteristics of cytochromes c_3: (i) due to their small size, the hemes are packed close together and intramolecular electron transfer is fast, estimated to be faster than 10^8 s^{-1} based on electrochemical measurements;[128] (ii) at the concentrations typically used for NMR samples (1–2 mM) the intermolecular electron transfer is slow, less than $4 \times 10^2 s^{-1}$;[117] (iii) NMR spectroscopy provides spectral discrimination of the four hemes, allowing the cross-assignment of the signals to specific hemes in the structure. Parsing the effect of redox interactions from the effect of pH dependence of the reduction potentials with a minimal number of fitted parameters requires the measurement of the NMR data at several pH values to determine the macroscopic pK_a of the acid-base center(s).[107,129] This information was used to establish the order of reduction potentials of the hemes for various cytochromes c_3, reported in Table 4. It also allowed the identification of pairs of hemes that display positive cooperativities that reduce or even invert the

Table 4. Order of heme reduction potentials in tetraheme cytochromes c_3 from SRB.

Organism	First to last[a]				Ref.
Type I					
D. gigas	I	II	III	IV	106
D. vulgaris Hildenborough	III	II	I	IV	106
D. vulgaris Miyazaki F	III	II	I	IV	107
D. desulfuricans ATCC 27774	I	II	IV	III	106
D. africanus	I	IV	II	III	106
D. norvegicum	II	I	IV	III	104
D. baculatum	II	I	IV	III	104
Type II					
D. africanus	II	I	III	IV	132

[a] Hemes are numbered with Roman numerals according to the order of attachment to the polypeptide chain. Shaded entries indicate the pair of hemes displaying positive cooperativity.

expected electrostatic repulsion between charges of the same sign.[106,107,117,130] These positive cooperativities revealed redox-linked structural changes in the cytochromes, that were later identified in crystallographic and NMR structures that are described in Section IV.C.d.

It is evident from Table 4 that despite the structural homology between the various cytochromes c_3, to be discussed in Section IV.C.d, the order of heme reduction potentials is different for different proteins. Also, the pairs of hemes involved in positive cooperativity are different. Nonetheless, this does not translate into functional variability and a common theme is found among all TpI-c_3 with positive cooperativity between hemes as the basis for concerted multi-electron transfer, while the redox-Bohr effect led to the proposal that TpI-c_3 couple the transfer of electrons and protons at physiological pH values.[102,103] TpII-c_3 have a similar size as TpI-c_3 and are associated with the membrane-bound Tmc redox complex (described in Section VI.B, see also Table 8).[131] Contrary to TpI-c_3, the single example of TpII-c_3 studied in detail does not exhibit positive cooperativity between any pair of hemes.[132]

The states of TpI-c_3 as it interacts with the physiological partners can be described as standing in the vertices of a cube (Figure 12). The experimental data shows that conformational changes leading to cooperative electron transfer are coupled to proton transfer in the physiological pH range. As mentioned above, the putative functional consequences of these properties for the interaction with the physiological partner were given the name "proton-thrusting".[133] The experimental data does not allow the identification of the specific acid-base groups that contribute to the observed pK_a values. Theoretical calculations based on high resolution structures reported in Section IV.C.d showed that the observed pH

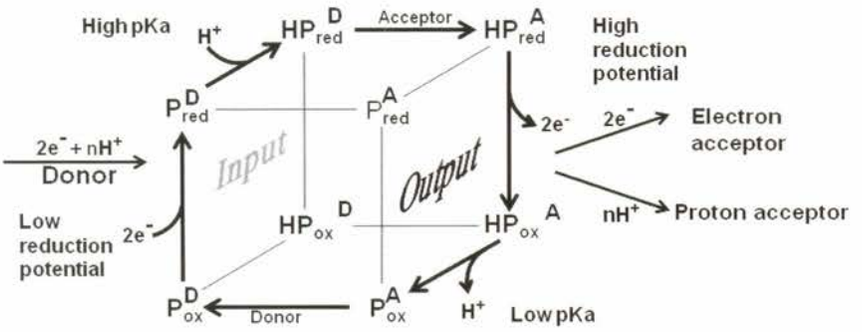

Figure 12. Cube diagram for the changes in redox and acid-base properties of TpI-c_3 when it receives electrons and protons from hydrogenase (donor) and releases them to the acceptor. The proposed cyclic and ordered interconversion of states leads to the acidification of protons at the expense of redox power in a process that dispenses the presence of a membrane. Adapted from Ref. 102.

dependence of the reduction potentials corresponds to the overall contribution of partial titration of various groups in the cytochromes.

(ii) Kinetic studies

The reduction of multiheme cytochromes c_3 with sodium dithionite was kinetically studied, which allowed the parsing of the kinetic contribution of the individual hemes in the absence of spectral discrimination using UV-visible spectroscopy.[134]

These studies showed that in the absence of recognition and binding of the physiological donor, electron uptake occurs through different hemes in different cytochromes. Access of the reducing agent to the hemes is an important factor in establishing the rates of electron transfer, but not the dominant one.[106]

(iii) Site-directed mutagenesis studies

Given the extensive interest surrounding the functional properties of cytochromes c_3, site-directed mutations were performed on this protein. This was a non-trivial endeavor, given that many molecular biology tools were unavailable at the time of the initial attempts. Also, at that time full amino acid sequences including the signal peptide for translocation of the apocytochrome into the periplasm (where heme *c* insertion takes place) were unavailable.

The first report of cloning of a cytochrome c_3 gene was published by Voordouw and Brenner in 1986 for the TpI-c_3 from *D. vulgaris* Hildenborough.[135] However, original attempts to express the protein in *E. coli* were unsuccessful[136] with production of only the apoprotein. In the early 1990s the expression in *D. alaskensis* G20 allowed purification of sufficient recombinant protein for

functional and structural characterization.[137] Early targets were the distal axial ligands of the hemes.[138] Replacement of these ligands with methionines increases the reduction potentials and reduces the thermal stability showing the structural and functional importance of the heme coordination,[139,140] as well-known from earlier studies on monoheme cytochromes[141]. Another target for site-directed mutagenesis was a phenylalanine (Phe20 in the mature *D. vulgaris* Hildenborough protein) which is one of the few conserved residues among the various tetraheme cytochromes c_3. The structural studies (see Section IV.C.d) showed that the aromatic plane of this residue also assumes a conserved position relative to hemes I and III, and both observations suggest an important role for this residue in controlling the rate of intramolecular electron-transfer.[142] However, replacement by isoleucine resulted only in minor changes in the redox properties of the cytochrome.[143] A F20L mutated cytochrome was also characterized.[144] The thermostability of this mutated cytochrome remained very high and the kinetics of reduction by the physiological partner were identical to the wild type protein. However, it was not possible to determine the rates of intramolecular electron transfer, which could have been affected by this mutation. The redox- and the electron-proton cooperative effects in cytochromes c_3 were also analyzed by mutating Lys45 (residue numbering of the mature protein) of cytochrome c_3 from *D. vulgaris* Hildenborough.[143] This residue is located close to the propionates of heme I and the replacement modified the pH dependence of the reduction potentials. The most dramatic effect was observed for the K45Q mutant for which a structure was obtained by NMR.[145] This residue is located in a loop that changes position depending on the oxidation state of the cytochrome and therefore modulates electrostatic interactions within the protein; this mutation led to reduced positive cooperativity and changes in the electron-proton coupling. Another mutant was made on Thr24, a residue whose side chain changes conformation with the protein redox state. In this mutated cytochrome the reduction potential of heme III is lowered, unbalancing the network of cooperativities exhibited by the cytochrome.[146]

In the year 2000, strategies for expression of multiheme cytochromes in *E. coli* were finally reported that relied on the co-expression with the *E. coli* cytochrome *c* maturation (*ccm*) gene cluster for incorporation of the hemes.[147–150]

(iv) Physiological studies

Due to its high abundance in the cell, TpI-c_3 was believed to be essential for sulfate respiration. Odom and Peck proposed a mechanism of hydrogen cycling to explain energy conservation during growth of *D. vulgaris* Hildenborough with lactate/sulfate that requires the involvement of this protein as an electron acceptor to periplasmic hydrogenases.[151]

Electron transfer between cytochromes c_3 and various physiological and non-physiological redox partners was studied. Cytochromes c_3 are known to enhance hydrogenase activity at low pH,[102] and are reduced by [NiFe]-hydrogenases faster than other cytochromes present in the periplasmic space of SRB.[77,81,152,153] Of particular bioremediation significance is the identification of the hydrogenase/cytochrome c_3 system as the physiological enzymatic system responsible for reductive precipitation of uranium and chromium leachates in contaminated ground waters.[154,155] Interaction with hydrogenase is favored in the oxidized state, and interaction with the electron-accepting multiheme cytochromes is favored in the reduced state of cytochrome c_3, enhancing directionality in electron transfer within the redox chain.[156]

d. *Structural studies*

The first three-dimensional structure of a TpI-c_3 to be determined was that from *D. vulgaris* Miyazaki F, shown in Figure 13 and published in 1984 by Higuchi *et al.*;[157] this structure was followed by those of the TpI-c_3 from *D. vulgaris* Hildenborough[158,159] and *D. norvegicum*,[160] establishing the "cytochrome c_3 fold" as a fundamental structural motif, where a single polypeptide chain is wrapped around a compact core of four non-parallel heme groups, which are exposed to solvent.

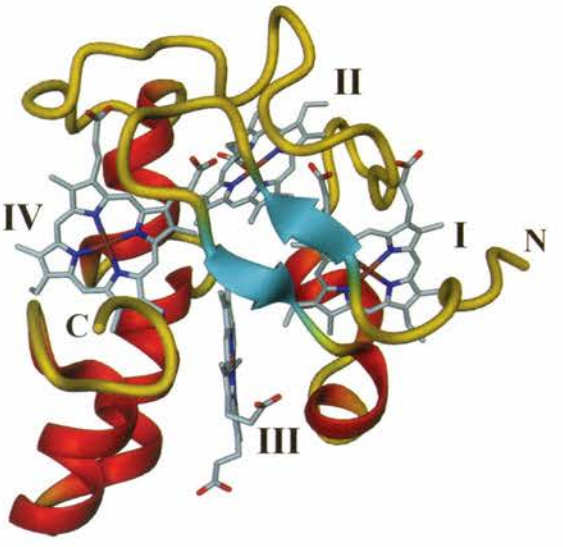

Figure 13. Three-dimensional structure of type I cytochrome c_3 from *D. vulgaris* Miyazaki F (PDB 2cdv, Ref. 157). The protein chain is represented as ribbons highlighting the secondary structure elements: the α-helices are colored red and the β-strands are shown in cyan. The heme groups are represented as sticks, with atom colors blue for nitrogen, red for oxygen, light cyan for carbon and brown for iron. The roman numerals indicate the heme groups in the order in which they are bound to the protein chain. Figure prepared with DINO.[91]

Table 5. Published structures of tetraheme cytochromes c_3 from SRB up to 2011.

PDB id	Year	Method	Resolution (Å)	Ref.	Remarks
D. baculatum					
1w7o	2004	X-ray diffraction	1.81	104	Type I
D. norvegicum (formerly known as *D. desulfuricans* Norway 4)					
2cy3	1994	X-ray diffraction	1.70	160	Type I
D. africanus					
3cao	1999	X-ray diffraction	1.60	161	Type II, oxidized
3car	1999	X-ray diffraction	1.90	161	Type II, reduced
2bq4	2005	X-ray diffraction	1.68	123	Type I
D. desulfuricans ATCC 27774					
3cyr	1997	X-ray diffraction	1.60	162	Type I
1gm4	2001	X-ray diffraction	2.05	129	Type I, oxidized
1gmb	2001	X-ray diffraction	2.00	129	Type I, reduced
1upd	2003	X-ray diffraction	1.40	163	Type I, oxidized
1up9	2003	X-ray diffraction	1.35	163	Type I, reduced
2kmy	2010	solution NMR	—	121	Type I, oxidized
2ksu	2010	solution NMR	—	121	Type I, reduced
D. desulfuricans Essex 6					
1i77	2001	X-ray diffraction	1.95	164	Type I
D. alaskensis G20 (formerly known as *D. desulfuricans* G20)					
2a3m	2006	X-ray diffraction	1.50	165	Type I, oxidized
2a3p	2006	X-ray diffraction	2.30	165	Type I, reduced
D. gigas					
1wad	1996	X-ray diffraction	1.80	166	Type I
1qn1	2000	solution NMR	—	119	Type I, oxidized
1qn0	2000	solution NMR	—	119	Type I, reduced
D. vulgaris Hildenborough					
2cym	1991	X-ray diffraction	2.00	159	Type I
2cth	1997	X-ray diffraction	1.67	162	Type I
2a2i	1998	solution NMR	—	120	Type I
1mdv	1999	X-ray diffraction	2.30	144	Type I, F20L mutant
2bpn	2006	solution NMR	—	145	Type I, oxidized
—	2006	solution NMR	—	145	Type I, K45Q mutant
D. vulgaris Miyazaki F					
2cdv	1984	X-ray diffraction	1,80	157	Type I
1it1	2002	Solution NMR	—	122	Type I, reduced
1j0o	2003	X-ray diffraction	1.15	167	Type I, oxidized
1j0p	2003	X-ray diffraction	0.91	167	Type I, oxidized, Y45L mutant
2ewi	2006	X-ray diffraction	1.00	168	Type I, oxidized, F20Y mutant
2ewu	2006	X-ray diffraction	1.10	168	Type I, oxidized, F20H mutant
1wr5	2003	X-ray diffraction	1.40	169	Type I, oxidized, E41K mutant
2ffn	2006	X-ray diffraction	1.80	169	Type I, oxidized, E41Q mutant
2ewk	2008	X-ray diffraction	1.00	170	Type I, oxidized, T24V mutant
2yxc	2008	X-ray diffraction	1.50	170	Type I, oxidized, H25M mutant
2yyw	2008	X-ray diffraction	1.33	168	Type I, oxidized, F20M mutant
2yyx	2008	X-ray diffraction	1.00	168	Type I, oxidized, Y65A mutant
2z47	2008	X-ray diffraction	1.60	168	Type I, oxidized, Y66L mutant

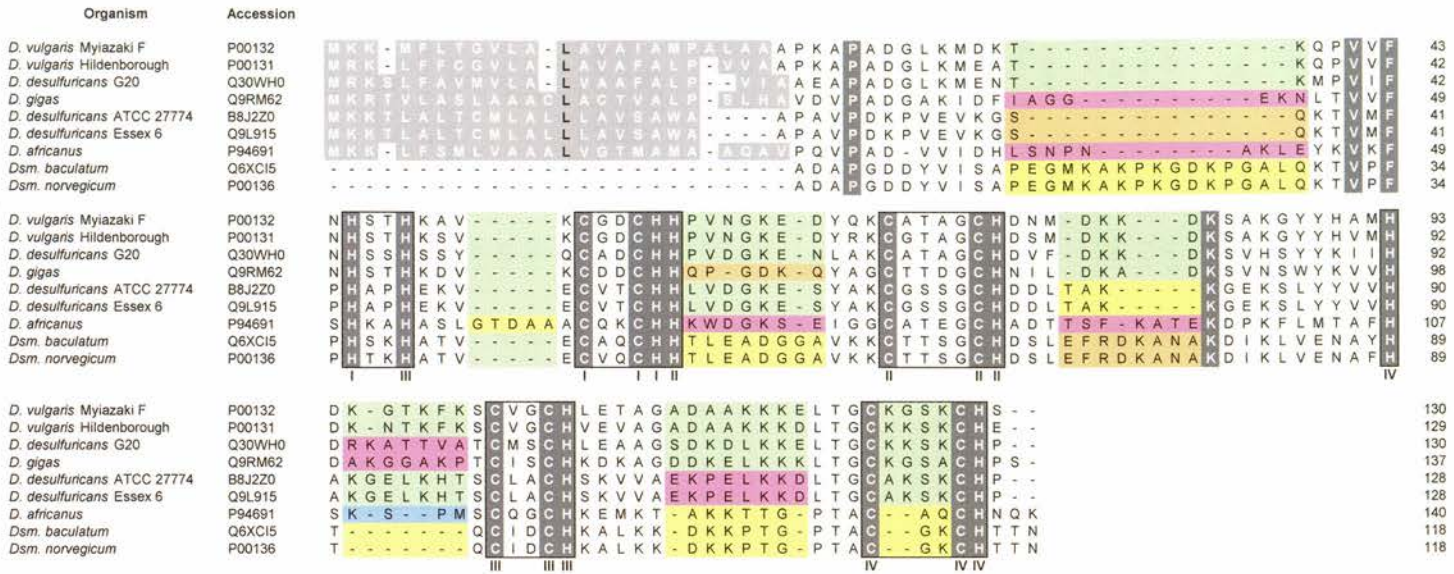

Figure 14. Amino acid sequence alignment of the TpI-c_3 of known structures (this work). Conserved residues are highlighted in dark grey boxes and the signal peptides are highlighted in light gray boxes. Numbering includes the signal peptides, when available. UniProt accession codes are also listed. For *D. norvegicum* and *D. baculatum* proteins only the sequence of the mature protein is known. The initial sequence alignment was carried out with CLUSTAL 2.1 at UniProt (http://www.uniprot.org/). The results were subsequently refined by superposition of the 3D structures of the cytochromes in COOT[171] using the Secondary Structure Matching (SSM) algorithm.[172] The variable regions are highlighted in color. Cytochromes c_3 of similar structure in a given variable region are highlighted in the same color. The Roman numerals indicate to which heme group the labeled residues are bound.

Many structures of cytochromes c_3 from SRB have been determined since, by X-ray crystallography and solution NMR, of proteins in the oxidized and reduced states as well as of site-directed mutants. A summary of the structures known up to 2011 is presented in Table 5 and an amino acid sequence alignment of the TpI-c_3 of known structures is shown in Figure 14.

In spite of a local high sequence similarity in more closely related organisms (e.g., *D. vulgaris* strains Miyazaki F and Hildenborough) the primary sequence similarity is rather low, and the family of cytochromes c_3 actually provides a striking example of how the overall three-dimensional protein structure is conserved, despite a low amino acid identity. Indeed, apart from the cysteine and histidine residues that bind the heme groups, only four more residues, Pro24, Val41, Phe43 and Lys83 (in *D. vulgaris* Miyazaki F numbering, including the signal peptide) are strictly conserved outside the signal peptide in the nine sequences aligned. An increasing divergence in sequence similarity is also reflected in larger differences at the atomic level, as illustrated in Table 6. The cytochrome c_3 fold thus appears to be largely determined by the need to accommodate four heme groups within a compact and globular protein structure, in which the heme-binding residues play a major role.

Table 6. Summary of the SSM results for the tetraheme cytochromes c_3 from SRB.

Organism	PDB	Ref.	1j0o	2cth	1wad	2a3m	1i77	1upd	2bq4	1w7o	2cy3	3cao
DvMF	1j0o	167	—	0.58	0.81	0.96	1.07	1.14	1.57	1.75	1.75	1.92
DvH	2cth	162	88	—	0.98	1.05	1.07	1.18	1.61	1.29	1.38	1.91
Dg	1wad	166	53	51	—	1.13	1.21	1.23	1.56	1.86	1.59	2.11
DaG20	2a3m	165	64	63	53	—	1.23	1.27	2.03	1.64	1.64	2.54
DdE6	1i77	164	43	47	40	43	—	0.54	2.01	1.78	1.80	4.98
Dd27k	1upd	163	42	47	42	43	82	—	2.04	1.80	1.73	3.40
Da-I	2bq4	123	40	38	34	31	34	33	—	1.96	2.08	2.09
Db	1w7o	104	35	40	38	33	41	37	39	—	0.36	2.35
Dn	2cy3	160	35	39	38	35	41	37	40	97	—	2.34
Da-II	3cao	161	32	33	29	25	14	17	29	35	32	—

The PDB coordinates representing each cytochrome c_3 are those from the highest resolution crystal structure available of the oxidized form. If the structure contained more than one chain, chain A was chosen. The SSM calculations were performed with the PDBfold server at the European Bioinformatics Institute (http://www.pdbe.org/fold). Abbreviations used are: DvMF — *D. vulgaris* Miyazaki F; DvH — *D. vulgaris* Hildenborough; Dg — *D. gigas*; DaG20 — *D. alaskensis* G20; DdE6 — *D. desulfuricans* Essex 6; Dd27k — *D. desulfuricans* ATCC 27774; Da-I — *D. africanus* Type I; Db — *D. baculatum*; Dn — *D. norvegicum*; Da-II — *D. africanus* Type II. The top half of the table lists the root mean square deviations in Å, calculated between C^{α} atoms of matched residues for the best 3D superposition of the query and target structures. The bottom half of the table shows the % amino acid sequence identity, calculated after 3D structural alignment as the fraction of pairs of identical residues among all aligned. The color highlights represent ranges of Q-score values, a complex function describing the "quality of alignment" (http://www.ebi.ac.uk/msd-srv/ssm/rl_qscore.html):

Q-score ≥ 0.7 0.7 ≥ Q-score ≥ 0.5 0.5 ≥ Q-score ≥ 0.3 Q-score < 0.3

An initial long variable loop containing a short two-stranded antiparallel β-sheet is followed by a α-helical turn containing the two histidine residues that axially bind hemes I and III, completing the coordination sphere of their iron atoms. In *D. gigas* and *D. africanus* cytochromes structures, a Ca(II) ion is found with octahedral coordination, supplied by residues in this loop as well as by both propionate groups of heme IV. Next, another variable loop is followed by a α-helical turn containing the CXXCH binding motif of heme I, immediately followed by another histidine which completes the axial coordination of heme II. A third variable loop is continued by a β-turn containing the CXXXXCH binding region of heme II. After a fourth variable loop, there is a long α-helical region, which in all but the *D. baculatum* and *D. norvegicum* structures is divided into two shorter segments by an insertion loop. The first segment includes the CXXCH linkage of heme III, while the second axial histidine residue coordinating heme IV is located at the beginning of the second segment. Finally, in all structures except those from *D. africanus*, *D. baculatum* and *D. norvegicum* cytochromes, the C-terminal region contains a short α-helical region followed by a ω-loop formed by the CXXXXCH binding motif of heme IV, just before the C-terminus of the protein chain. In *D. africanus*, *D. baculatum* and *D. norvegicum* cytochromes this short α-helix is replaced by a loop which packs against heme III, lowering its solvent accessibility, followed by a α-helical turn containing the CXXCH binding motif of heme IV. These structural differences are illustrated in Figures 14 and 15.

The first determined three-dimensional structure of a TpII-c_3 was that from *D. africanus*.[161] Homologs of this cytochrome have been characterized in several other *Desulfovibrio* sp. such as *D. vulgaris* Hildenborough and *D. alaskensis* G20, but no other crystal structures have been determined up to 2011. A comparison between the 3D structures of the *D. africanus* TpI-c_3 and TpII-c_3 (see Figure 16) shows that both heme arrangement and overall protein fold are very similar. However, the structure of the TpII-c_3 presents several differences: the initial short two-stranded anti-parallel β-sheet is absent, the first short α-helix containing the two histidine residues is slightly longer, all heme-binding motifs are of the form CXXCH and occur in α-helical turns, the third and fourth variable loops surrounding heme II are more pronounced, and the long α-helix is unbroken. In addition, the TpII-c_3 molecule lacks the positively charged surface region around heme IV, typical of TpI-c_3, and instead displays a negatively charged surface region surrounding a more exposed heme I. Indeed, the TpII-c_3 is efficiently reduced by the pair hydrogenase/TpI-c_3[101,153] and heteronuclear ^{1}H–^{15}N multidimensional NMR spectroscopy combined with docking experiments established that in *D. africanus* and *D. vulgaris* Hildenborough, heme IV of the TpI-c_3 interacts with heme I of the TpII-c_3.[123]

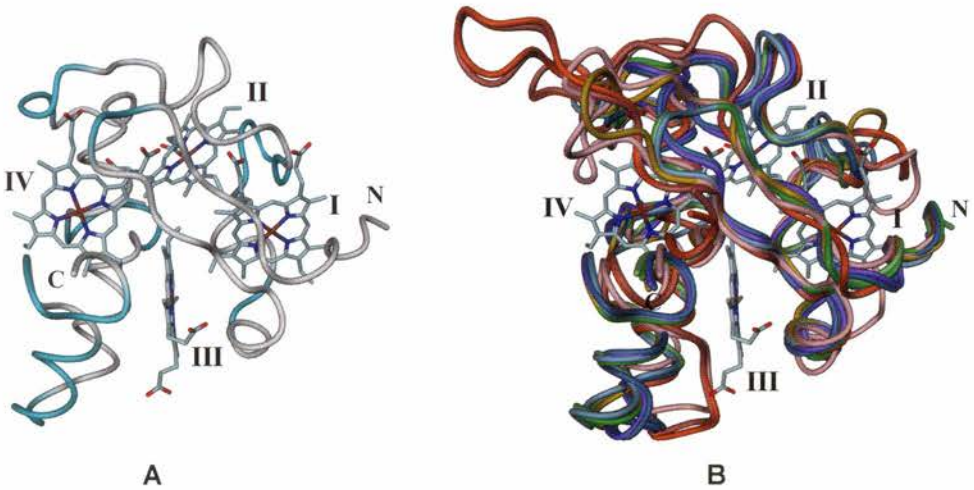

Figure 15. Variations in the cytochrome c_3 fold. (A) Location of the variable regions in the cytochrome c_3 fold, highlighted in cyan in the structure of *D. vulgaris* Miyazaki F TpI-c_3 (PDB 1j0o, Ref. 167). (B) C^{α} tube representation of the superposed nine known TpI-c_3 structures from SRB. *D. vulgaris* Miyazaki F — light green, *D. vulgaris* Hildenborough (PDB 2cth, Ref. 162) — lime green, *D. gigas* (PDB 1wad, Ref. 166) — goldenrod, *D. alaskensis* G20 (PDB 2a3m, Ref. 165) — sky blue, *D. desulfuricans* ATCC 27774 (PDB 1upd, Ref. 163) — steel blue, *D. desulfuricans* Essex 6 (PDB 1i77, Ref. 164) — light slate blue, *D. africanus* (PDB 2bq4, Ref. 123) — light pink, *D. baculatum* (PDB 1w7o, Ref. 104) — Indian red, *D. norvegicum* (PDB 2cy3, Ref. 160) — orange red. For clarity, only the *D. vulgaris* Miyazaki F heme groups are represented as sticks, with atom colors blue for nitrogen, red for oxygen, light cyan for carbon and brown for iron. The roman numerals indicate the heme groups in the order in which they are bound to the protein chain. Figure prepared with DINO.[91]

The comparison of the 3D structures of *D. vulgaris* Hildenborough TpI-c_3 at 2 Å resolution and *D. vulgaris* Miyazaki F TpI-c_3 at 1.8 Å resolution showed both structures to be very similar, and led Morimoto *et al.*[159] to conclude that the 14 different amino acids of these cytochromes had no structural implications, since all the amino acid replacements involving bulky side chains in either *D. vulgaris* Hildenborough or *D. vulgaris* Miyazaki F, potentially capable of causing significant structural changes, were located on the protein surface. Messias *et al.*[120] determined the structure of reduced *D. vulgaris* Hildenborough TpI-c_3 in solution using 2D ^{1}H-NMR, and its comparison with the crystal structure of the oxidized state at 1.67 Å resolution[162] revealed a localized displacement of the backbone of residues Arg44-Lys45-Cys46-Gly47 (*D. vulgaris* Hildenborough TpI-c_3 numbering for the mature protein) towards the propionate edge of heme I, with a concomitant disruption of the salt bridge between Lys45 and propionate 17 of heme I (propionate A in the PDB coordinates), and of the hydrogen bond between the amide proton of Cys46 with propionate 13 of heme I (propionate D in the PDB coordinates). This region includes one of the

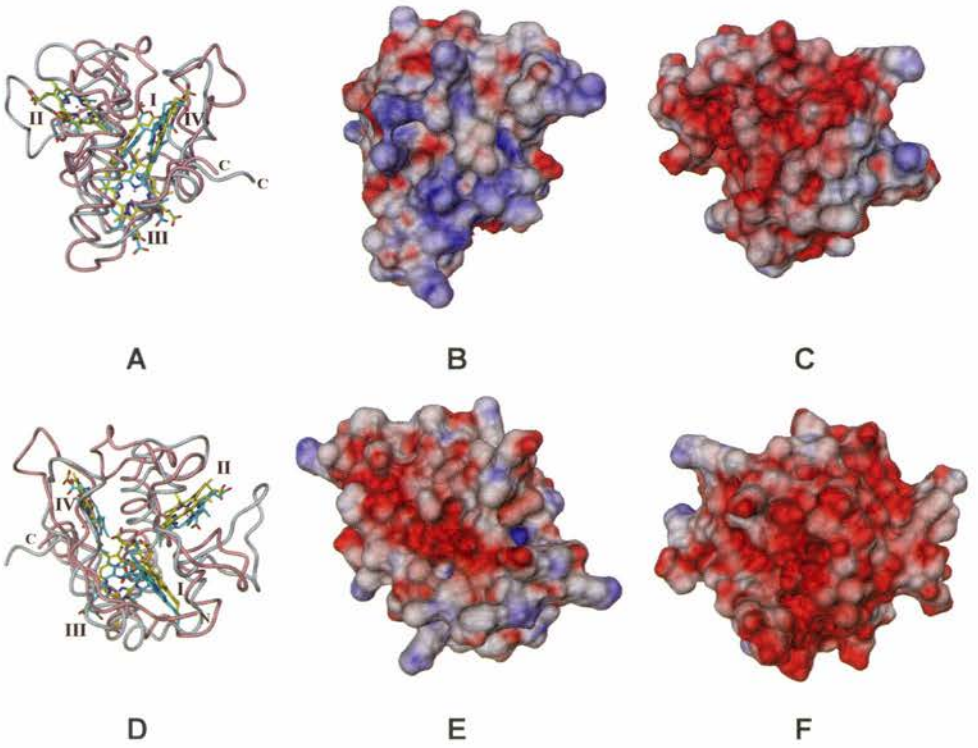

Figure 16. TpI-c_3 *vs.* TpII-c_3 cytochrome c_3. (A) and (D) Superposition of the 3D structures of the Type I (PDB 2bq4, Ref. 123) and Type II (PDB 3cao, Ref. 163) cytochromes c_3 from *D. africanus* using the SSM[172] algorithm in COOT.[171] The protein chains are represented as C^{α} tubes, colored light pink and light cyan for Types I and II cytochromes c_3, respectively; the heme groups are represented as sticks, with atom colors blue for nitrogen and red for oxygen in both structures, yellow for carbon and brown for iron in TpI-c_3, and cyan for carbon and salmon for iron in TpII-c_3. The roman numerals indicate the heme groups in the order in which they are bound to the protein chain. In (A) the view is down the plane of heme IV and in (B) it is down the plane of heme I. (B,C,E,F): electrostatic potential mapped at the molecular surface of the Type I (B,E) and Type II (C,F) cytochromes c_3. In (B) and (C) the view is the same as in (A), and in (E) and (F) it is the same as in (D). The range of potentials shown spans from −15 (red) to +15 kT/e (blue) units. The molecular surface is represented as semitransparent and was calculated with MSMS[173] using atomic radii from PDB2PQR[174] and a probe radius of 1.4 Å. The atomic charges were calculated with PDB2PQR using the CHARMM22[175] all-atom force field for the protein and heme group atoms. The electrostatic potentials were calculated with MEAD[176], assuming an ionic strength of 0.1 M, T = 300 K, $\varepsilon_{int} = 4$, $\varepsilon_{ext} = 80$ and a solvent probe radius of 1.4 Å. Figure prepared with DINO.[91]

cysteine residues binding heme II, and these observations led to the suggestion that the region comprising Lys45, Cys46, heme II and both propionate groups of heme I is the basic structural motif behind the coupled two-proton transfer step observed in the redox-Bohr cooperativity for this cytochrome,[177] as well as of the functional network of cooperativities governing the proposed concerted transfer of two electrons

and two protons from its physiological partner hydrogenase.[102] These conclusions were confirmed in 2006 by Turner and coworkers[145] that reported the structures of the oxidized forms of the wild-type and K45Q mutant of *D. vulgaris* Hildenborough TpI-c_3 determined in solution by 2D ^{1}H-NMR spectroscopy. El Antak *et al.*[124] studied the electron-transfer complex between *D. vulgaris* Hildenborough TpI-c_3 and [FeFe]-hydrogenase by heteronuclear NMR combined with soft-docking calculations using the 3D structures of *D. desulfuricans* ATCC 7757 [FeFe]-hydrogenase (identical to the *D. vulgaris* Hildenborough enzyme)[92] and *D. vulgaris* Hildenborough TpI-c_3,[162] having concluded that *D. vulgaris* Hildenborough TpI-c_3 accepts electrons from [FeFe]-hydrogenase through heme IV.

Brennan *et al.*[119] determined the structures of oxidized and reduced *D. gigas* TpI-c_3 in solution by 2D ^{1}H-NMR at pH conditions below the onset of redox-Bohr effects (pH 5.1 and 7.3 for the oxidized and reduced states, respectively) and confirmed that the positive redox cooperativity measured between hemes II and III could be related to redox-linked conformational changes in residues Lys80 and Lys90, and that propionate 13 of heme I was the major contributor to the redox-Bohr effect observed in this cytochrome. A similar role for this propionate group in TpI-c_3 from *D. baculatum* and *D. norvegicum* was established by Correia *et al.*,[104] based on the respective crystal structures[160] in combination with thermodynamic and kinetic studies.

Louro *et al.*[129] studied *D. desulfuricans* ATCC 27774 TpI-c_3 by X-ray crystallography and theoretical methods. Using the crystal structures of the oxidized and reduced forms of this cytochrome at pH 7.6 and 2 Å resolution, and the previously crystal structure determined at pH 4.0 and 1.67 Å,[162] these authors identified a redox-linked conformation change of Glu61 to be strongly related to the redox cooperativity observed between hemes I and II.[116] In addition, one of the two previously characterized redox-linked protonation sites[116] was recognized as arising from the propionate groups of heme I while the second was assigned to the combined effect of propionate 13 of heme IV and His76. This work was continued by Bento *et al.*[178] using the crystal structures of the oxidized and reduced protein refined to higher resolution (1.40 Å and 1.35 Å resolution, respectively) in combination with more advanced theoretical methods. Their results showed the redox-linked structural changes in *D. desulfuricans* ATCC 27774 TpI-c_3 to be almost entirely located in protein regions surrounding hemes I and II, whereas those around hemes III and IV were mainly invariant. The key role of Glu61 in the redox cooperativity between hemes I and II was confirmed, but minor contributions to this effect from His76 and the propionate 13 of heme II were also identified. His76, together with the propionate 17 of heme I and the propionate 13 of heme IV were identified as the main contributors to the capture, upon reduction, of two protons by this cytochrome. These groups changed their protonation state

by more than 0.2 protons upon reduction, for an overall capture of 1.4 protons quantified in this work. Paixão *et al.*[121] determined the fully oxidized and reduced structures of *D. desulfuricans* ATCC 27774 TpI-c_3 by NMR in solution at pH values below the onset of redox-Bohr effects in this cytochrome (4.2 and 6.4 respectively) to study the redox-linked conformational changes without the influence of pH-related structural modifications. Their results showed significant differences between the structures of the oxidized and reduced protein, in the segments comprising residues Val11–Phe20, Gly47–Ser63 and Arg71–Lys75. Some of these differences were also reported by Bento *et al.*,[178] but it is likely that these motions were somewhat restricted in the crystal structure of the reduced cytochrome due to crystal packing effects. The NMR structural data also supported the role of Glu61 and propionate 13 of heme II in the positive cooperativity between hemes I and II. The interaction between *D. desulfuricans* ATCC 27774 TpI-c_3 and its physiological partner [NiFe]-hydrogenase was assessed using molecular modelling methods by Matias *et al.*,[179] and, similarly to *D. vulgaris* Hildenborough, the lowest energy docking solutions found corresponded to an interaction between the distal $[4Fe4S]^{2+/1+}$ cluster of hydrogenase with the heme IV region of *D. desulfuricans* ATCC 27774 TpI-c_3; a second best-set of docking solutions was found to correspond to an interaction of the heme II region of the cytochrome c_3 with a surface region of the hydrogenase located directly above a Mg(II) ion near the [NiFe] active site. These two solutions provide structural snapshots that agree with the observed coupling of transfer of electrons and protons between these two proteins.

Harada *et al.*[122] determined the solution structure by NMR of the reduced *D. vulgaris* Miyazaki F TpI-c_3 to study the redox-coupled conformational changes between the oxidized and reduced states, and concluded that the cooperative reduction of hemes I and II is based on conformational changes in propionate 13 of heme I, the aromatic ring of Tyr43, and the interaction between His34 and His35 (*D. vulgaris* Miyazaki F TpI-c_3 numbering for the mature protein). The aromatic ring of Tyr43 is placed nearly parallel to the imidazole ring of His34 coordinating heme I, and its role was further investigated by Ozawa *et al.*[167] through the determination of the 3D structures of the Y43F and Y43L mutants of *D. vulgaris* Miyazaki F TpI-c_3 in combination with NMR spectroscopy, electrochemical, and laser flash photolysis studies. The results showed that the aromatic ring in position 43 contributes to lowering the reduction potential of heme I, and participates in the regulation of the reduction kinetics in this cytochrome. Tyr43 forms a hydrogen bond with Glu41, and Yahata *et al.*[169] assessed the role of this residue by combining NMR spectroscopy and electrochemical measurements with the 3D structure determination of the E41K and E41Q mutants of *D. vulgaris* Miyazaki F TpI-c_3, concluding that Glu41 is important to stabilize the

molecular structure in the region between hemes I and II and affects the redox properties of the cytochrome, without influencing the electron transfer kinetics from *D. vulgaris* Miyazaki F [NiFe]-hydrogenase. Following up on earlier work by Dolla *et al.*,[139] crystals of the H25M mutant were obtained by Takayama *et al.*,[170] and the determination of its 3D structure showed the structural changes introduced by the mutation to be local, with Met25 replacing His25 as the sixth ligand of heme III. These studies were continued by Takyama *et al.*[168] who determined the 3D structures of five mutants of *D. vulgaris* Miyazaki F TpI-c_3 involving replacement of conserved non-heme coordinated aromatic residues: F20H, F20M, F20Y, Y65A and Y66L (numbering for the mature protein). These authors combined their X-ray crystallographic work with measurements by NMR spectroscopy of the C2 proton chemical shifts (i.e., the hydrogen atom bonded to atom $C^{\varepsilon 1}$ in the PDB coordinates) of the heme-coordinated histidines that were induced by the mutations, and suggested that although the structural changes introduced by the mutations were local, all these conserved aromatic residues contributed to modulate the reduction potentials displayed by this cytochrome c_3, and that the most pronounced effect was observed for the mutations involving Phe20. The aromatic ring of this conserved residue is almost parallel to the porphyrin ring of heme I and nearly perpendicular to the porphyrin ring of heme III. It is also almost perpendicular to His22, one of the axial ligands of heme I, and approximately parallel to His25, one of the axial ligands of heme III. Interestingly, these two histidine residues are located in a conserved HXXH sequence motif found not only in all Type I and Type II tetraheme cytochromes c_3, but also in cytochromes c_3 with higher heme content that contain tetraheme structural motifs (to be described in the Sections IV.C.2–4). The results obtained by Takyama *et al.*[168] showed that in *D. vulgaris* Miyazaki F TpI-c_3 Phe20 is involved in π–π interactions with the imidazole ring of His25 and the porphyrin ring of heme I.

2. *Octaheme Cytochrome* c_3

The so-called octaheme cytochromes c_3 are actually proteins made of two identical tetraheme cytochrome c_3 sub-units and as such they are also often referred to as di-tetraheme cyrochromes c_3. Octaheme cytochromes c_3 have been identified in *D. gigas*,[180] *D. norvegicum*[181] and *D. africanus*[109] but a full amino acid residue sequence has only been determined for the proteins from *D. gigas* and *D. norvegicum*. These two cytochromes show no significant sequence similarity either between themselves or with the tetraheme cytochromes c_3 found in those organisms, as illustrated in Figure 17. Besides the heme-binding residues, only

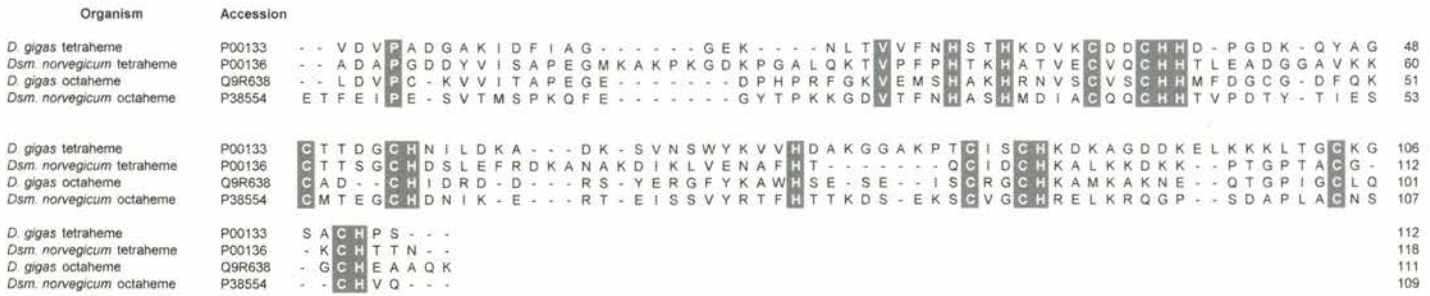

Figure 17. Amino acid sequence alignment of the octaheme cyrochromes c_3 of known sequence and structure with the TpI-c_3 from the same organisms (this work). The sequences of the mature proteins are represented as retrieved from the UniProt database (http://www.uniprot.org/) under the listed accession codes. Conserved residues are highlighted in dark gray boxes. The initial sequence alignment was carried out with CLUSTAL 2.1 at UniProt (http://www.uniprot.org/). The results were subsequently refined by superposition of the 3D structures of the cytochromes using the SSM[172] algorithm in COOT.[171]

two residues are conserved, and this makes the identification of other octaheme cyrochromes c_3 from sequence databases rather difficult. It is likely that octaheme cyrochromes c_3 occur in other SRB but their isolation and characterization will be required in order for their presence to be established.

All three octaheme cytochromes c_3 have been shown to accept electrons from hydrogenases,[109,180,181] but their function remains to be established. The octaheme cytochrome c_3 from *D. norvegicum* can use the corresponding TpI-c_3 as mediator for electron transfer, which is in agreement with the proposed role for TpI-c_3 as the primary electron acceptor from hydrogenases.[152]

The 3D structures of the octaheme cytochromes c_3 from *D. norvegicum* (native and Y73E mutant)[182,183] and *D. gigas*[184] have been determined by X-ray crystallography and are represented in Figure 18. Both cytochromes are homodimers of tetraheme subunits with the typical cytochrome c_3 fold, with an interface formed by the protein regions surrounding both hemes I, which adopt an almost parallel arrangement. The N-terminus of one monomer interacts with a protein region of the other monomer a few residues downstream of the heme I binding motif. In addition to this interaction, in *D. gigas* the two monomers are cross-linked by two disulfide bridges between Cys5 and Cys46 residues from each monomer, which correspond to Glu7 and Tyr49 in the *D. norvegicum* octaheme cytochrome c_3. In contrast with most tetraheme cytochromes c_3 already described, the second heme binding motif in *D. gigas* octaheme cytochrome is of the form CXXCH and the fourth is of the unusual CXXXCH type, with three residues inserted between the cysteines that bind the heme group. In the octaheme cytochrome c_3 from *D. norvegicum*, the last heme-binding motif is of the

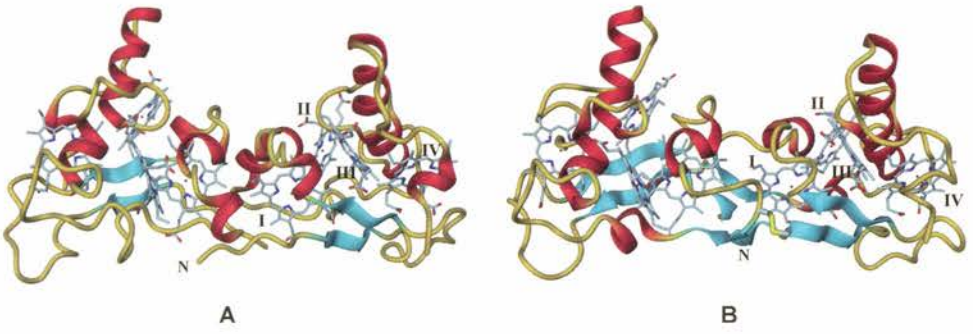

Figure 18. Three-dimensional structures of octaheme cytochromes c_3 from (A) *D. norvegicum* (PDB 1czj, Ref. 182) and (B) *D. gigas* (PDB 1gyo, Ref. 184). The protein chains are represented as ribbons highlighting the secondary structure elements: the α-helices are colored red and the β-strands are shown in cyan. The heme groups are represented as sticks, with atom colors blue for nitrogen, red for oxygen, light cyan for carbon and brown for iron. The roman numerals indicate the heme groups in the order in which they are bound to the protein chain of one of the monomers. Figure prepared with DINO.[91]

form CXXCH, as found in the TpI-c_3 from *D. africanus*, *D. norvegicum* and *D. baculatum*.

The amino acid residue Tyr73 in the *D. norvegicum* octaheme cytochrome c_3 is also structurally conserved in the *D. gigas* homolog, as well as in the *D. vulgaris* Miyazaki F, *D. vulgaris* Hildenborough and *D. alaskensis* G20 TpI-c_3, with its aromatic ring oriented almost parallel to the imidazole ring of the second axial histidine ligand coordinating the iron atom in heme IV. Its replacement by a glutamic acid in the *D. norvegicum* protein had the effect of destabilizing the complex formed between the octaheme cytochrome c_3 and [NiFeSe]-hydrogenase, but without preventing electron transfer to take place.[183] This effect was attributed to the conformational changes observed in the side chains of the neighboring residues Lys22 and Arg66 which become involved in interactions with the mutated residue. The physiological significance of these experiments remains to be established since, as mentioned above, the electron transfer between the hydrogenases and the other multiheme cytochromes is mediated by the TpI-c_3.

3. *Nine-heme Cytochrome c_3*

A nine-heme cytochrome c_3 (also known as nonaheme cytochrome c_3 or NhcA, see Section VI) was first discovered in *D. desulfuricans* ATCC 27774,[94] with higher expression in sulfate- than in nitrate-grown cells.[185] It was initially believed to be a dodecaheme cytochrome, and the true heme content was revealed by the determination of its 3D structure by Matias *et al.*[186] using the anomalous dispersion properties of the heme iron atoms; the complete primary structure of this cytochrome was subsequently determined by Saraiva *et al.*[187] Like all *c*-type cytochromes, the nine-heme cytochrome c_3 contains a signal peptide, an indication of its periplasmic location in the cell, and the mature protein is 296 residues in length. The structure of this cytochrome (Figure 19) contains two tetraheme cytochrome c_3 domains connected by a linker region, which has an isolated heme group. Surprisingly, this isolated heme is heme IV (considering the order in which the hemes are bound to the protein chain) and not heme V, meaning that heme IV is intercalated in the first tetraheme cytochrome c_3 domain. The histidine residue that completes the octahedral coordination of the isolated heme IV is located in the second tetraheme cytochrome c_3 domain. The location of heme IV between the two tetraheme cytochrome c_3 domains very likely allows interdomain electron transfer. The linker region is constituted by two consecutive α-helices followed by a segment of extended chain, and might allow some interdomain flexibility. However, this flexibility should be limited by the rigidity conferred by the presence of the heme group, coordinated by residues from both tetraheme cytochrome c_3 domains. Contrary to TpI-c_3, all heme-binding motifs are of the form CXXCH,

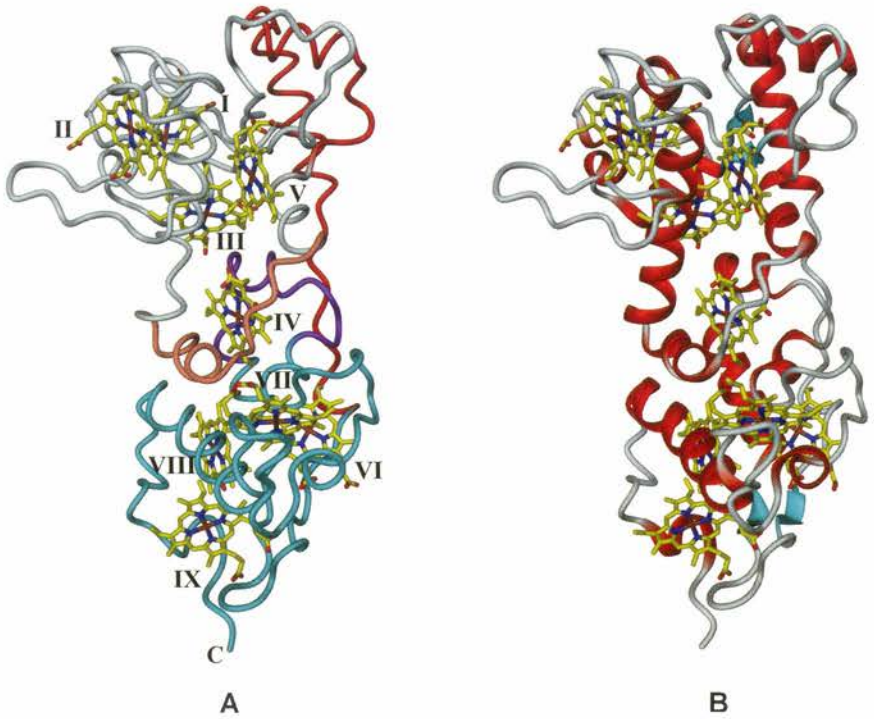

Figure 19. Three-dimensional structures of the nine-heme cytochromes c_3 from (A) *D. desulfuricans* ATCC 27774 (PDB 1h9c, Ref. 186) and (B) *D. desulfuricans* Essex 6 (PDB 1duw, Ref. 189). In (A) the protein chain is represented as a C^{α} tube, colored according to the protein region it belongs to: light cyan and cyan for the tetraheme cytochrome c_3 regions of the N-terminal and C-terminal domains, pink and purple respectively for the N-terminal and C-terminal domain insertions containing the binding regions of the isolated heme group, red for the linker region between the two domains. In (B) the protein chain is represented as ribbons highlighting the secondary structure elements: the α-helices are colored red and the β-strands are shown in cyan. In both panels the heme groups are represented as sticks, with atom colors blue for nitrogen, red for oxygen, yellow for carbon and brown for iron. The roman numerals in (A) indicate the heme groups in the order in which they are bound to the protein chain. Figure prepared with DINO.[91]

located in short α-helices. The modular structure of this cytochrome also suggests different roles for the two domains.

By amino acid sequence comparison, a striking similarity was found between the nine-heme cytochrome c_3 from *D. desulfuricans* ATCC 27774 and the C-terminal region of the sixteen-heme high-molecular weight cytochrome (HmcA) from *D. vulgaris* Hildenborough (Section IV.C.4), leading to the addition of the nine-heme cytochrome c_3 to the Hmc family and raising the possibility of its inclusion in a transmembrane electron transfer complex.[186] Indeed, in 2001 this cytochrome was identified as NhcA, the first of four subunits of the Nhc complex,[185] described in Section VI.B. In addition, kinetic experiments showed that, similarly to HmcA

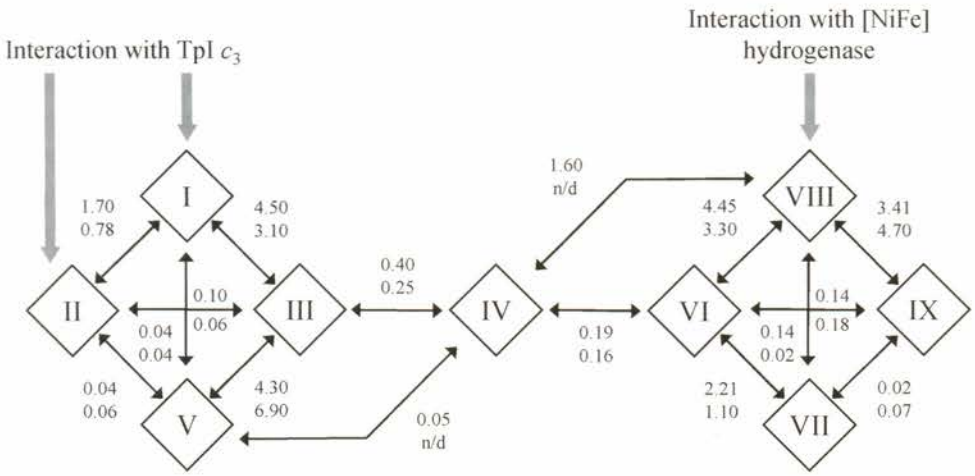

Figure 20. Electron transfer coupling factors (multiplied by 1,000) for the nine-heme cytochromes c_3 from *D. desulfuricans* Essex 6 (top row) and *D. desulfuricans* ATCC 27774 (bottom row). The heme groups predicted to interact with the physiological partners TpI-c_3 and [NiFe]-hydrogenase are indicated by arrows. Adapted from Refs. 188 and 189.

in *D. vulgaris* Hildenborough, in *D. desulfuricans* ATCC 27774 the nine-heme cytochrome c_3 could be reduced by the [NiFe]-hydrogenase, and that its reduction was faster in the presence of TpI-c_3.[186] The electron transfer properties of the nine-heme cytochrome c_3 and its interaction with TpI-c_3 from *D. desulfuricans* ATCC 27774 were studied by Matias *et al.*[188] using theoretical methods (Figure 20), and a specific interaction was found between heme IV of TpI-c_3 and heme I or heme II of the nine-heme cytochrome c_3. The only other known structure of a nine-heme cytochrome c_3 is that of the corresponding protein from *D. desulfuricans* Essex 6.[189] The structure is very similar to that of the *D. desulfuricans* ATCC 27774 cytochrome, but this protein exhibits a higher direct reduction rate by the [NiFe]-hydrogenase.[190] Umhau *et al.*[189] also studied the electron transfer properties of the *D. desulfuricans* Essex 6 nine-heme cytochrome c_3 by theoretical methods (Figure 20) and proposed that it can accept electrons directly from the [NiFe]-hydrogenase *via* heme VIII, followed by fast intramolecular electron transfer. A patch of positively charged residues surrounds heme VIII in the *D. desulfuricans* Essex 6 cytochrome, and can interact with the negatively charged tip of [NiFe]-hydrogenase harboring the distal iron-sulfur cluster (Figure 9). In addition, heme VIII shows the highest electronic coupling factors with other heme groups, in particular heme IV.[189] In *D. desulfuricans* ATCC 27774 the positive patch around heme VIII is less pronounced, but this heme also shows the highest coupling factors with other heme groups, although the coupling factor to heme IV was not calculated.[188] In contrast with less complex tetraheme cytochromes, experimental measurements of the heme–heme interactions for any nine-heme cytochrome are not

yet available in 2011, because of the spectral complexity that thus far has prevented the full assignment of spectral features in paramagnetic NMR spectra,[191] However, since the nine-heme cytochrome c_3 is part of a transmembrane redox complex of as yet unknown structure, the physiological relevance of a direct interaction with hydrogenase is uncertain.

Like for TpI-c_3, experimental evidence for a redox-Bohr effect was reported for the nine-heme cytochrome c_3 from *D. desulfuricans* ATCC 27774[192] and this effect was studied by Bento *et al.*[163] by analyzing the 3D structures of the oxidized and reduced forms of this cytochrome at pH 7.5 using theoretical methods. The calculations predicted a capture of 2.4 protons upon reduction, in agreement with the inclusion of two acid-base centers in the thermodynamic model used to interpret the experimental data.[192] The groups predicted to be most relevant to the redox-Bohr effect were the two propionates from hemes I and IV, propionate 17 from heme III and propionates 13 from hemes V and IX. The analysis of the calculated statistical correlation between the protonation/reduction of heme groups suggested no significant interactions between the N-terminal domain hemes I, II, III and V, and the C-terminal domain hemes VI, VII, VIII and IX, although high correlation values were determined for the heme groups in each domain. Also, the isolated heme IV was found to interact more strongly with the hemes of the N-terminal domain than with those in the C-terminal domain. These results suggested the N-terminal domain of the nine-heme cytochrome c_3 from *D. desulfuricans* ATCC 27774 (including heme IV) to be the most active region in terms of binding of protons and electrons.

Based on CD spectra, Fritz *et al.*[190] reported a redox-dependent conformational change in the nine-heme cytochrome c_3 from *D. desulfuricans* Essex 6. Due to the difficulty in crystallizing the protein in its reduced form, Bento *et al.* obtained the reduced form of the cytochrome by reducing crystals of the oxidized form with sodium dithionite.[163] Most of the observed redox-linked structural changes were found in the region of the isolated heme IV, and it is possible that in this crystal structure the extent of these structural changes may have been hindered by the crystal packing.

In addition to *D. desulfuricans* ATCC 27774 and *D. desulfuricans* Essex 6, a UniProt database search identified only two more organisms containing a nine-heme cytochrome c_3: *Desulfovibrio piger* ATCC 29098 and *Desulfovibrio* sp. 3_1_syn3. The sequence alignment is shown in Figure 21. The remaining high-scoring matches corresponded to HmcA cytochromes (see Section IV.C.4).

4. *Sixteen-heme Cytochrome c_3*

The sixteen-heme cytochrome c_3 also known as high-molecular weight cytochrome, hexadecaheme cytochrome or HmcA is, until 2011, the largest cytochrome of the class III family characterized in SRB. Higuchi *et al.* isolated,

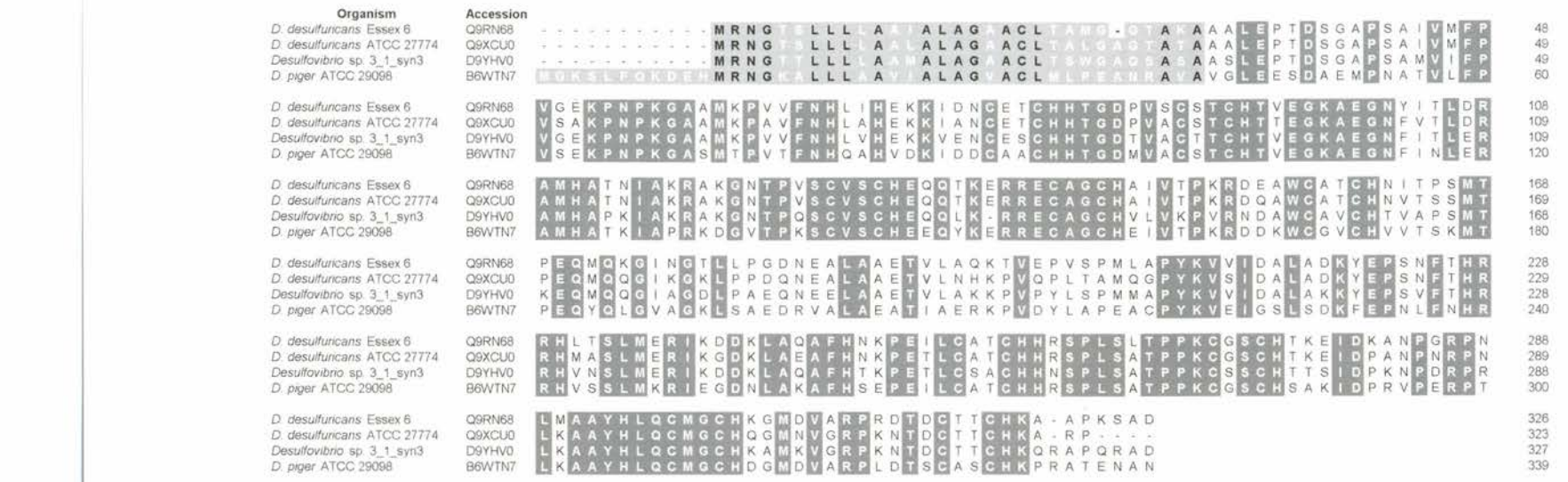

Figure 21. Amino acid sequence alignment of the known nine-heme cytochromes c_3 from *Desulfovibrio sp* (this work). The sequences were retrieved by a BLAST search of the UniProt database against the sequence of the protein from *D. desulfuricans* ATCC 27774. The percentage of identity with this sequence is 85% for *D. desulfuricans* Essex 6, 76% for *Desulfovibrio* sp. 3_1_syn3 and 65% for *D. piger* ATCC 29098. UniProt accession codes are also listed. The sequence alignment was carried out with CLUSTAL 2.1 at UniProt (http://www.uniprot.org/). The signal peptides are highlighted in light gray boxes with conserved residues displayed in black boldface. Signal peptides are known for the *D. desulfuricans* Essex 6 and *D. desulfuricans* ATCC 27774 cytochromes, and inferred in the basis of the sequence alignment for the other two proteins. Conserved residues in the mature proteins are highlighted in dark grey boxes.

purified and crystallized HmcA from *D. vulgaris* Hildenborough,[193] and Voordouw *et al.* cloned, sequenced and expressed the respective encoding gene, and determined its heme content.[194] This cytochrome is the first of six subunits of the Hmc complex,[195] which will be described in Section VI.B. From the amino acid sequence Voordouw *et al.*[194] proposed that one of the heme groups would lack its second axial ligand, and also predicted a modular structure for HmcA, formed by four tetraheme cytochrome c_3 domains, the first of which with only three heme groups, and an isolated heme. HmcA was purified and characterized from *D. vulgaris* Miyazaki F in 1993[196] and from *D. gigas* in 1994.[197] EPR and Mössbauer spectroscopy showed that one or two heme groups in the HmcA from *D. vulgaris* Hildenborough and *D. gigas* were high-spin, an unprecedented feature in multiheme class III cytochromes.[197–199]

The three-dimensional structure of the sixteen-heme cytochrome c_3 from *D. vulgaris* Hildenborough was determined by Czjzek *et al.*,[200] Matias *et al.*[201] and Sato *et al.*,[202] confirming the modular domain structure proposed by Voordouw *et al.* In agreement with the earlier prediction by Matias *et al.*,[186] based on the high sequence similarity between the nine-heme cytochrome c_3 from *D. desulfuricans* ATCC 27774 and the C-terminal region of the HmcA from *D. vulgaris* Hildenborough, the isolated and the high-spin heme groups were identified as heme XI and heme XV respectively, instead of heme XII. This domain structure is illustrated in Figure 22. In the displayed orientation, it can be seen that the HmcA molecule is Λ-shaped: one leg is *ca.* 60 Å long and contains the first two domains, whereas the other extends for about 70 Å and includes the third and fourth domains, which are structurally very similar to the nine-heme cytochrome c_3 described in Section IV.C.3. The first domain contains only three heme groups as expected, and its structure resembles that of the tri-heme cytochrome c_7 from *Desulforomonas acetoxidans*, a sulfur-reducing bacterium,[203] in which the protein region involved in the binding of heme II in a tetraheme cytochrome c_3 has been replaced by a shorter loop. The way in which the legs are joined allows for a degree of flexibility that may facilitate its binding to the other partners in the Hmc complex. The heme arrangement in this cytochrome can therefore be succintly described as 3-4-4-1-4, and an interesting aspect is that if one looks at HmcA in the orientation given in Figure 22 a "top-to-bottom arrangement" is observed, which in the case of the first two domains contradicts what might be expected from the sequence. Thus, heme III (and not heme I) is located at the bottom of the tri-heme domain and heme I (instead of heme III) is found at the top, interacting with heme VII from the first tetraheme domain (equivalent to heme IV in tetraheme cytochrome c_3) while heme IV (equivalent to heme I) is found at the top of the domain, close to heme VIII (corresponding to heme I in the first tetraheme region of the nine-heme cytochrome c_3 domain). Sato *et al.*[202] also determined the

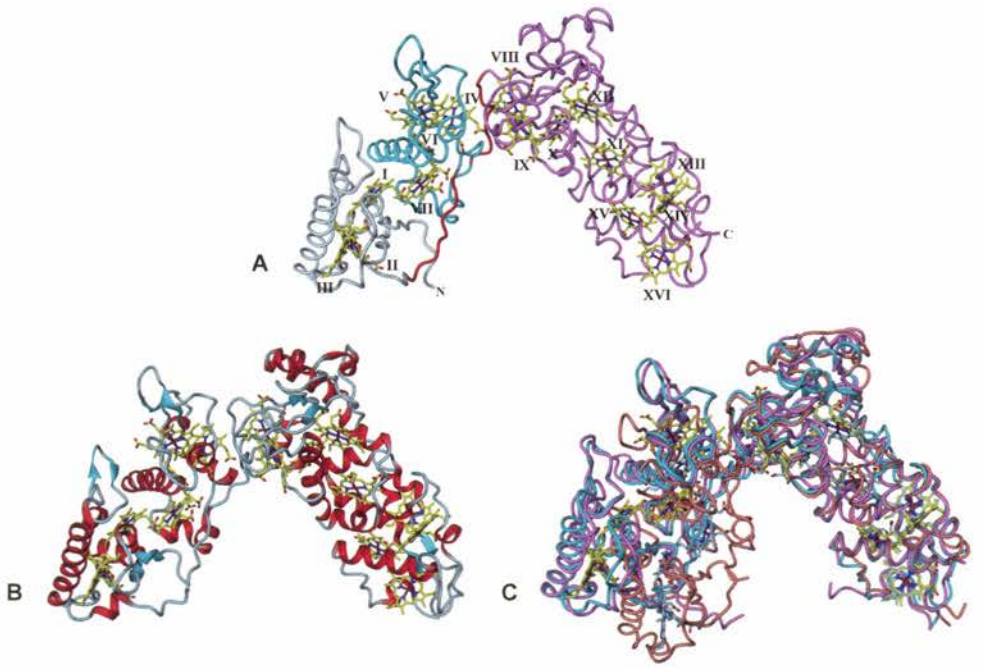

Figure 22. Known three-dimensional structures of the sixteen-heme cytochrome c_3 (HmcA). (A) C^{α} tube diagram of the HmcA from *D. vulgaris* Hildenborough (PDB 1h29, Ref. 201) colored to highlight the domain structure: the N-terminal tri-heme and tetraheme cytochrome c_3 domains are colored light blue and cyan, respectively, and the C-terminal nine-heme cytochrome c_3 domain is colored violet. The heme groups are represented as sticks, with atom colors blue for nitrogen, red for oxygen, yellow for carbon and brown for iron. The roman numerals indicate the heme groups in the order in which they are bound to the protein chain. (B) Ribbon diagram of the HmcA from *D. vulgaris* Hildenborough (PDB 2gws, Ref. 200) showing the secondary structure elements: the α-helices are colored red and the β-strands are shown in cyan. The hemes are represented as in (A). (C) C^{α} tube diagrams of the superposed HmcA structures from three different SRB: the HmcA from *D. vulgaris* Hildenborough (PDB 2cvc, Ref. 202) is colored cyan, HmcA from *D. vulgaris* Miyazaki F (PDB 2e84, Ref. 204) is colored violet and the HmcA from *D. gigas* (PDB 1z1n, Ref. 205) is colored salmon. The hemes from PDB 2cvs are represented as in (A), while the hemes from PDB 2e84 overlap with those of PDB 2cvs and are omitted for clarity. The hemes from 1z1n are shown as in (A), but with carbon atoms colored light blue. The three structures were superimposed with reference to their C-terminal nine-heme cytochrome c_3 domain to emphasize the different relative orientations of the N-terminal and C-terminal regions in the *D.gigas* protein. Figure prepared with DINO.[91]

three-dimensional structure of this cytochrome in the reduced form by exposure to synchrotron radiation, taking advantage of the known fact that intense beams of X-rays, as available at synchrotrons, can induce photoelectron reduction of metal centers in protein crystals. However, the low resolution (2.8 Å) of the diffraction data did not allow a detailed analysis of the structural differences between the oxidized and reduced molecules.

In addition to *D. vulgaris* Hildenborough, the three-dimensional structures of the HmcA from *D. gigas*[205] and *D. vulgaris* Miyazaki F[204] were also determined. These structures are very similar to that of *D. vulgaris* Hildenborough HmcA, with an identical domain structure and heme arrangement, and in both heme XV is high-spin with a five-coordinated iron atom and an isoleucine residue replacing the canonical axial histidine that usually completes the heme coordination. Nevertheless, Figure 22 shows that in *D. gigas* the angle between the legs of the Λ-shaped HmcA is shallower, which probably results from a combination of the interdomain flexibility and packing interactions in the crystal. Also, *D. gigas* HmcA contains a glycosylated asparagine residue near the tip of the Λ-shaped HmcA. Three *N*-acetyl-D-glucosamine molecules (GlcNAc) were identified by matrix-assisted laser desorption/ionization time-of-flight (MALDI-TOF) mass spectrometry, two of which were visible in the electron density maps and included in the structural model. Finally, the binding motif of heme IX is of the form CXXXCH, with three residues between the cysteines, as previously mentioned in Section IV.C.2 for heme IV in each monomer of the octaheme cytochrome c_3 from the same organism.

A BLAST search of all protein sequence databases with the *D. vulgaris* Hildenborough HmcA sequence produced a total of 17 significant hits in terms of protein length and sequence identity. Due to the protein length and number of hits the full alignment results are too extensive to be presented here and instead a summary is given in Table 7. There are two striking results that emerged from this analysis. First, not all HmcA orthologs are sixteen-heme cytochromes c_3: in *D. baculatum* DSM 4028 and *D. aespoeensis* ATCC 700646 the cytochromes contain fifteen heme binding sites, lacking respectively the heme V and the heme IX binding motifs, and in *D. desulfuricans* ND132 the corresponding gene codes for a fourteen-heme cytochrome, lacking both heme V and IX binding motifs. Secondly, a conserved isoleucine residue in the sequence alignment suggests that the heme corresponding to heme XV in *D. vulgaris* Hildenborough HmcA will be high-spin in all these organisms except the one from *Thermodesulfovibrio yellowstonii* ATCC 51303, where it is replaced by a methionine residue and therefore a low-spin heme XV with His/Met coordination is possible in this cytochrome.

By analogy with their studies on the interaction between the *D. desulfuricans* ATCC 27774 nine-heme cytochrome c_3 and its corresponding TpI-c_3, Matias *et al.*[201] suggested that the *D. vulgaris* Hildenborough HmcA interacts with TpI-c_3 *via* the surface region around heme VIII (which is equivalent to heme I in the nine-heme cytochrome c_3), whereas the concave molecular regions as well as the N-terminal and C-terminal ends may be involved in interactions with the membrane-bound proteins of the complex. On the other hand, Czjzek *et al.*[200] used a combination of NMR spectroscopy and docking calculations to derive a structural

Table 7. Summary of the BLAST and sequence alignment results for *D. vulgaris* Hildenborough sixteen-heme cytochrome c_3.

Organism[a]	UniProt Accession	Length	% Identity	Heme arrangement	Heme XV axial neighbors
D. vulgaris Hildenborough	P24092	545	—	3-4-4-1-4	His, Ile
D. vulgaris Miyazaki F	B8DR59	556	67	3-4-4-1-4	His, Ile
D. gigas[b]	n/a	530	39	3-4-4-1-4	His, Ile
Other sulfate reducing bacteria					
D. vulgaris RCH1	E3IQD4	545	100	3-4-4-1-4	His, Ile
D. vulgaris DP4	A1VG55	545	99	3-4-4-1-4	His, Ile
D. alaskensis G20	Q315E2	555	52	3-4-4-1-4	His, Ile
Desulfohalobium retbaense DSM 5692	C8X171	557	45	3-4-4-1-4	His, Ile
D. aespoeensis ATCC 700646[c]	E6VRF1	527	47	3-4-3-1-4	His, Ile
D. salexigens ATCC 14822	C6BRK0	545	44	3-4-4-1-4	His, Ile
D. baculatum DSM 4028[d]	C7LX19	514	42	3-3-4-1-4	His, Ile
Uncultured *Desulfobacterium* sp.	E1YDG0	529	40	3-4-4-1-4	His, Ile
Desulfococcus oleovorans DSM 6200	A8ZUW4	538	42	3-4-4-1-4	His, Ile
D. magneticus ATCC 700980	C4XMI3	585	41	3-4-4-1-4	His, Ile
D. fructosovorans JJ	E1JTY2	587	41	3-4-4-1-4	His, Ile
Desulfovobrio sp. FW1012B	D2L404	588	39	3-4-4-1-4	His, Ile
D. desulfuricans ND132[e]	F0JEL9	531	40	3-3-3-1-4	His, Ile
Thermodesulfobacterium sp. OPB45	F8C3E3	577	32	3-4-4-1-4	His, Ile
Thermodesulfovibrio yellowstonii ATCC 51303	B5YFP9	523	31	3-4-4-1-4	His, Met
S-Reducing Bacteria[f]					
Bilophila wadsworthia 3_1_6	E5Y9L6	588	46	3-4-4-1-4	His, Ile

[a] The top three organisms are those for which crystal structures are available.
[b] The *D. gigas* HmcA sequence is not deposited. An independent BLAST using this sequence was done to obtain its % identity with *D. vulgaris* Hildenborough Hmc.
[c] Lacks the heme IX binding motif.
[d] Lacks the heme V binding motif.
[e] Lacks both heme V and heme IX binding motifs
[f] Bacteria that reduce other sulfur compounds.

model of the interaction complex between the HmcA and TpI-c_3 from *D. vulgaris* Hildenborough, where the interaction takes place between the C-terminal heme XVI of HmcA and heme IV of TpI-c_3. These authors also suggested that the HmcA is probably attached to the membrane part of the complex *via* the region corresponding to the tip of the Λ-shape in Figure 22, which contains several hydrophobic and aromatic residues exposed to the solvent. Santos-Silva *et al.*[205] noticed in the structure of *D. gigas* HmcA a similar hydrophobic patch highly exposed to the

solvent and near the glycosylated asparagine residue. N-Glycosylation sites in eukaryotic proteins occur at asparagine residues located within one of the consensus motifs NXT or NXS.[206] GlcNAc is one of the constituents of the cytoplasmic membrane in Gram-negative cells,[207] and may act as a membrane anchor for periplasmic-facing proteins. Santos-Silva *et al.*[205] therefore suggested that the NGT glycosylation site found in *D. gigas* HmcA provides evidence of its attachment point to the membrane. Although no such N-glycosylation was observed in either *D. vulgaris* Hildenborough or *D. vulgaris* Miyazaki F HmcA structures, *D. vulgaris* Hildenborough HmcA does contain a NGT motif, also located at the top of the nine-heme cytochrome c_3 domain of HmcA but in a different solvent-exposed loop from that containing the *D. gigas* HmcA glycosylation site. *D. vulgaris* Miyazaki F HmcA also has a putative N-glycosylation site of the form NCT, but this sequence motif overlaps the heme IX binding region and is therefore unlikely to become glycosylated. A PROSITE search for N-glycosylation sites in the HmcA sequences referenced in Table 7 was carried out with the San Diego Computing Centre Biology Workbench (http://workbench.sdsc.edu) and showed that most analyzed proteins have one or more possible glycosylation sites. However, when a sequence alignment with *D. vulgaris* Hildenborough HmcA is used to identify the approximate structural location of these sites, many are found to be overlapping heme binding motifs, as well as in protein regions unlikely to be exposed to the solvent. Only in eight out of the sixteen analyzed sequences of HmcA proteins with unknown structure are these regions located in solvent-exposed regions. Six are located at the top of the nine-heme cytochrome c_3 domain, one at the top of the first tetraheme cyrochrome c_3 domain and one is found near the C-terminal region of the HmcA. However, our present knowledge of glycosylation in bacteria is still limited, and other types of glycosylation corresponding to different sequence motifs may exist.

Therefore, while the existence of a conserved glycosylation site in HmcA is at present unknown, the notion of a HmcA membrane attachment through the tops of the N- and C-terminal regions is appealing, since electrons might be captured by both ends of the molecule from either TpI-c_3 or from other as yet undiscovered periplasmic physiological partner, and then quickly transferred to the other proteins in the complex.[205] The analysis of the interaction between HmcA and TpI-c_3 in *D. vulgaris* Hildenborough by Matias *et al.*[201] conflicts with the NMR-assisted docking calculations of Czjzek *et al.*,[200] but both suffer from the difficulties arising from dealing with HmcA in its soluble form, i.e., not associated with the other complex proteins. This may lead to artefacts as it is being assumed that the TpI-c_3 is interacting with what each group of authors believes to be the most favorable region of HmcA, without knowledge of whether that region will be actually available for interaction in the integral complex. The determination of the structure of

this complex, even at low resolution (e.g., by Small Angle X-ray Scattering or Cryoelectron Microscopy) is a challenge for the future and will certainly provide important clues to settle this issue.

D. Multiheme Cytochromes — The Cytochrome *c* Nitrite Reductase NrfHA

Two other widespread cytochromes *c* in SRB are NrfA and NrfH (from the *E. coli* nomenclature of nitrite reduction with formate),[208] which form a membrane-bound complex that reduces nitrite to ammonia.[209,210] This cytochrome *c* nitrite reductase was originally believed to be constituted by a single hexaheme *c*-type cytochrome, named cytochrome c_{552},[211] and several spectroscopic studies were interpreted with this assumption.[212,213] Subsequently, it was shown that in fact the enzyme comprises two subunits,[214,215] both of which are *c*-type cytochromes. The catalytic subunit is NrfA, a pentaheme cytochrome that includes a high-spin heme for binding of nitrite,[216] and the tetraheme cytochrome NrfH is a membrane-associated protein responsible for electron transfer from menaquinol to NrfA.[217] Subsequent studies re-evaluated the spectroscopic properties taking into account this composition, and allowed the assignment of reduction potentials to individual hemes, including the NrfA high-spin catalytic heme (–80 mV) and an unusual bis-His coordinated heme with high reduction potential (+150 mV).[218] The NrfA nitrite reductase is quite widespread in bacteria,[210,219] usually in organisms that grow by nitrate or nitrite ammonification. In some organisms, e.g., *E. coli*, the system responsible for menaquinol to nitrite reduction involves different proteins.[208] The *E. coli* NrfA enzyme forms a soluble complex with its electron donor, the pentaheme cytochrome *c* NrfB, which receives electrons from the membrane proteins NrfCD that oxidize menaquinol.[220] In SRB, the ability to reduce nitrate is limited to a few organisms, whereas that of reducing nitrite is much more common in this group of bacteria,[221] which is reflected by the distribution of the *nrfHA* genes in sulfate-reducing organisms.[21] However, the NrfHA nitrite reductase is present in organisms, such as *D. vulgaris* Hildenborough, which cannot grow with nitrite as electron acceptor.[222] Nitrite is toxic to these organisms by acting as an inhibitor of sulfate reduction, and instead this enzyme is responsible for nitrite detoxification.[223,224] In *D. vulgaris* Hildenborough, nitrite leads to an upregulation of the *nrfHA* genes.[224,225] Interestingly, the NrfHA nitrite reductase is also capable of reducing sulfite. However, the fact that the catalytic site of NrfA is facing the periplasm argues against its involvement in the dissimilatory sulfate reduction process.[214,226]

The first three-dimensional structure of an NrfA was that of the protein isolated from the sulfur-reducing organism *Sulfurospirillum deleyianum*, which was

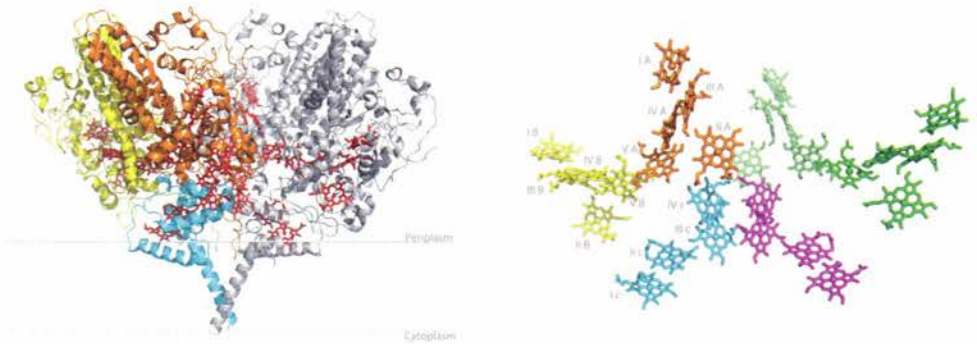

Figure 23. Three-dimensional structure of *D. vulgaris* Hildenborough cytochrome *c* nitrite reductase NrfHA (PDB 2j7a, Ref. 228). (A) Secondary structure of NrfHA ($\alpha_4\beta_2$ assembly), viewed parallel to the proposed position in the membrane (delimited by gray lines) with hemes drawn as red sticks. One NrfA dimer is shown in orange and yellow with NrfH in cyan; (B) Heme arrangement (total of 28 groups) in the same orientation as in (A). Hemes are numbered according to the order of their binding motifs in the protein chain. Hemes bound to NrfA chains are colored orange/yellow and light green/green, and hemes bound to NrfH are colored cyan and magenta. Figure made with PyMOL.[68]

determined at 1.9 Å resolution.[227] To date, two structures from SRB proteins have been obtained, that of NrfA from *D. desulfuricans* ATCC 27774[216] and that of NrfHA from *Desulfovibrio vulgaris* Hildenborough.[228,229] NrfA has a predominantly α-helical fold and forms a homodimer with approximate dimensions $100 \times 80 \times 50$ Å, with a six-helix bundle at the dimer interface (Figure 23). Hemes are numbered according to the order of their binding motifs in the sequence, and *D. vulgaris* Hildenborough NrfHA is used as the reference structure. Each monomer contains four bis-histidinyl-coordinated hemes *c* (**2**) and an unusual catalytic heme *c* (heme I), where a lysine from a CXXCK motif is the proximal axial ligand instead of the usual histidine, as was initially shown by Cole and coworkers.[230] Heme I iron is coordinated by the N^{ζ} atom of Lys 151 (in *D. vulgaris* Hildenborough NrfA numbering), whereas the distal axial position is vacant for substrate binding (Figure 24A). The active site pocket is formed by three conserved residues Arg114, Tyr218 and His277, and is solvent accessible by a positively charged channel that facilitates the entry of the substrate nitrite ions, while a negatively charged pathway exists that can drive the positively charged ammonium ions to the exterior of the enzyme. Moreover, a conserved calcium-binding site is observed near heme I, although its role still remains unclear. A second Ca(II) ion is also present in the vicinity of hemes III and IV in *D. vulgaris* Hildenborough and *D. desulfuricans* ATCC 27774 NrfA. A mechanism for the six-electron reduction of nitrite to ammonia by NrfA has been proposed, which

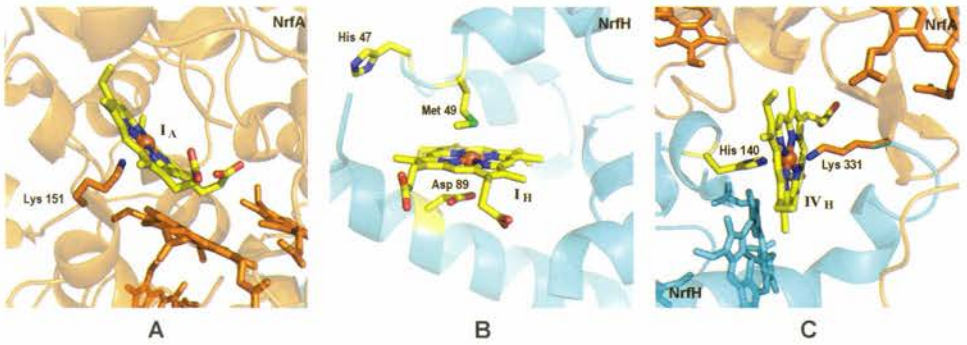

Figure 24. Detail views of the three-dimensional structure of *D. vulgaris* Hildenborough cytochrome *c* nitrite reductase NrfHA in complex with HQNO (PDB 2vr0, Ref. 229). (A) Catalytic heme I from NrfA: Lys151 at the proximal axial site with the distal axial site free for substrate binding (nitrite); (B) Heme I from NrfH: Met49 is coordinated to the heme and Asp89 $O^{\delta 2}$ is ~3 Å away from Fe. His47 from the CXXCHXM motif is also displayed. NrfH heme I is the entry point of electrons from menaquinol; (C) Heme IV from NrfH has as proximal axial ligand His140 and as distal axial ligand Lys331 from a NrfA subunit. NrfH heme IV is proposed to transfer electrons from NrfH to hemes II and V of NrfA. The protein chains are represented as ribbons and are colored orange for NrfA and cyan for NrfH. The heme groups and protein residues are displayed as sticks, and for the relevant hemes and residues mentioned in the text, the atom colors are yellow (or orange) for carbon, blue for nitrogen, red for oxygen, green for sulfur and brown for iron. Figure made with PyMOL.[68]

suggests that catalysis starts with heterolytic cleavage of the N–O bond.[231] Subsequently, it has been shown that nitrite binding to NrfA induces a transition from the high-spin to the low-spin configuration in the catalytic heme, which also favors the heterolytic route for catalysis.[232]

The X-ray structure of the *D. vulgaris* Hildenborough NfrHA complex, formed by the catalytic subunit cytochrome *c* nitrite reductase NrfA and the electron partner subunit NrfH, has been determined at 2.3 Å resolution.[228] It revealed that one NrfH is tightly bound to two NrfA molecules, where a dimer of $NrfHA_2$ units has approximate dimensions of $150 \times 120 \times 95$ Å and a total surface area of about 76,000 $Å^2$. This $\alpha_4\beta_2$ arrangement was proposed to be the biologically active form of the complex (Figure 23A).[228]

The NrfH subunit belongs to a family of cytochrome *c* quinol dehydrogenases, which are present in many proteobacteria, and mediate electron transfer between quinols and various periplasmic enzymes.[209,233,234] Members of this family include one-domain tetraheme cytochromes, as in the case of NrfH, NapC in periplasmic nitrate reductases (Nap), NirT in periplasmic cd_1 nitrite reductases (Nir) and CymA, a membrane-anchored tetraheme cytochrome *c* first isolated from *Shewanella oneidensis* MR-1, or may contain an additional monoheme domain as

in the case of TorC in trimethylamine N-oxide reductase (Tor), as well as DorC and DmsC in dimethyl sulfoxide reductases (Dor/Dms).[234] NrfH is the more common member of this family.[235] NrfH is essential for electron transfer between menaquinol and NrfA, and also serves to anchor the enzyme to the membrane.[217,236] The first and, until 2011, only structure of a cytochrome *c* quinol dehydrogenase is that of *D. vulgaris* Hildenborough NrfH in complex with NrfA.[228] NrfH comprises a N-terminal transmembrane helix, another helix which should be embedded in the membrane and a hydrophilic globular domain that binds four hemes *c* (**2**). The two pairs of heme groups display alternating parallel stacking and perpendicular diheme motifs, an arrangement also observed in other multiheme *c*-type cytochromes,[78,237] such as NrfA, hydroxylamine oxidoreductase and tetrathionate reductase[238] (Figure 23B). *D. vulgaris* Hildenborough NrfH displays an unprecedented heme ligation. Heme I has a methionine residue (Met49) from a CXXCHXM motif as proximal axial ligand (S^{δ} to Fe distance is 2.8 Å), rather than the more usual histidine. $O^{\delta 2}$ from an aspartate residue, Asp89, is *ca.* 3 Å away to the heme iron occupying the distal axial ligand position, but not bound to the iron (Figure 24B). This aspartate residue is replaced by a histidine in many NrfH proteins or a glutamate among NapC proteins. Another remarkable feature of *D. vulgaris* Hildenborough NrfH is the distal axial coordination of heme IV by a lysine residue (Lys331) from the closest NrfA protein, with a histidine as proximal axial ligand (Figure 24C). Heme IV is located at the interface between the NrfH and NrfA subunits and is the gateway for electrons in transit from NrfH to NrfA. Lys331 is conserved in other NrfH proteins that interact with NrfA. The other two NrfH hemes (II and III) are bis-histidinyl coordinated.

The X-ray structure of *Desulfovibrio vulgaris* Hildenborough NrfHA nitrite reductase complex bound to 2-heptyl-4-hydroxyquinoline-*N*-oxide (HQNO), determined at 2.8 Å resolution, elucidated the menaquinol binding site of NrfH.[229] HQNO is a competitive inhibitor of the NrfH quinol oxidation activity. The structure reveals that the inhibitor binds close to NrfH heme I, where it establishes polar contacts with two essential residues: Asp89, the residue occupying the heme distal axial ligand position, and Lys82, a strictly conserved residue. Site-directed mutants have also shown these residues to be essential for menaquinol oxidation.[235] The menaquinol binding cavity has a wide opening to the protein surface and lies at the periplasmic interface of the membrane, suggesting that protons from menaquinol oxidation are liberated to the periplasm. Although NrfH is not a multi-span membrane protein, its quinol binding site has several characteristics similar to quinone binding sites, such as the presence of an acidic residue that is hydrogen bonded to the oxygen from the quinone ring.[229]

V. The Terminal Step of Sulfate Reduction — The Dissimilatory Sulfite Reductase

A key heme-containing protein in sulfate-reducing organisms is the dissimilatory sulfite reductase (DsrAB), which is responsible for the terminal reduction step of sulfite to sulfide.[239,240] The enzyme is composed of two subunits, DsrA and DsrB, in a ~200 kDa $\alpha_2\beta_2$ arrangement.[1] It belongs to an enzyme super-family characterized by the presence of a unique cofactor where an iron tetrahydroporphyrin of the isobacteriochlorin class, termed siroheme (**4**), is coupled through its cysteine axial ligand to a $[4Fe4S]^{2+/1+}$ cluster. This family includes also assimilatory sulfite and nitrite reductases, and other types of sulfite reductases, a topic reviewed in Refs. 241–243. The *dsrA* and *dsrB* genes are paralogous, and phylogenetic analysis suggested that they originated from a gene duplication event that preceded the separation of the Archaea and Bacteria domains, in agreement with the proposed early onset of biological sulfite reduction.[244–247]

Most studies of dissimilatory sulfite reductases have focused on desulfoviridin, the enzyme of *Desulfovibrio* sp. This protein has a characteristic and redox-insensitive band at ~628 nm due to the presence of sirohydrochlorin, the iron-free form of siroheme, which is responsible for the protein green colour (Figure 25). Several spectroscopic studies have provided a detailed characterization of the cofactors.[240,248,249] In contrast to assimilatory sulfite reductases, which reduce sulfite directly to sulfide, the *in vitro* product of dissimilatory sulfite reductases is not sulfide, but a mixture of products including also trithionate and thiosulfate.[250] There is some controversy regarding the mechanism of sulfite

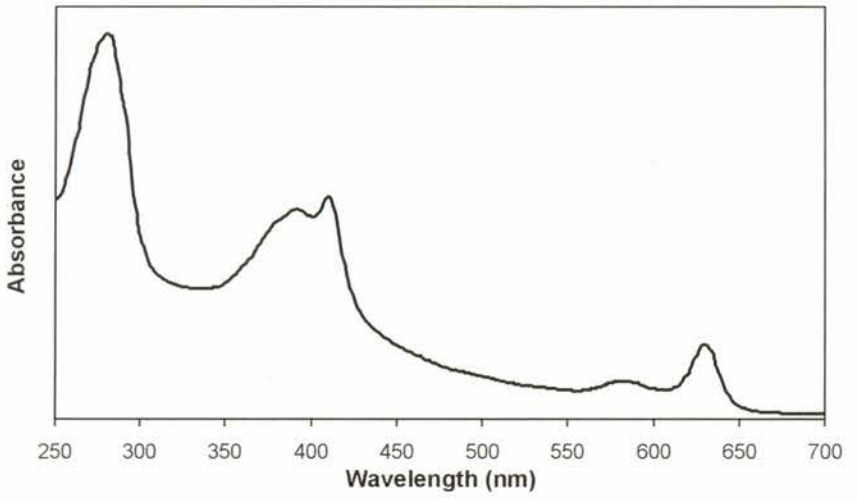

Figure 25. UV-visible spectra of the as isolated desulfoviridin from *D. vulgaris* Hildenborough. Adapted from Ref. 240.

reduction to sulfide, namely as to whether this involves thiosulfate and trithionate as necessary intermediates.[1] In 2008, Oliveira *et al.* presented evidence (see below) to indicate that other proteins may be required for the complete reduction to sulfide.[27]

The first crystal structures of dissimilatory sulfite reductases, from the bacterium *D. vulgaris* Hildenborough[27] and the hyperthermophilic archaeon *A. fulgidus*,[55] provided very important insights into the catalytic action of the enzymes and their physiological partners DsrC and the DsrMKJOP complex. Subsequently, the structures of the dissimilatory sulfite reductases from *D. gigas*[251] and *D. norvegicum*[51] were reported. The *A. fulgidus* enzyme is arranged as a dimer of DsrAB units ($\alpha_2\beta_2$), whereas in the bacterial structures DsrAB is complexed with the DsrC protein, and is organized as $\alpha_2\beta_2\gamma_2$, with approximate dimensions of 125 × 60 × 100 Å and a total surface area of about 55,700 Å^2 (Figure 26A). When the presence of DsrC in DsrAB preparations was first reported, this protein was regarded as a third subunit of the dissimilatory sulfite reductases,[252] but it has since been recognized that it is an independent protein that interacts with DsrAB.[253–257]

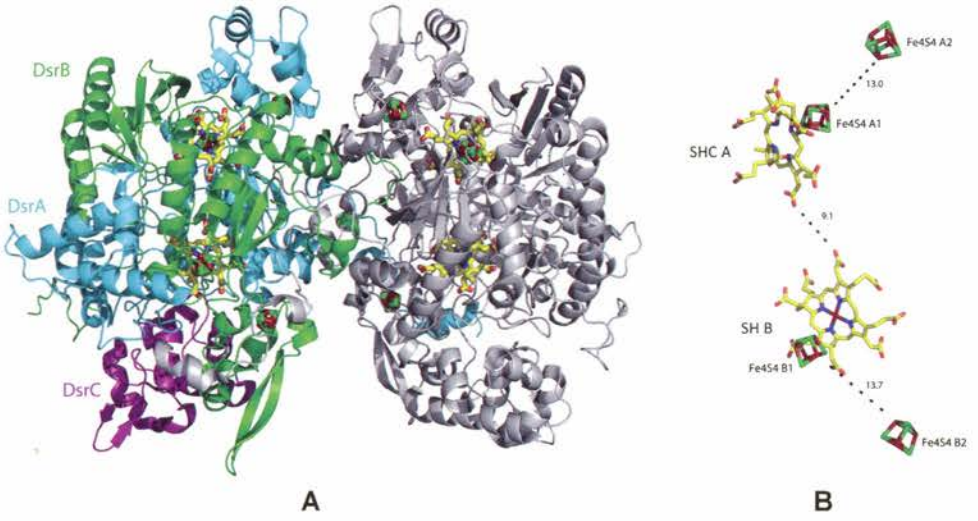

Figure 26. (A) Overall fold of the $\alpha_2\beta_2\gamma_2$ assembly of the *D. vulgaris* Hildenborough dissimilatory sulfite reductase DsrAB bound to DsrC (PDB 2v4j, Ref. 27). The protein chains are represented as ribbons and the cofactors in ball-and-stick mode. In one of the $\alpha\beta\gamma$ units DsrA, DsrB and DsrC are colored cyan, green and magenta, respectively, and the other $\alpha\beta\gamma$ unit is drawn in gray. (B) Arrangement of the cofactors in one DsrABC unit. Atom colors are are yellow for carbon, blue for nitrogen, red for oxygen, green for sulfur and brown for iron, SHC A represents the sirohydrochlorin from subunit A, SH B is the siroheme from subunit B, and the [4Fe4S]$^{2+/1+}$ in both subunits (A,B) are labeled as Fe4S4. Distances between cofactors (dotted lines) are given in A. Figure made with PyMOL.[68]

The buried area between the two $\alpha\beta$ units represents ~10% of the entire surface. This interface is mainly hydrophilic with an important contribution from the C-terminal tails of both subunits that are either wrapped around the other $\alpha\beta$ unit or encapsulated by it, corroborating the $\alpha_2\beta_2$ minimal composition proposed for all dissimilatory sulfite reductases. DsrA and DsrB subunits are structurally very similar, as predicted from their amino acid sequence analysis. In the *D. vulgaris* Hildenborough and *D. gigas* dissimilatory sulfite reductase structures, DsrA binds a sirohydrochlorin (a demetalled siroheme) very close to a $[4Fe4S]^{2+/1+}$ cluster, which is coordinated by four cysteines from a $CX_5CX_nCX_3C$ motif (SHC A and Fe_4S_4 A1 in Figure 26B). This had been previously proposed as the sequence motif for binding the $[4Fe4S]^{2+/1+}$ center of the siroheme-$[4Fe4S]^{2+/1+}$ cofactor in both assimilatory and dissimilatory sulfite reductases.[244,258] In the *A. fulgidus* and *D. norvegicum* enzymes this sirohydrochlorin is replaced by a siroheme. The enzyme from *D. norvegicum* has the trivial name desulforubidin, since it is red, due to the presence of fully metallated sirohydrochlorins. However, in all cases the siroheme bound by DsrA is considered to be catalytically inactive, because it is not solvent accessible, and several conserved basic residues important for substrate binding are missing at the heme distal side. Interestingly, in assimilatory sulfite reductases the corresponding cofactor-binding site is empty. In DsrB the catalytic siroheme is coupled to an iron-sulfur cluster coordinated by four cysteines, as proposed in 1983 by Siegel and coworkers on the basis of Mössbauer studies of the *E. coli* sulfite reductase,[259] that revealed the presence of an exchange-coupled pair of a siroheme and a $[4Fe4S]^{2+/1+}$ center. The coordinating cysteines are arranged in a different sequence motif, CX_nCCX_3C, unusual in that two consecutive cysteine residues are bound to the cluster (SH B and Fe4S4 B1 in Figure 26B). Both DsrA and DsrB bind a second $[4Fe4S]^{2+/1+}$ cluster, inserted in a domain with a typical ferredoxin fold, which is 6.5 Å away from the protein surface and 13 Å from the catalytic center (Fe4S4 A2 and Fe4S4 B2 in Figure 26B). This arrangement suggests that this second cluster is positioned to transfer electrons from an as yet unidentified external electron donor to the cluster of the catalytic cofactor. The ferredoxin domain was proposed to result from the insertion of a ferredoxin-encoding gene into an ancestral gene coding for a siroheme-$[4Fe4S]^{2+/1+}$ binding reductase.[244]

The siroheme and sirohydrochlorin groups are buried in the protein interior, sitting at the interface between DsrA and DsrB (Figure 26A). The proximal side of the catalytic siroheme is formed by residues from DsrB, including the cysteine that is a ligand to the siroheme iron (~2.3 Å) and to the $[4Fe4S]^{2+/1+}$ cluster (~2.5 Å) (SH B and Fe4S4 B1 in Figures 26B and 27). This $[4Fe4S]^{2+/1+}$ cluster is bound exclusively by residues from the DsrB subunit. Moreover, DsrA provides the basic residues (Arg83, Arg101, Arg172, Lys213, Lys215, Lys217, Arg231, Arg376 and

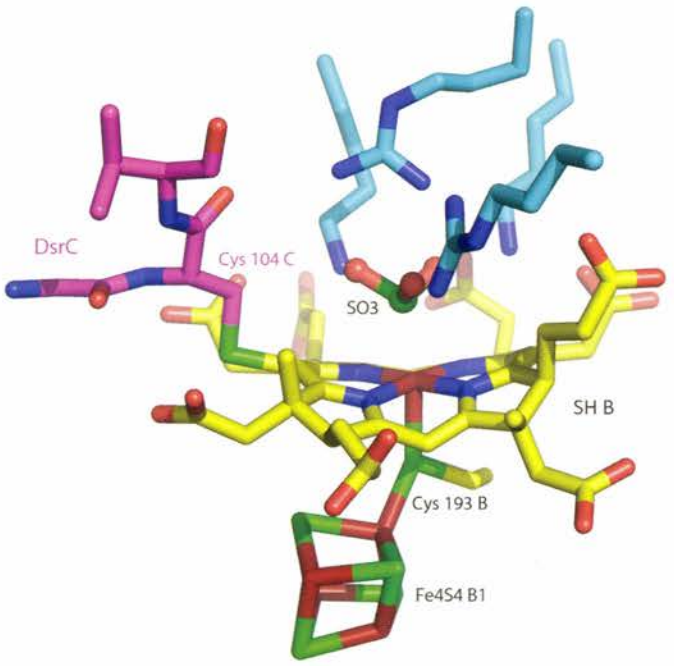

Figure 27. View of the catalytic siroheme in *D. vulgaris* Hildenborough DsrB, showing a bound sulfite with its interacting basic residues from DsrA, and the cross-linked Cys104C from DsrC (PDB 2v4j, Ref. 27). The cofactors and protein residues are drawn as sticks. Atom colors are blue for nitrogen, red for oxygen, green for sulfur and brown for iron. Carbon atoms in DsrA, DsrB and DsrC are colored cyan, yellow and magenta, respectively. Figure made with PyMOL.[68]

Arg378, *D. vulgaris* Hildenborough numbering) for substrate binding at the distal site. These strictly conserved residues, mostly lysine and arginine in dissimilatory sulfite reductases, create a positive pocket in the active site that favors the binding of sulfite and compensates the negative charge of the siroheme propionate groups, as also observed in assimilatory sulfite and nitrite reductases.[260] In all SRB dissimilatory sulfite reductase structures characterized to date, a sulfite ion is bound at the distal side of the siroheme through its sulfur atom (~2.4 Å), while its oxygen atoms are hydrogen-bonded to some of the basic residues mentioned above (Arg101, Arg172, Lys213 and Lys215) and two water molecules (Figure 27).[27,51,55,251]

DsrC is a small 11 kDa protein containing a very conserved C-terminal arm that includes two strictly conserved cysteines (Cys93 and the penultimate Cys104 residue, in *D. vulgaris* DsrC numbering).[253,255,257] It belongs to a larger family of proteins, including *E. coli* TusE (from the Tus system, tRNA 2-thiouridine synthesizing proteins), that are involved in biosynthetic sulfur-transfer reactions, and in which only the cysteine near the C-terminus is conserved.[261,262] The strict

conservation of the two DsrC cysteines in all organisms performing dissimilatory sulfite reduction is a strong indication for the involvement of these residues in this process. The C-terminal arm of DsrC is very flexible and can adopt two different conformations: an extended and loose conformation, and another one where the arm is retracted, bringing the two cysteines in close enough contact to allow disulfide bond formation.[253,255] The structure of the *D. vulgaris* Hildenborough DsrAB–DsrC complex showed that in this situation the C-terminal arm of DsrC protrudes into a cleft between DsrA and DsrB, such that the strictly conserved penultimate Cys of DsrC is positioned right next to the substrate-binding site (Figure 27).[27] This strongly suggests that this Cys is involved in the process of sulfite reduction, and led to the proposal of a new mechanism for this process.[27] In this mechanism, two of the six electrons required to fully reduce sulfite derive from the thiol form of DsrC, which in the process is oxidized forming an intramolecular disulfide bond between the two Cys.[27] This oxidized form of DrsC is proposed to be reduced back to the thiol form by the conserved DsrMKJOP membrane complex (see Section VI.A). Thus, two of the electrons for sulfite reduction would derive from the menaquinone pool (*via* DsrMKJOP and DsrC), and the other four would derive from the unknown electron donor to DsrAB.

Unexpectedly, the S^{γ} of the conserved penultimate cysteine (Cys104C in *D. vulgaris* Hildenborough) is covalently linked to the catalytic siroheme (carbon 20 of the porphyrin ring, CHA in the PDB coordinates) (Figure 27), providing an explanation for the strong interaction between DsrAB and DsrC in the bacterial enzymes, and for the fact that very little siroheme is extracted upon protein precipitation.[27,51,251] This bond is most likely formed as the result of unspecific oxidation by a π-cation radical at the siroheme and should not be physiologically relevant. Mass spectrometric studies have shown that, in solution, the purified bacterial dissimilatory sulfite reductases are not homogeneous, but present different oligomeric states in which one $DsrA_2B_2$ unit binds one, two or no DsrC molecules.[51] Thus, the crystallization process seems to select the $DsrA_2B_2C_2$ form found in the structures. Interestingly, in the *D. gigas* DsrAB-DsrC complex structure additional DsrC conformations are observed: in the major form crystallized, 70% of the molecules contain a covalent bond between the penultimate cysteine of DsrC and the siroheme, whereas in the remaining 30% the C-terminal arm of DsrC is retracted bringing the two conserved cysteines in close contact (3.4–4.0 Å apart), although not forming a disulfide bond.[251] In a second crystallized form an additional conformation is observed for DsrC, where the arm is extended but there is no covalent bond to the heme, and the penultimate cysteine is actually closer to the sulfite molecule present at the active site.[251] The presence of these additional conformations of the DsrC arm in the *D. gigas* DsrAB-DsrC structure lends support to the proposed involvement of the DsrC cysteine residues in the catalytic cycle.[27]

VI. Membrane Complexes

Sulfate respiration is associated with a set of unique membrane-bound respiratory complexes (see Figure 28 and nomenclature in Table 8) that include as subunits

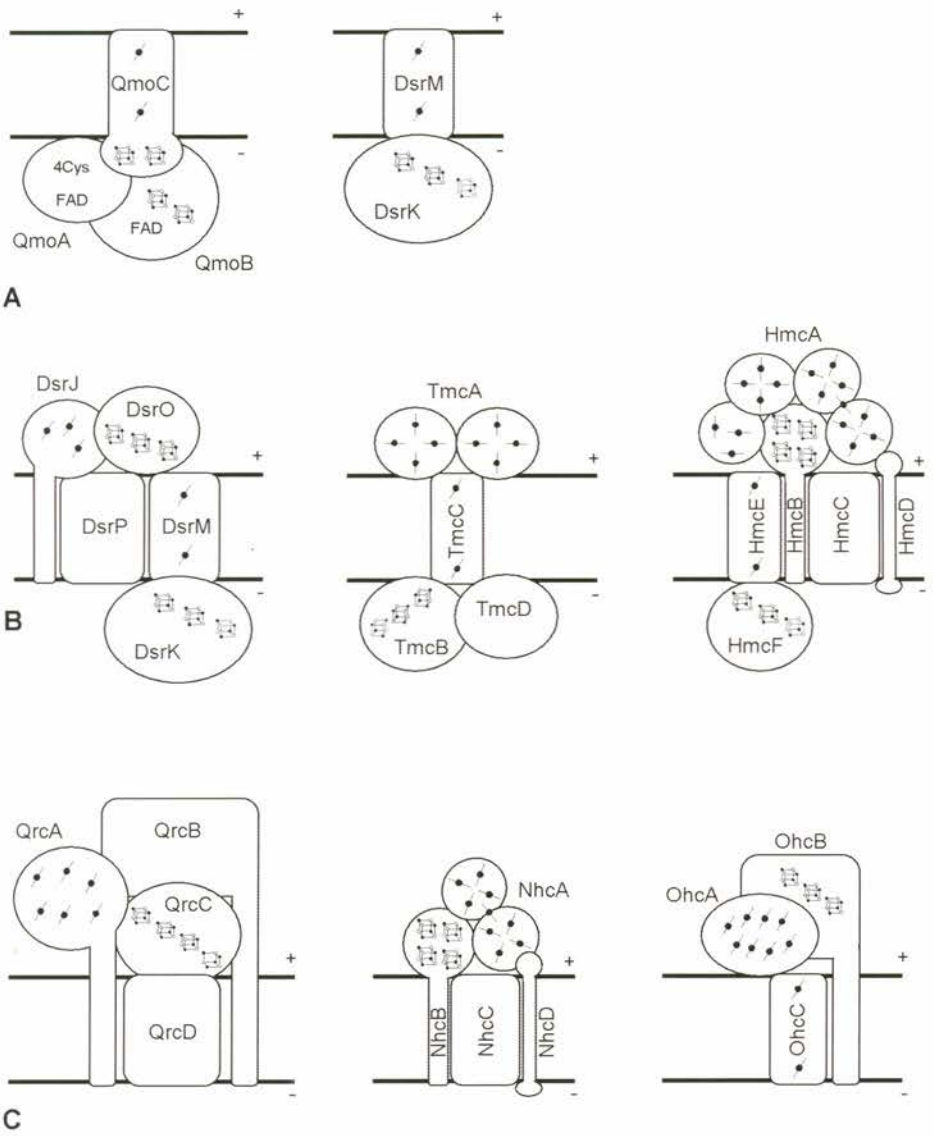

Figure 28. Schematic representation of membrane-bound electron transfer complexes of SRB grouped according to proposed function. (A) menaquinol oxidation; (B) transmembrane electron transfer; (C) menaquinone reduction. The predicted number of heme groups and iron-sulfur clusters is represented for each member of the complex. The (+) and (–) signs denote respectively the periplasmic and cytoplasmic sides of the membrane. Adapted from Ref. 21.

Table 8. Nomenclature of membrane complexes in SRB.

Abbreviation	Name	Composition	Gene locus tag[a]
Qmo	Quinone-interacting membrane oxidoreductase complex	QmoABC	DVU0848, DVU0849, DVU0850[b]
Dsr	Dissimilatory sulfite reductase complex	DsrMKJOP[c]	DVU1290, DVU1289, DVU1288, DVU1287, DVU1286[b]
Hmc	High-molecular weight cytochrome complex	HmcABCDEF	DVU0536, DVU0535, DVU0534, DVU0533, DVU0532, DVU0531[b]
Tmc	Tetraheme membrane cytochrome complex	TmcABCD	DVU0263, DVU0264, DVU0265, DVU0266[b]
Nhc	Nine-heme cytochrome complex	NhcABCD	Ddes_2038, Ddes_2039, Ddes_2040, Ddes_2041[d]
Ohc	Octaheme cytochrome complex	OhcABC	DVU3143, DVU3144, DVU3145[b]
Qrc	Quinone reductase complex	QrcABCD	DVU0695 (with frame shift), DVU0694, DVU0693, DVU0692[b]

[a] Full information can be retrieved from http://img.jgi.doe.gov/cgi-bin/w/main.cgi.
[b] in *D. vulgaris* Hildenborough genome.[33]
[c] DsrMK is a simpler version of this complex found in some SRB.
[d] in *D. desulfuricans* ATCC 27774 genome.[264]

cytochromes *c* and/or cytochromes *b*.[263] Two of them, the QmoABC and DsrMKJOP complexes, are present in all sulfate reducers and are deemed essential for sulfate respiration, whereas a group of others (Qrc, Hmc Tmc, Nhc and Ohc) are present only in sulfate reducers that are characterized by a high content of multiheme cytochromes *c* (mainly the deltaproteobacterial SRB). The cytochrome *c* subunits of the membrane complexes are involved in electron exchange with periplasmic redox partners, whereas the cytochrome *b* subunits are integral membrane proteins responsible for electron exchange with the menaquinone pool (the physiological quinone in SRB) and/or for transmembrane electron transfer between periplasmic and cytoplasmic subunits. It should be noted that up to 2011 there have been no studies regarding the exact location of the "soluble" subunits of these complexes. Their predicted location is therefore based on the presence or absence of recognizable signal peptides and the information available for similar proteins from other organisms. However, co-translocation of subunits is possible in the Tat (twin-arginine translocation) system, and a Tat signal peptide is present in some of the iron–sulfur subunits (e.g. DsrO and HmcB), so in theory other subunits could be co-translocated to the periplasm (e.g. DsrK and HmcF). This is believed to be unlikely, considering the cytoplasmic location of similar proteins (e.g. HdrD, the catalytic subunit of membrane-bound

heterodisulfide reductases from methanogens) and the fact that simpler versions of the complexes (e.g. DsrMK, see below) have no periplasmic subunits.

A. The Qmo and Dsr Complexes

The QmoABC complex (Figure 28A, left) is constituted by three subunits.[263,265] QmoA and QmoB are both cytoplasmic iron–sulfur flavoproteins related to the HdrA subunit of soluble heterodisulfide reductases (HDRs) from methanogens.[266,267] QmoA is predicted to bind one flavin and possibly one iron–sulfur cluster due to the presence of four conserved cysteines, and QmoB is predicted to bind also one flavin and two $[4Fe4S]^{2+/1+}$ clusters. QmoC has an integral membrane domain that binds two hemes *b* (**1**) and a cytoplasmic domain predicted to ligate two $[4Fe4S]^{2+/1+}$ clusters. Sequence analysis shows that there are no recognizable signal petides associated with the QmoABC subunits suggesting there are no periplasmic subunits and that Qmo is involved in electron transfer between the menaquinone pool and cytoplasmic proteins. Both QmoC hemes are reduced by menadiol, a menaquinol analog, supporting their role in electron transfer with the menaquinone/menaquinol pool. In most sulfate reducers the *qmoABC* genes are adjacent to the *aprAB* genes coding for APS reductase, which led to the proposal that Qmo transfers electrons from the quinone pool to AprAB, in a process that may result in energy conservation.[265] Indeed, deletion of the *qmoABC* genes in *D. vulgaris* Hildenborough resulted in the inability to grow by sulfate, but not sulfite, reduction.[268] The reduction potentials of the two hemes *b* in the Qmo complex were determined to be −20 and +75 mV. These potentials are in a suitable range to be involved in electron transfer from menaquinol ($E_0' = -70$ mV) to APS (E_0' APS/$SO_3^{2-} = -60$ mV). If the oxidation of menaquinol by QmoC occurs at the heme closest to the positive periplasmic side of the membrane, protons may be released to the periplasm during this process and electrons transferred to the negative cytoplasmic side of the membrane to QmoAB to subsequently reduce APS. Hence, electron transfer through QmoABC may contribute to the establishement of a transmembrane difference of electrochemical potential, through a redox loop mechanism. The importance of the Qmo complex is reflected in the fact that it is present in almost all sulfate reducers analyzed so far (with the single exception of the archaeon *Caldirviga maquilingensis*).[21] However, in Gram-positive sulfate reducers the *qmoC* gene is absent and is replaced is some organisms by the *hdrBC* genes that encode soluble subunits of HDRs, suggesting that the reduction of APS reductase may involve soluble electron donors rather than quinones.[21,269]

The genes encoding the DsrMKJOP complex (Figure 28B, left) were first shown to be part of a gene cluster having also the genes coding for the dissimilatory

sulfite reductase (DsrAB) in the sulfur-oxidizing bacterium *Allochromatium vinosum*.[270] This complex is present not only in sulfate reducing and sulfur-oxidizing bacteria, but in all organisms that reduce sulfite dissimilatorily.[263,271] In sulfate reducers, the DsrMKJOP complex from *A. fulgidus*[272] and *D. desulfuricans* ATCC 27774[256] were described. It includes two periplasmic subunits, the triheme cytochrome *c* DsrJ and the iron-sulfur protein DsrO; two transmembrane subunits, the diheme cytochrome *b* DsrM and DsrP (that in *A. vinosum* also contains hemes *b*, not detected in SRB[273]); and finally the cytoplasmic iron–sulfur protein DsrK that is similar to HdrD. DsrK binds two canonical $[4Fe4S]^{2+/1+}$ clusters and a special $[4Fe4S]^{3+/2+}$ cluster, that in heterodisulfide reductases is the catalytic site responsible for heterodisulfide reduction.[274] This suggests that DsrK is involved in a disulfide-thiol reaction, and its proposed substrate is the oxidized form of the DsrC protein with an intramolecular disulfide bond (see Section V).[256] Indeed, in many sulfate reducers the *dsrMKJOP* genes are often part of gene clusters that also include genes for the dissimilatory sulfite reductase (*dsrAB*) and its small interacting protein (*dsrC*),[21] described in Section V. In the Gram-positive sulfate reducers and in the archaeon *Caldivirga maquilingensis* only the *dsrMK* genes are present.[21] Gram-positive bacteria lack a periplasmic space, which may explain the absence of DsrJO, and in these organisms DsrMK (Figure 28A, right) must transfer electrons between the menaquinone pool and cytoplasmic acceptors, while in organisms with the DsrMKJOP complex the electron transfer likely involves also periplasmic components.

The DsrJ cytochrome shows no relationship to cytochromes c_3, and in fact it belongs to a novel family of cytochromes *c*. It is possibly membrane-anchored through a hydrophobic signal peptide that is not cleaved off, and its three hemes show distinct coordination modes in both proteins from *D. desulfuricans* ATCC 27774[256] and *A. vinosum*[273]: bis-His, His/Met and one with His/Cys coordination. In the latter organism, this heme-coordinating cysteine was shown to be essential for the function of DsrJ in the oxidation of intracellular sulfur.[273] It is still not clear whether DsrJ is involved in catalysis of sulfur chemistry in the periplasm or it is simply an electron transfer protein. In *D. vulgaris* Hildenborough this cytochrome does not accept electrons from the hydrogenase/TpI-c_3 couple,[256] in contrast to other transmembrane redox complexes (see below). Based on sequence and spectroscopic data, the hemes *b* in DsrM are proposed to be bis-His ligated. In the *D. desulfuricans* ATCC 27774 Dsr complex, the hemes are reduced between +100 and −200 mV, except for the His/Cys coordinated heme that cannot be fully reduced.[256] Treatment with the quinol analog 2,3-dimethyl-1,4-naphthoquinol ($DMNH_2$) led to 40% reduction of the hemes in the complex.

The EPR spectrum of the oxidized DsrMKJOP complex from *D. desulfuricans* ATCC 27774 shows several resonances assigned to low-spin hemes (Figure 29,

line ***a***).[256] Three signals with g_{max} values of 3.44, 2.96 and 2.84, attributed to bis-histidine or bis-methionine bound hemes, have a relative intensity of approximately 1:2:1, suggesting that they account for four hemes. Additionaly, a broad absorption resonance at g_{max} 2.55 was attributed to the heme with His/Cys coordination, as observed for the SoxA subunit of the SoxAX complex involved in thiosulfate oxidation[275,276] and in the 40 kDa triheme cytochrome PufC bound to the photosynthetic reaction center.[277] In the oxidized state, another intense resonance was observed in the g~2 region, with g-values at 2.027, 1.991 and 1.94 (Figure 29, lines ***a*** and ***c***). This signal is very similar to those displayed by the *A. fulgidus* Dsr complex[272] and *A. profundus* DsrMK proteins,[278] and was attributed to a $[4Fe4S]^{3+/2+}$ cluster, as proposed for that observed in heterodisulfide reductases upon addition of one of the thiol substrates to the oxidized enzyme,[279] and also to the signals displayed by *A. fulgidus* Dsr complex[272] and *A. profundus* DsrMK proteins.[279] Upon reduction with sodium dithionite the rhombic signal with $g_{max} = 2.027$ disappears and is replaced by a complex signal in the g~2 region (Figure 29, line ***b***), which is indicative of the presence of several reduced $[4Fe4S]^{2+/1+}$ centers, as predicted by sequence analysis. The line shape and g-values observed indicate there are multiple magnetic interactions between these centers.

B. Other Cytochrome *c*-Associated Membrane Complexes

Another family of membrane redox complexes is found only in those sulfate reducers that contain the tetraheme TpI-c_3.[21,263] Some of these complexes have subunits in the periplasm, membrane and cytoplasm suggesting involvement in transmembrane electron transfer (Hmc and Tmc), whereas others have only subunits in the periplasm and membrane suggesting electron exchange between periplasmic proteins and the quinone pool (Qrc, Nhc and Ohc). In several cases, the cytochrome *c* subunits also belong to the cytochrome c_3 family (e.g. HmcA, NhcA and TmcA, also known as TpII-c_3), whereas others do not (QrcA and OhcA). The study of molecular interactions between the TpI-c_3 and some of these cytochrome *c* subunits has been reviewed in Ref. 100 (see also Section IV.C).

The above-mentioned six-subunit Hmc complex from *D. vulgaris* Hildenborough (Figure 28B, right) was the first membrane complex described in *Desulfovibrio* sp.[195] Its composition is strikingly similar to the Dsr complex in terms of the type of subunits present: a possibly catalytic cytoplasmic FeS protein related to HdrD, two integral membrane proteins belonging to the NarI (membrane subunit of the respiratory nitrate reductase) and NrfD (*E. coli* membrane protein associated with the dissimilatory nitrite reductase NrfA) families, a periplasmic ferredoxin-like protein and a periplasmic cytochrome *c*. Although the composition of the Hmc and Dsr complexes may suggest that the two complexes have related functions, the low amino acid sequence identity between subunits

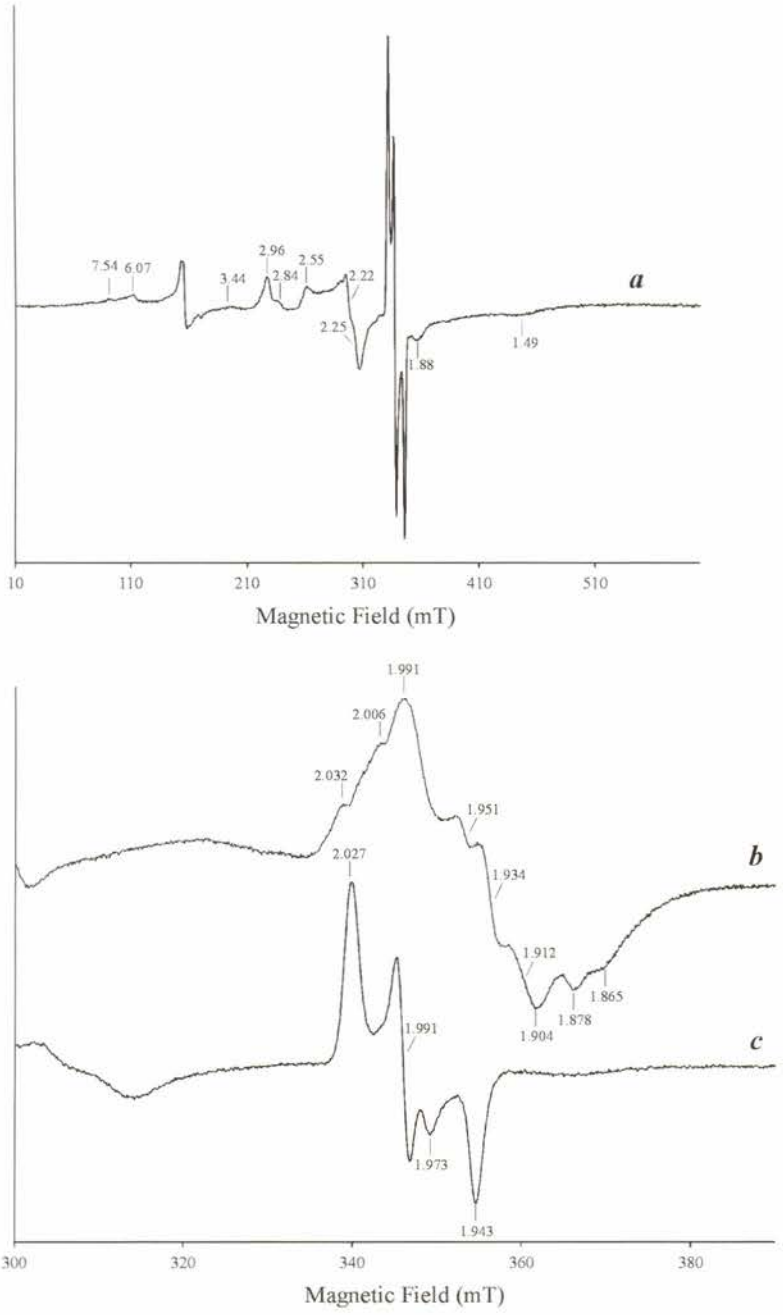

Figure 29. EPR spectra of the *D. desulfuricans* 27774 Dsr complex in the oxidized state (lines ***a*** and ***c***) and after reduction with dithionite (line ***b***). Experimental conditions were: microwave frequency, 9.64 GHz; microwave power 2.4 mW, modulation frequency 100 kHz and modulation amplitude 1 mT. Temperature is 10 K for lines a and b, and 15 K for line c. Adapted from Ref. 256.

indicates that they are not similar. The multiheme cytochrome *c* subunit is the most dissimilar between the two complexes since it is a large, 65 kDa, sixteen-heme cytochrome in Hmc (HmcA) and a small 15 kDa triheme cytochrome in Dsr (DsrJ). Only the HmcA subunit has been characterized thus far. Its structure has been determined and is described in Section IV.C.4. HmcA can accept electrons from periplasmic hydrogenases *via* the TpI-c_3,[81,100,152,156] but this is not observed for DsrJ.[256] Initial studies suggested the involvement of the Hmc complex in accepting electrons from periplasmic hydrogen oxidation.[280,281] However, the expression of the *hmc* genes is down-regulated in cells grown with hydrogen as electron donor.[282,283] Subsequently, this complex was proposed to be involved in iron reduction and corrosion,[284,285] and also to play a role during syntrophic growth of *D. vulgaris*, where it was suggested to be implicated in electron transfer from the cytoplasm to the periplasm.[286] Its function remains to be established.

The Tmc complex (Figure 28B, middle) includes four subunits, TmcABCD, and its subunit architecture is closely related to the Hmc complex, but with a simpler composition.[131] TmcA is the above mentioned (Section IV.C.1) Type II tetraheme cytochrome c_3, initially described as acidic cytochrome c_3.[101,287] TmcB is a cytoplasmic iron-sulfur protein, of the same family as DsrK, HmcF and HrdD, which also binds a similar catalytic $[4Fe4S]^{3+/2+}$ cluster.[131] TmcC is an integral membrane cytochrome *b* of the same family as HmcE, DsrM and HdrE. TmcD is a tryptophan-rich protein that shows no similarity to any proteins in the databases, except for its homologs from SRB. As for the other cytochromes that are part of the membrane complexes Hmc, Qrc and Nhc, the TpI-c_3 seems to be the physiological electron donor to the TpII-c_3.[101,123,288] The reduction potentials for the hemes *c* in the complex are similar to those reported for the isolated TpII-c_3: −170 mV, −235 mV, −260 mV and −325 mV at pH 7.6,[101] and the reduction potentials for the hemes *b* are approximately −155 and −45 mV.[131] In *D. vulgaris* Hildenborough the *tmc* genes show a much higher transcript abundance than the *hmc* genes in a range of conditions,[289] and they are up-regulated in cells grown with hydrogen as electron donor.[283] All redox centers in the Tmc complex are reduced with H_2 and hydrogenase/TpI-c_3,[131] showing that the Tmc complex can transfer electrons that result from periplasmic hydrogen oxidation to cytoplasmic acceptors. The presence of a similar cytoplasmic subunit in the Dsr, Hmc and Tmc complexes (DsrK, HmcF and TmcB) suggests that all three are capable of reducing the same cytoplasmic partner, proposed to be DsrC.[27,256]

Genes encoding for two other complexes related to Tmc and Hmc are present in the genomes of sulfate reducers. One includes the nine-heme cytochrome *c* and is designated as Nhc complex (Figure 28C, middle),[185] while the other includes a cytochrome *c* with eight canonical heme binding sites, and was designated as Ohc (Figure 28C, right).[290] The Nhc complex is composed of four subunits

NhcABCD,[185] of which only the nine-heme cytochrome *c* subunit NhcA has been isolated and characterized.[94,190,291] whereas the Ohc complex contains three subunits, OhcABC. The NhcA cytochrome, described in Section IV.C.3, has a structure similar to that of the C-terminal domain of HmcA, and is also reduced by the hydrogenase/TpI-c_3 couple,[186,189] whereas OhcA belongs to a different cytochrome family and is not related to the octaheme cytochrome c_3 described in Section IV.C.2.

Nhc lacks the heme *b* and cytoplasmic subunits of Hmc, but includes two transmembrane subunits (NhcC and NhcD) and a periplasmic iron–sulfur subunit (NhcB) that display a high amino acid sequence identity to the corresponding subunits of Hmc. Ohc also includes OhcB, a periplasmic iron–sulfur subunit, and OhcC, a cytochrome *b* of the NarI family, while NhcC membrane subunit belongs to the NrfD family. Both Nhc and Ohc can transfer electrons only to the level of the quinone pool. These two complexes have a more limited distribution in deltaproteobacterial sulfate reducers than either Hmc or Tmc.[21]

The Qrc complex (Figure 28C, left) was first isolated from *D. vulgaris* Hildenborough.[292] It is composed of four subunits, QrcABCD, of which the three QrcBCD proteins have strong sequence similarity with the catalytic, electron transfer and membrane subunits of the so-called complex iron–sulfur molybdoenzymes (also known as dimethyl sulfoxide reductase family).[293] In addition, the Qrc complex is closely related to the so-called alternative complex III present in many bacteria,[294] which was first isolated from *Rhodothermus marinus*.[295] The Qrc complexes belong to a large family of proteins present in aerobic and anaerobic bacteria, which were initially named MFIc and MFIcc.[296] However, these names were misleading, since the purified complexes do not contain any molybdopterin cofactor or even molybdenum. QrcA is a hexaheme cytochrome *c* that is also not related to other cytochromes *c* from sulfate reducing bacteria. The reduction potentials of the hemes range from +60 to −130 mV.[297] QrcB belongs to the family of molybdopterin oxidoreductases (but binds no molybdenum cofactor), QrcC is a periplasmic protein binding four iron-sulfur clusters and QrcD is a transmembrane protein, also belonging to the NrfD family. The *qrc* genes are present in sulfate reducers that have periplasmic hydrogenases and/or formate dehydrogenases that lack a membrane subunit for direct quinone reduction, and instead use the TpI-c_3 as their electron acceptor.[21,292] In fact, Qrc was the first complex in SRB shown to reduce menaquinone with electrons from periplasmic hydrogen or formate oxidation, having activity as a TpI-c_3:menaquinone oxidoreductase.[292] A deletion mutant strain of the *qrcB* gene is unable to grow with H_2 or formate as electron donors, but grows normally with lactate,[298] corroborating the role of Qrc in H_2 and formate oxidation. Furthermore, in *D. vulgaris* Hildenborough Qrc was shown to form a supercomplex with the [NiFe]-hydrogenase and TpI-c_3.[297] It has been proposed

that the Qrc and Qmo complexes constitute the two arms of an energy conserving redox loop, contributing to proton motive force generation during sulfate reduction with H_2 or formate.[292]

VII. Respiratory Oxygen Reductases

As mentioned in Section I, SRB are usually described as strict anaerobic bacteria, namely in the sense that growth would stop in the presence of oxygen. However, an increasing body of experimental evidence for a more complex behaviour of SRB upon contact with oxygen has been presented, including a report of effective SRB growth up to atmospheric levels of oxygen[86]. These results were reviewed in Ref. 16. Some authors have proposed that the hydrogenase/TpI-c_3 system could lead to a complete reduction of oxygen to water. This is not possible, however, not only because low-spin cytochromes are incapable of performing such a reaction, but also because reduced cytochromes upon oxidation by oxygen produce ROS, namely the superoxide anion. Nevertheless, as already pointed out in Section I, SRB do contain genes encoding canonical, membrane-bound, oxygen reductases of the *bd* and heme-copper families that, in fact, fully reduce O_2 to water without the release of ROS.

A. Oxygen Reductases of *bd* Type

The cytochrome *bd* oxygen reductases are quinol oxidases, formed by two transmembrane subunits, which contain three hemes: b_{558} (in subunit I), b_{595} and *d* (for a review see Ref. 299). The two last hemes are only present in the holo heterodimer. It is believed that hemes b_{595} and *d* (**3**) form a di-heme site where reduction of oxygen occurs; nevertheless, this is hypothetical since no crystal structure is yet available in 2011. Another alternative is that heme b_{595} simply delivers electrons to heme *d*. Cytochromes *bd* are electrogenic, contributing to the formation of a transmembrane difference of electrochemical potential by charge separation, i.e., they are energy-conserving enzymes. However, and in contrast with the heme-copper enzymes, they do not pump protons, and the apparent lower efficiency in energy conservation may be compensated by a higher turnover rate and by their higher affinity to the dioxygen molecule. Cytochromes *bd* are mainly expressed under microaerophilic and anaerobic conditions, enabling energy conservation and ATP formation under oxygen-limiting conditions; these cytochromes have also been proposed to act in oxygen detoxification in anaerobes. However, even if this should be their function, the detoxification would still allow energy conservation. A survey of the SRB genomes for which the complete sequences are available shows that all these these organisms contain genes for cytochrome *bd*.[21]

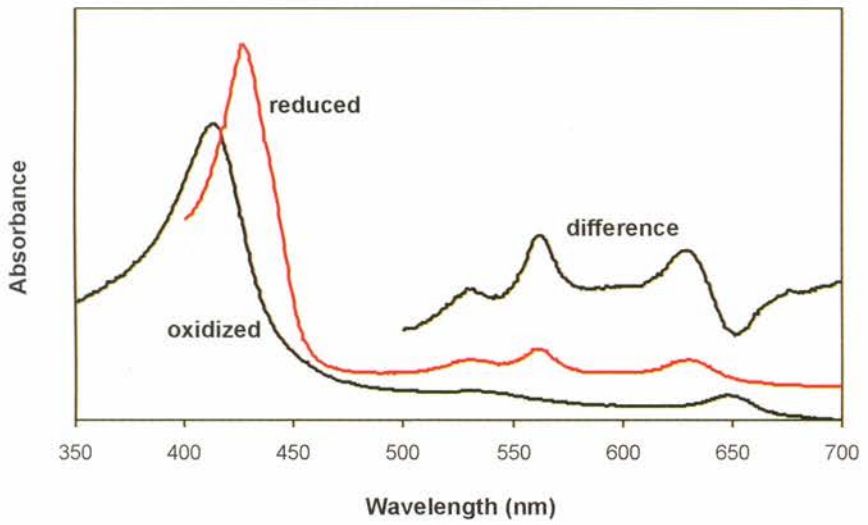

Figure 30. UV-Visible spectra of the isolated cytochrome *bd* oxygen reductase from *D.gigas* in the oxidized state (black line) and reduced with dithionite (red line). The redox spectrum (oxidized minus reduced) is shown above these spectra. Adapted from Ref. 14.

Up to 2011, only the cytochrome *bd* from *D. gigas* was purified and characterized.[14] The protein was isolated from *D. gigas* membranes of cells grown on fumarate/sulfate, and is composed by two subunits with molecular masses of 40 and 29 kDa. The UV-visible absorption spectrum of the oxidized and reduced forms of the purified enzyme is identical to those of other proteins of this family, resulting from the contributions of hemes *b* and heme *d* (Figure 30). The spectrum of the oxidized form is dominated by a band at 650 nm due to heme *d*; in more concentrated samples, a band at 600 nm is also observed due to the α-band of the high-spin heme b_{559}. Upon reduction, the 650 nm band shifts to 630 nm (heme *d*), and the α and β bands at 530 and 561 nm of the ferrous heme *b* appear. It was further demonstrated that *D. gigas* membranes are capable of reducing oxygen to water, with a rate comparable to those of aerobic organisms; these studies, conjugated with experiments done with specific inhibitors, also suggested that the oxygen consumption was probably due not only to the *bd* oxygen reductase but also to a heme-copper enzyme, which is in agreement with the presence in the genomes of several SRB of genes encoding putative heme-copper proteins, as it will be described in the following section.

B. Heme-Copper Oxygen Reductases

Heme-copper reductases (HCOs) are the terminal oxygen reductases most commonly present in the aerobic respiratory chains of organisms belonging to the

three life domains. They are membrane proteins with a common transmembrane α-helical catalytic subunit (subunit I) containing a low-spin, hexacoordinated heme, and a binuclear active site formed by a high-spin, pentacoordinated heme, and a copper ion (Cu_B). These enzymes fully reduce oxygen to water and are electrogenic, receiving electrons from the periplasmic side of the membrane and protons from the cytoplasmic side. Furthermore, they also function as proton pumps, with a stoichiometry of 0.5 to 1 H^+/e^-. Therefore, these enzymes conserve energy very efficiently, in the form of a transmembrane difference of electrochemical potential. Since the catalytic site is deep inside the protein and far from the protein surface, these enzymes have intramolecular proton channels, both to deliver protons for the chemical reaction and to transfer the pumped protons. According to a classification based on the analysis of the proton channels and on the comparison of amino acid sequences[300,301] there are three types of heme-copper reductases: A (subdivided into A1 and A2), B and C (the cbb_3 enzymes). In SRB of the *Desulfovibrio* genus, the enzymes are of type A2, being characterized by the absence of a glutamate residue close to the active center that was proposed to be substituted by a tyrosine-serine motif; nevertheless, they are proton pumps, as efficient as the mitochondrial-like A1-type enzymes.[302,303] HCOs oxidizing soluble periplasmic electron carriers (such as monoheme cytochromes *c*) contain a binuclear copper center in subunit II. In several organisms, those subunits have an extra C-terminal domain of the monoheme cytochrome *c* family, in which the heme is covalently bound to the canonical CXXCH motif, with histidine and methionine as axial ligands. Interestingly, the subunits II of the A2 enzymes from *Desulfovibrio* sp. have two consecutive monoheme cytochrome *c* domains, as demonstrated biochemically for the enzyme from *D.vulgaris* Hildenborough.[86] Those two domains are highly similar between themselves, and most probably result from a gene duplication event. The structure of the homologous domain from the *R. marinus* caa_3 enzyme was solved and, together with an extensive amino acid sequence analysis, revealed that those cytochrome *c* domains form a new subfamily of monoheme cytochromes *c*,[86,304] related to the heme subunits of the cbb_3 oxygen reductases.[305]

In some SRB, oxygen reductases of the *bd* type coexist with those of the heme-copper superfamily.[21] As already mentioned in Section IV.A, cytochrome c_{553} was proposed to be the electron donor to the HCOs in SRB.[85,86] Up to 2011, no heme-copper reductase has been purified from any SRB, and therefore the heme types present in the catalytic subunit remain to be firmly established. In 2011, HPLC analysis of the heme content of *D. vulgaris* Hildenborough membranes by Lamrabet *et al.* revealed the presence of *o*-type hemes (**6**) and the absence of the more frequent *a*-type heme.[26] These authors proposed that the HCO from *D. vulgaris* Hildenborough is of a novel $cc(o/b)o_3$ type.

All the transcriptional evidence related to the expression of genes encoding the *bd* and heme-copper oxygen reductases in *D. vulgaris* Hildenborough and *D. gigas* suggests that these enzymes are expressed constitutively.[26,47,86] Whether these proteins only have a role in oxygen detoxification, or if they allow to sustain growth under microaerophilic conditions, remains to be clarified. Nevertheless, they certainly constitute the main systems for complete reduction of oxygen to water, without releasing harmful oxygen species.

VIII. Quinol:Fumarate Oxidoreductases

Several SRB are capable of growth in fumarate, either by disproportonation, or by using it as a terminal electron acceptor in an anaerobic respiratory process. Therefore, these bacteria contain genes encoding quinol:fumarate oxidoreductases (QFRs). QFRs are quite similar to the respiratory and citric acid cycle enzyme succinate:quinone oxidoreductase (SQR). In fact, solely on the basis of their amino acid sequences, it is not possible to discriminate the two types of enzymes, which catalyze opposite reactions. The enzymes from SRB were reviewed in Refs. 306–308, and are of the B-type, i.e., they are composed of three distinct subunits: subunit A is a cytoplasm-facing protein containing the catalytic FAD moiety; subunit B is another cytoplasm-facing protein harboring three iron–sulfur centers of the $[2Fe2S]^{2+/1+}$, $[4Fe4S]^{2+/1+}$ and $[3Fe4S]^{1+/0}$ types, that transfers electrons between subunit A and the third subunit C; finally, subunit C is a transmembrane α-helical protein (5 helices) with two *b*-type hemes. Subunit C is where the interaction with the quinone/quinol partner occurs, and its heme groups are located near each side of the cytoplasmic or mytochondrial membranes. Subunit C is involved either in energy conservation or dissipation through redox-loop mechanisms. The 3D structures of several of these enzymes were determined by X-ray crystallography and reviewed in Ref. 309. Both hemes have bis-histidine axial coordination, but whereas in one of the hemes the planes of the two imidazole rings are parallel, in the other they are perpendicular. This arrangement is observed in the 3D structures and is also inferred from the EPR data. In SRB only the *D. gigas* enzyme, grown in the presence of fumarate, was purified and characterized up to 2011; under these growth conditions, the expression of this QFR is significantly increased. It is a canonical B-type QFR and, interestingly, both hemes show a significant pH-dependence of the reduction potentials,[14] with $pK_{a,ox} \leq 6$ and $pK_{a,red}$ of 7.7 and 8.1, well within the physiological pH range. This observation may be physiologicaly relevant, as the heme propionates of the QFR from *W. succinogens* have been implicated in proton transport.[310] While the function of these enzymes in organisms capable of growth in fumarate is clear, in other SRB their role remains to be established.[311]

IX. Final Comments

The study of SRB and their metabolism offers a window to life conditions in a younger planet Earth. These organisms were probably once widespread across oceans and continents, but became confined to more restricted environments due to advent of cyanobacteria that caused the largest upheaval in the ecosystem of our world, by releasing over several million years the vast quantities of molecular oxygen present in our atmosphere and that allowed the development of the more complex life forms respiring oxygen. Nevertheless, anaerobes still constitute a large majority of the microbial world, which are the predominant life forms. SRB play a key role in today's ecosystems, in the biogeochemical cycles of carbon and sulfur, and their impact in the oil and food industries, has provided an additional incentive to promote their study. The SRB heme proteins described in this chapter represent several decades of research by groups from all over the world. While in 2011 much is known about these bacteria and many of their proteins, much more is yet to be learned. As with other organisms, the challenge that lies ahead for SRB is that of obtaining the 3D structures of their larger protein complexes, such as the membrane complexes described in Section VI, and the unveiling of the still large number of unknown proteins encoded in their genomes. The large protein complexes have a degree of complexity that makes them intractable by X-ray crystallography in the foreseeable future. The current trend in structural biology is to address increasingly larger systems by combining different methods capable of delivering complementary information about biological macromolecules. Thus, Small-Angle X-ray Scattering and Single Particle Cryo Electron microscopy are being increasingly used in addition to the more classical methods of X-ray crystallography and Nuclear Magnetic Resonance spectroscopy. It will be a fascinating exercise to look back in five or even ten years' time to realize how much our knowledge of the structures of SRB complexes containing some of the heme proteins described in this chapter has progressed, in parallel with a deeper understanding of their biological functions, which calls for a recognition of the importance of the transdisciplinar biochemical approaches.

X. Acknowledgments

Some of the work described here was carried out at our Institute and has been financed by several grants from Fundação para a Ciência e Tecnologia and PEst-OE/EQB/LA0004/2011. SAL is a recipient of a FCT post doctoral grant SFRH/BPD/63944/2009. CVR is supported by *Programa Ciência* (POPH/QREN). We would like to thank all our past and present collaborators, whose names appear in the references. The continued research on sulfate-reducing bacteria at our Institute

is a legacy of the pioneering work by the late professors António V. Xavier and Jean LeGall, as well as a tribute to their memory.

XI. References

1. Rabus, R.; Hansen, T.; Widdel, F. In *The Prokaryotes*; 3rd ed.; Dworkin, M., Falkow, S., Rosenberg, E., Schleifer, K.-H., Stackebrandt, E., Eds.; Springer-Verlag: New York, **2006**; Vol. 2, pp. 659–768.
2. Muyzer, G.; Stams, A. J. *Nat. Rev. Microbiol.* **2008**, *6*, 441–454.
3. Barton, L. L.; Fauque, G. D. *Adv. Appl. Microbiol.* **2009**, *68*, 41–98.
4. Widdel, F.; Hansen, T. A. In *The Prokaryotes* Balows, A., Truper, H. G., Dworkin, M., Harder, W., Scheifer, K. H., Eds.; Springer-Verlag: New York, **1992**; Vol. I, pp. 583–624.
5. Stahl, D. A.; Loy, A.; Wagner, M. In *Sulphate-Reducing Bacteria: Environmental and Engineered Systems*; Barton, L. L., Hamilton, W. A., Eds.; Cambridge University Press: Cambridge, **2007**, pp. 39–115.
6. Thauer, R. K.; Stackebrandt, E.; Hamilton, W. A. In *Sulphate-Reducing Bacteria: Environmental and Engineered Systems*; Barton, L. L., Hamilton, W. A., Eds.; Cambridge University Press: Cambridge, **2007**, pp. 1–38.
7. Barton, L. L. (Ed.) *Sulfate-Reducing Bacteria*; Plenum Press: New York, **1995**.
8. Barton, L. L.; Hamilton, W. A. (Eds.) *Sulphate-Reducing Bacteria: Environmental and Engineered Systems*; Cambridge University Press: Cambridge, **2007**.
9. Fournier, M.; Zhang, Y.; Wildschut, J. D.; Dolla, A.; Voordouw, J. K.; Schriemer, D. C.; Voordouw, G. *J. Bacteriol.* **2003**, *185*, 71–79.
10. Zhang, W.; Culley, D. E.; Scholten, J. C. M.; Hogan, M.; Vitiritti, L.; Brockman, F. J. *Anton. Leeuw. Int. J. G.* **2006**, *89*, 221–237.
11. Sass, H.; Cypionka, H. In *Sulphate-Reducing Bacteria: Environmental and Engineered Systems*; Barton, L. L., Hamilton, W. A., Eds.; Cambridge University Press: Cambridge, **2007**, pp. 167–184.
12. Mukhopadhyay, A.; Redding, A. M.; Joachimiak, M. P.; Arkin, A. P.; Borglin, S. E.; Dehal, P. S.; Chakraborty, R.; Geller, J. T.; Hazen, T. C.; He, Q.; Joyner, D. C.; Martin, V. J.; Wall, J. D.; Yang, Z. K.; Zhou, J.; Keasling, J. D. *J. Bacteriol.* **2007**, *189*, 5996–6010.
13. Lobo, S. A.; Melo, A. M.; Carita, J. N.; Teixeira, M.; Saraiva, L. M. *FEBS Lett.* **2007**, *581*, 433–436.
14. Lemos, R. S.; Gomes, C. M.; Santana, M.; LeGall, J.; Xavier, A. V.; Teixeira, M. *FEBS Lett.* **2001**, *496*, 40–43.
15. Fareleira, P.; Legall, J.; Xavier, A. V.; Santos, H. *J. Bacteriol.* **1997**, *179*, 3972–3980.
16. Dolla, A.; Kurtz Jr., D. M.; Teixeira, M.; Voordouw, G. In *Sulphate-Reducing Bacteria: Environmental and Engineered Systems*; Barton, L. L., Hamilton, W. A., Eds.; Cambridge University Press: Cambridge, **2007**, pp. 185–214.
17. Rabus, R.; Strittmatter, A. In *Sulphate-Reducing Bacteria: Environmental and Engineered Systems*; Barton, L. L., Hamilton, W. A., Eds.; Cambridge University Press: Cambridge, **2007**, pp. 117–140.
18. Taguchi, Y.; Sugishima, M.; Fukuyama, K. *Biochemistry* **2004**, *43*, 4111–4118.
19. Fritz, G.; Roth, A.; Schiffer, A.; Buchert, T.; Bourenkov, G.; Bartunik, H. D.; Huber, H.; Stetter, K. O.; Kroneck, P. M.; Ermler, U. *Proc. Natl. Acad. Sci. USA.* **2002**, *99*, 1836–1841.
20. Akagi, J. M. In *Sulfate-reducing bacteria*; Barton, L. L., Ed.; Plenum Press: New York, **1995**, pp. 89–111.

21. Pereira, I. A. C.; Ramos, A. R.; Grein, F.; Marques, M. C.; da Silva, S. M.; Venceslau, S. S. *Front. Microbiol.* **2011**, *2*, 69.
22. Fontecilla-Camps, J. C.; Volbeda, A.; Cavazza, C.; Nicolet, Y. *Chem. Rev.* **2007**, *107*, 4273–4303.
23. Baltazar, C. S. A.; Marques, M. C.; Soares, C. M.; DeLacey, A. M.; Pereira, I. A. C.; Matias, P. M. *Eur. J. Inorg. Chem.* **2011**, *2011*, 948–962.
24. Zhou, J.; He, Q.; Hemme, C. L.; Mukhopadhyay, A.; Hillesland, K.; Zhou, A.; He, Z.; Van Nostrand, J. D.; Hazen, T. C.; Stahl, D. A.; Wall, J. D.; Arkin, A. P. *Nat. Rev. Microbiol.* **2011**, *9*, 452–466.
25. Marfarlane, G. T.; Cummings, J. H.; Macfarlane, S. In *Sulphate-Reducing Bacteria: Environmental and Engineered Systems*; Barton, L. L., Hamilton, W. A., Eds.; Cambridge University Press: Cambridge, **2007**, pp. 503–522.
26. Lamrabet, O.; Pieulle, L.; Aubert, C.; Mouhamar, F.; Stocker, P.; Dolla, A.; Brasseur, G. *Microbiology* **2011**, *157*, 2720–2732.
27. Oliveira, T. F.; Vonrhein, C.; Matias, P. M.; Venceslau, S. S.; Pereira, I. A.; Archer, M. *J. Biol. Chem.* **2008**, *283*, 34141–34149.
28. Romão, C. V.; Louro, R.; Timkovich, R.; Lubben, M.; Liu, M. Y.; LeGall, J.; Xavier, A. V.; Teixeira, M. *FEBS Lett.* **2000**, *480*, 213–216.
29. Timkovich, R.; Burkhalter, R. S.; Xavier, A. V.; Chen, L.; LeGall, J. *Bioorg. Chem.* **1994**, *22*, 284–293.
30. Heinemann, I. U.; Jahn, M.; Jahn, D. *Arch. Biochem. Biophys.* **2008**, *474*, 238–251.
31. Gibson, K. D.; Laver, W. G.; Neuberger, A. *Biochem. J.* **1958**, *70*, 71–81.
32. Jahn, D.; Verkamp, E.; Soll, D. *Trends Biochem. Sci.* **1992**, *17*, 215–218.
33. Heidelberg, J. F.; Seshadri, R.; Haveman, S. A.; Hemme, C. L.; Paulsen, I. T.; Kolonay, J. F.; Eisen, J. A.; Ward, N.; Methe, B.; Brinkac, L. M.; Daugherty, S. C.; Deboy, R. T.; Dodson, R. J.; Durkin, A. S.; Madupu, R.; Nelson, W. C.; Sullivan, S. A.; Fouts, D.; Haft, D. H.; Selengut, J.; Peterson, J. D.; Davidsen, T. M.; Zafar, N.; Zhou, L.; Radune, D.; Dimitrov, G.; Hance, M.; Tran, K.; Khouri, H.; Gill, J.; Utterback, T. R.; Feldblyum, T. V.; Wall, J. D.; Voordouw, G.; Fraser, C. M. *Nat. Biotechnol.* **2004**, *22*, 554–559.
34. Jaffe, E. K. *Bioorg. Chem.* **2004**, *32*, 316–325.
35. Erskine, P. T.; Coates, L.; Newbold, R.; Brindley, A. A.; Stauffer, F.; Wood, S. P.; Warren, M. J.; Cooper, J. B.; Shoolingin-Jordan, P. M.; Neier, R. *FEBS Lett.* **2001**, *503*, 196–200.
36. Erskine, P. T.; Norton, E.; Cooper, J. B.; Lambert, R.; Coker, A.; Lewis, G.; Spencer, P.; Sarwar, M.; Wood, S. P.; Warren, M. J.; Shoolingin-Jordan, P. M. *Biochemistry* **1999**, *38*, 4266–4276.
37. Jaffe, E. K. *Chem. Biol.* **2003**, *10*, 25–34.
38. Bollivar, D. W.; Clauson, C.; Lighthall, R.; Forbes, S.; Kokona, B.; Fairman, R.; Kundrat, L.; Jaffe, E. K. *BMC Biochem.* **2004**, *5*, 17.
39. Kokona, B.; Rigotti, D. J.; Wasson, A. S.; Lawrence, S. H.; Jaffe, E. K.; Fairman, R. *Biochemistry* **2008**, *47*, 10649–10656.
40. Tang, L.; Stith, L.; Jaffe, E. K. *J. Biol. Chem.* **2005**, *280*, 15786–15793.
41. Lobo, S. A.; Brindley, A.; Warren, M. J.; Saraiva, L. M. *Biochem. J.* **2009**, *420*, 317–325.
42. Jordan, P. M.; Warren, M. J. *FEBS Lett.* **1987**, *225*, 87–92.
43. Jordan, P. M.; Warren, M. J.; Williams, H. J.; Stolowich, N. J.; Roessner, C. A.; Grant, S. K.; Scott, A. I. *FEBS Lett.* **1988**, *235*, 189–193.
44. Shoolingin-Jordan, P. M.; Warren, M. J.; Awan, S. J. *Biochem. J.* **1996**, *316 (Pt 2)*, 373–376.
45. Gomes, C. M.; Silva, G.; Oliveira, S.; LeGall, J.; Liu, M. Y.; Xavier, A. V.; Rodrigues-Pousada, C.; Teixeira, M. *J. Biol. Chem.* **1997**, *272*, 22502–22508.

46. Vicente, J. B.; Justino, M. C.; Gonçalves, V. L.; Saraiva, L. M.; Teixeira, M. *Methods Enzymol.* **2008**, *437*, 21–45.
47. Rodrigues, R.; Vicente, J. B.; Félix, R.; Oliveira, S.; Teixeira, M.; Rodrigues-Pousada, C. *J. Bacteriol.* **2006**, *188*, 2745–2751.
48. Schubert, H. L.; Phillips, J. D.; Heroux, A.; Hill, C. P. *Biochemistry* **2008**, *47*, 8648–8655.
49. Anderson, P. J.; Entsch, B.; McKay, D. B. *Gene* **2001**, *281*, 63–70.
50. Battersby, A. R.; Sheng, Z.-C. *J. Chem. Soc. Chem. Commun.* **1982**, 1393–1394.
51. Oliveira, T. F.; Franklin, E.; Afonso, J. P.; Khan, A. R.; Oldham, N. J.; Pereira, I. A. C.; Archer, M. *Front. Microbiol.* **2011**, *2*.
52. Romão, C. V.; Ladakis, D.; Lobo, S. A.; Carrondo, M. A.; Brindley, A. A.; Deery, E.; Matias, P. M.; Pickersgill, R. W.; Saraiva, L. M.; Warren, M. J. *Proc. Natl. Acad. Sci. USA.* **2011**, *108*, 97–102.
53. Bali, S.; Lawrence, A. D.; Lobo, S. A.; Saraiva, L. M.; Golding, B. T.; Palmer, D. J.; Howard, M. J.; Ferguson, S. J.; Warren, M. J. *Proc. Natl. Acad. Sci. USA.* **2011**.
54. Hsieh, Y. C.; Liu, M. Y.; Wang, V. C.; Chiang, Y. L.; Liu, E. H.; Wu, W. G.; Chan, S. I.; Chen, C. J. *Mol. Microbiol.* **2010**, *78*, 1101–1116.
55. Schiffer, A.; Parey, K.; Warkentin, E.; Diederichs, K.; Huber, H.; Stetter, K. O.; Kroneck, P. M.; Ermler, U. *J. Mol. Biol.* **2008**, *379*, 1063–1074.
56. Lai, K. K.; Moura, I.; Liu, M. Y.; LeGall, J.; Yue, K. T. *Biochim. Biophys. Acta* **1991**, *1060*, 25–27.
57. Seki, Y.; Nagai, Y.; Ishimoto, M. *J. Biochem.* **1985**, *98*, 1535–1543.
58. Warren, M. J.; Bolt, E. L.; Roessner, C. A.; Scott, A. I.; Spencer, J. B.; Woodcock, S. C. *Biochem. J.* **1994**, *302*, 837–844.
59. Stroupe, M. E.; Leech, H. K.; Daniels, D. S.; Warren, M. J.; Getzoff, E. D. *Nat. Struct. Biol.* **2003**, *10*, 1064–1073.
60. Raux, E.; McVeigh, T.; Peters, S. E.; Leustek, T.; Warren, M. J. *Biochem J* **1999**, *338 (Pt 3)*, 701–708.
61. Raux, E.; Leech, H. K.; Beck, R.; Schubert, H. L.; Santander, P. J.; Roessner, C. A.; Scott, A. I.; Martens, J. H.; Jahn, D.; Thermes, C.; Rambach, A.; Warren, M. J. *Biochem. J.* **2003**, *370*, 505–516.
62. Dailey, H. A. *Biochem. Soc. Trans.* **2002**, *30*, 590–595.
63. Brindley, A. A.; Raux, E.; Leech, H. K.; Schubert, H. L.; Warren, M. J. *J. Biol. Chem.* **2003**, *278*, 22388–22395.
64. Lobo, S. A.; Brindley, A. A.; Romão, C. V.; Leech, H. K.; Warren, M. J.; Saraiva, L. M. *Biochemistry* **2008**, *47*, 5851–5857.
65. Buchenau, B.; Kahnt, J.; Heinemann, I. U.; Jahn, D.; Thauer, R. K. *J. Bacteriol.* **2006**, *188*, 8666–8668.
66. Ishida, T.; Yu, L.; Akutsu, H.; Ozawa, K.; Kawanishi, S.; Seto, A.; Inubushi, T.; Sano, S. *Proc. Natl. Acad. Sci. USA.* **1998**, *95*, 4853–4858.
67. Matthews, J. C.; Burkhalter, R. S.; Timkovich, R. *Bioorg. Chem.* **1998**, *26*, 221–231.
68. DeLano, W. L. **2002**, http://www.pymol.org.
69. Storbeck, S.; Rolfes, S.; Raux-Deery, E.; Warren, M. J.; Jahn, D.; Layer, G. *Archaea* **2010**, *2010*, 175050.
70. Romão, C. V.; Regalla, M.; Xavier, A. V.; Teixeira, M.; Liu, M. Y.; Le Gall, J. *Biochemistry* **2000**, *39*, 6841–6849.
71. Andrews, S. C. *Adv. Microb. Physiol.* **1998**, *40*, 281–351.
72. Watt, G. D.; Frankel, R. B.; Papaefthymiou, G. C.; Spartalian, K.; Stiefel, E. I. *Biochemistry* **1986**, *25*, 4330–4336.
73. Matias, P. M.; Morais, J.; Coelho, A. V.; Meijers, R.; Gonzalez, A.; Thompson, A. W.; Sieker, L.; LeGall, J.; Carrondo, M. A. *J. Biol. Inorg. Chem.* **1997**, *2*, 507–514.

74. Macedo, S.; Romão, C. V.; Mitchell, E.; Matias, P. M.; Liu, M. Y.; Xavier, A. V.; LeGall, J.; Teixeira, M.; Lindley, P.; Carrondo, M. A. *Nat. Struct. Biol.* **2003**, *10*, 285–290.
75. Le Brun, N. E.; Wilson, M. T.; Andrews, S. C.; Guest, J. R.; Harrison, P. M.; Thomson, A. J.; Moore, G. R. *FEBS Lett.* **1993**, *333*, 197–202.
76. da Costa, P. N.; Romão, C. V.; LeGall, J.; Xavier, A. V.; Melo, E.; Teixeira, M.; Saraiva, L. M. *Mol. Microbiol.* **2001**, *41*, 217–227.
77. Le Gall, J.; Payne, W. J.; Chen, L.; Liu, M. Y.; Xavier, A. V. *Biochimie* **1994**, *76*, 655–665.
78. Pereira, I. A. C.; Xavier, A. V. In *Encyclopedia of Inorganic Chemistry*; 2nd Ed. ed.; King, R. B., Ed.; John Wiley & Sons: Chichester, **2005**, pp. 3360–3376.
79. Yagi, T. *Biochim. Biophys. Acta* **1979**, *548*, 96–105.
80. Sebban, C.; Blanchard, L.; Bruschi, M.; Guerlesquin, F. *FEMS Microbiol. Lett.* **1995**, *133*, 143–149.
81. Pereira, I. A. C.; Romão, C. V.; Xavier, A. V.; LeGall, J.; Teixeira, M. *J. Biol. Inorg. Chem.* **1998**, *3*, 494–498.
82. Verhagen, M. F.; Wolbert, R. B.; Hagen, W. R. *Eur. J. Biochem.* **1994**, *221*, 821–829.
83. Sebban-Kreuzer, C.; Blackledge, M.; Dolla, A.; Marion, D.; Guerlesquin, F. *Biochemistry* **1998**, *37*, 8331–8340.
84. Sebban-Kreuzer, C.; Dolla, A.; Guerlesquin, F. *Eur. J. Biochem.* **1998**, *253*, 645–652.
85. Kitamura, M.; Mizugai, K.; Taniguchi, M.; Akutsu, H.; Kumagai, I.; Nakaya, T. *Microbiol. Immunol.* **1995**, *39*, 75–80.
86. Lobo, S. A. L.; Almeida, C. C.; Carita, J. N.; Teixeira, M.; Saraiva, L. M. *B.B.A. — Bioenergetics* **2008**, *1777*, 1528–1534.
87. Nakagawa, A.; Higuchi, Y.; Yasuoka, N.; Katsube, Y.; Yagi, T. *J. Biochem.* **1990**, *108*, 701–703.
88. Blackledge, M. J.; Medvedeva, S.; Poncin, M.; Guerlesquin, F.; Bruschi, M.; Marion, D. *J. Mol. Biol.* **1995**, *245*, 661–681.
89. Morelli, X.; Guerlesquin, F. *FEBS Lett.* **1999**, *460*, 77–80.
90. Morelli, X.; Dolla, A.; Czjzek, M.; Palma, P. N.; Blasco, F.; Krippahl, L.; Moura, J. J.; Guerlesquin, F. *Biochemistry* **2000**, *39*, 2530–2537.
91. Philippsen, A. **2003**, http://www.dino3d.org.
92. Nicolet, Y.; Piras, C.; Legrand, P.; Hatchikian, C. E.; Fontecilla-Camps, J. C. *Structure* **1999**, *7*, 13–23.
93. Morelli, X.; Czjzek, M.; Hatchikian, C. E.; Bornet, O.; Fontecilla-Camps, J. C.; Palma, N. P.; Moura, J. J.; Guerlesquin, F. *J. Biol. Chem.* **2000**, *275*, 23204–23210.
94. Liu, M. C.; Costa, C.; Coutinho, I. B.; Moura, J. J.; Moura, I.; Xavier, A. V.; LeGall, J. *J. Bacteriol.* **1988**, *170*, 5545–5551.
95. Moura, J. J. G.; Costa, C.; Liu, M. Y.; Moura, I.; LeGall, J. *B. B. A. — Bioenergetics* **1991**, *1058*, 61–66.
96. Abreu, I. A.; Lourenço, A. I.; Xavier, A. V.; LeGall, J.; Coelho, A. V.; Matias, P. M.; Pinto, D. M.; Carrondo, M. A.; Teixeira, M.; Saraiva, L. M. *J. Biol. Inorg. Chem.* **2003**, *8*, 360–370.
97. Devreese, B.; Costa, C.; Demol, H.; Papaefthymiou, V.; Moura, I.; Moura, J. J.; Van Beeumen, J. *Eur. J. Biochem.* **1997**, *248*, 445–451.
98. Rodriguez, J. A.; Abreu, I. A. *J. Phys. Chem. B* **2005**, *109*, 2754–2762.
99. Louro, R. O. *J. Biol. Inorg. Chem.* **2007**, *12*, 1–10.
100. Matias, P. M.; Pereira, I. A.; Soares, C. M.; Carrondo, M. A. *Prog. Biophys. Mol. Biol.* **2005**, *89*, 292–329.
101. Valente, F. M.; Saraiva, L. M.; LeGall, J.; Xavier, A. V.; Teixeira, M.; Pereira, I. A. *Chem. Biochem.* **2001**, *2*, 895–905.

102. Louro, R. O.; Catarino, T.; LeGall, J.; Xavier, A. V. *J. Biol. Inorg. Chem.* **1997**, *2*, 488–491.
103. Xavier, A. V. *FEBS Lett.* **2002**, *532*, 261–266.
104. Correia, I. J.; Paquete, C. M.; Coelho, A.; Almeida, C. C.; Catarino, T.; Louro, R. O.; Frazão, C.; Saraiva, L. M.; Carrondo, M. A.; Turner, D. L.; Xavier, A. V. *J. Biol. Chem.* **2004**, *279*, 52227–52237.
105. Papa, S.; Guerrieri, F.; Izzo, G. *FEBS Lett.* **1979**, *105*, 213–216.
106. Paquete, C. M.; Turner, D. L.; Louro, R. O.; Xavier, A. V.; Catarino, T. *Biochim. Biophys. Acta* **2007**, *1767*, 1169–1179.
107. Salgueiro, C. A.; Turner, D. L.; Gall, J. L.; Xavier, A. V.; LeGall, J. *J. Biol. Inorg. Chem.* **1997**, *2*, 343–349.
108. Ravi, N.; Moura, I.; Costa, C.; Teixeira, M.; LeGall, J.; Moura, J. J.; Huynh, B. H. *Eur. J. Biochem.* **1992**, *204*, 779–782.
109. Pieulle, L.; Haladjian, J.; Bonicel, J.; Hatchikian, E. C. *Biochim. Biophys. Acta* **1996**, *1273*, 51–61.
110. Ma, J. G.; Zhang, J.; Franco, R.; Jia, S. L.; Moura, I.; Moura, J. J.; Kroneck, P. M.; Shelnutt, J. A. *Biochemistry* **1998**, *37*, 12431–12442.
111. Simaan, A. J.; Murgida, D. H.; Hildebrandt, P. *Biopolymers* **2002**, *67*, 331–334.
112. Rivas, L.; Soares, C. M.; Baptista, A. M.; Simaan, J.; Di Paolo, R. E.; Murgida, D. H.; Hildebrandt, P. *Biophys. J.* **2005**, *88*, 4188–4199.
113. Guigliarelli, B.; Bertrand, P.; More, C.; Haser, R.; Gayda, J. P. *J. Mol. Biol.* **1990**, *216*, 161–166.
114. Moura, I.; Teixeira, M.; Huynh, B. H.; LeGall, J.; Moura, J. J. *Eur. J. Biochem.* **1988**, *176*, 365–369.
115. Moura, I.; Xavier, A.; Moura, J.; Fauque, G.; LeGall, J.; Moore, G.; Huynh, B. *Rev. Port. Quim.* **1985**, *27*, 212–215.
116. Louro, R. O.; Catarino, T.; LeGall, J.; Turner, D. L.; Xavier, A. V. *Chem. Biochem.* **2001**, *2*, 831–837.
117. Santos, H.; Moura, J. J.; Moura, I.; LeGall, J.; Xavier, A. V. *Eur. J. Biochem.* **1984**, *141*, 283–296.
118. Salgueiro, C. A.; Morgado, L.; Fonseca, B.; Lamosa, P.; Catarino, T.; Turner, D. L.; Louro, R. O. *FEBS J.* **2005**, *272*, 2251–2260.
119. Brennan, L.; Turner, D. L.; Messias, A. C.; Teodoro, M. L.; LeGall, J.; Santos, H.; Xavier, A. V. *J. Mol. Biol.* **2000**, *298*, 61–82.
120. Messias, A. C.; Kastrau, D. H.; Costa, H. S.; LeGall, J.; Turner, D. L.; Santos, H.; Xavier, A. V. *J. Mol. Biol.* **1998**, *281*, 719–739.
121. Paixão, V. B.; Vis, H.; Turner, D. L. *Biochemistry* **2010**, *49*, 9620–9629.
122. Harada, E.; Fukuoka, Y.; Ohmura, T.; Fukunishi, A.; Kawai, G.; Fujiwara, T.; Akutsu, H. *J. Mol. Biol.* **2002**, *319*, 767–778.
123. Pieulle, L.; Morelli, X.; Gallice, P.; Lojou, E.; Barbier, P.; Czjzek, M.; Bianco, P.; Guerlesquin, F.; Hatchikian, E. C. *J. Mol. Biol.* **2005**, *354*, 73–90.
124. ElAntak, L.; Morelli, X.; Bornet, O.; Hatchikian, C.; Czjzek, M.; Dolla, A.; Guerlesquin, F. *FEBS Lett.* **2003**, *548*, 1–4.
125. Louro, R. O.; Correia, I. J.; Brennan, L.; Coutinho, I. B.; Xavier, A. V.; Turner, D. L. *J. Am. Chem. Soc.* **1998**, *120*, 13240–13247.
126. Turner, D. L. *J. Biol. Inorg. Chem.* **2000**, *5*, 328–332.
127. Turner, D. L.; Brennan, L.; Chamberlin, S. G.; Louro, R. O.; Xavier, A. V. *Eur. Biophys. J.* **1998**, *27*, 367–375.
128. Sagara, T.; Nakajima, S.; Akutsu, H.; Niki, K.; Wilson, G. S. *J. Electroanal. Chem.* **1991**, *297*, 271–282.

129. Louro, R. O.; Bento, I.; Matias, P. M.; Catarino, T.; Baptista, A. M.; Soares, C. M.; Carrondo, M. A.; Turner, D. L.; Xavier, A. V. *J. Biol. Chem.* **2001**, *276*, 44044–44051.
130. Paquete, C. M.; Pereira, P. M.; Catarino, T.; Turner, D. L.; Louro, R. O.; Xavier, A. V. *Biochim. Biophys. Acta* **2007**, *1767*, 178–188.
131. Pereira, P. M.; Teixeira, M.; Xavier, A. V.; Louro, R. O.; Pereira, I. A. *Biochemistry* **2006**, *45*, 10359–10367.
132. Pereira, P. M.; Pacheco, I.; Turner, D. L.; Louro, R. O. *J. Biol. Inorg. Chem.* **2002**, *7*, 815–822.
133. Louro, R. O.; Catarino, T.; Turner, D. L.; Piçarra-Pereira, M. A.; Pacheco, I.; LeGall, J.; Xavier, A. V. *Biochemistry* **1998**, *37*, 15808–15815.
134. Catarino, T.; Turner, D. L. *Chem. Biochem.* **2001**, *2*, 416–424.
135. Voordouw, G.; Brenner, S. *Eur. J. Biochem.* **1986**, *159*, 347–351.
136. Pollock, W. B.; Chemerika, P. J.; Forrest, M. E.; Beatty, J. T.; Voordouw, G. *J. Gen. Microbiol.* **1989**, *135*, 2319–2328.
137. Voordouw, G.; Pollock, W. B.; Bruschi, M.; Guerlesquin, F.; Rapp-Giles, B. J.; Wall, J. D. *J. Bacteriol.* **1990**, *172*, 6122–6126.
138. Mus-Veteau, I.; Dolla, A.; Guerlesquin, F.; Payan, F.; Czjzek, M.; Haser, R.; Bianco, P.; Haladjian, J.; Rapp-Giles, B. J.; Wall, J. D.; *et al. J. Biol. Chem.* **1992**, *267*, 16851–16858.
139. Dolla, A.; Florens, L.; Bianco, P.; Haladjian, J.; Voordouw, G.; Forest, E.; Wall, J.; Guerlesquin, F.; Bruschi, M. *J. Biol. Chem.* **1994**, *269*, 6340–6346.
140. Dolla, A.; Florens, L.; Bruschi, M.; Dudich, I. V.; Makarov, A. A. *Biochem. Bioph. Res. Co.* **1995**, *211*, 742–747.
141. Moore, G. R.; Pettigrew, G. W. *Cytochromes c, Evolutionary, Structural and Physiochemical Aspects*; Springer-Verlag: Berlin, **1990**.
142. Yagi, T. *Biochim. Biophys. Acta* **1984**, *767*, 288–294.
143. Saraiva, L. M.; Salgueiro, C. A.; LeGall, J.; van Dongen, W. M. A. M.; Xavier, A. V. *J. Biol. Inorg. Chem.* **1996**, *1*, 542–550.
144. Dolla, A.; Arnoux, P.; Protasevich, I.; Lobachov, V.; Brugna, M.; Giudici-Orticoni, M. T.; Haser, R.; Czjzek, M.; Makarov, A.; Bruschi, M. *Biochemistry* **1999**, *38*, 33–41.
145. Messias, A. C.; Aguiar, A. P.; Brennan, L.; Salgueiro, C. A.; Saraiva, L. M.; Xavier, A. V.; Turner, D. L. *Biochim. Biophys. Acta* **2006**, *1757*, 143–153.
146. Salgueiro, C. A.; da Costa, P. N.; Turner, D. L.; Messias, A. C.; van Dongen, W. M.; Saraiva, L. M.; Xavier, A. V. *Biochemistry* **2001**, *40*, 9709–9716.
147. da Costa, P. N.; Conte, C.; Saraiva, L. M. *Biochem. Bioph. Res. Co.* **2000**, *268*, 688–691.
148. Herbaud, M. L.; Aubert, C.; Durand, M. C.; Guerlesquin, F.; Thony-Meyer, L.; Dolla, A. *Biochim. Biophys. Acta* **2000**, *1481*, 18–24.
149. Arslan, E.; Schulz, H.; Zufferey, R.; Kunzler, P.; Thony-Meyer, L. *Biochem. Biophys. Res. Co.* **1998**, *251*, 744–747.
150. Reincke, B.; Thony-Meyer, L.; Dannehl, C.; Odenwald, A.; Aidim, M.; Witt, H.; Ruterjans, H.; Ludwig, B. *Biochim. Biophys. Acta* **1999**, *1411*, 114–120.
151. Odom, J. M.; Peck Jr., H. D. *FEMS Microbiol. Lett.* **1981**, *12*, 47–50.
152. Aubert, C.; Brugna, M.; Dolla, A.; Bruschi, M.; Giudici-Orticoni, M. T. *Biochim. Biophys. Acta* **2000**, *1476*, 85–92.
153. Valente, F. M.; Oliveira, A. S.; Gnadt, N.; Pacheco, I.; Coelho, A. V.; Xavier, A. V.; Teixeira, M.; Soares, C. M.; Pereira, I. A. *J. Biol. Inorg. Chem.* **2005**, *10*, 667–682.
154. Lovley, D. R.; Phillips, E. J. *Appl. Environ. Microbiol.* **1992**, *58*, 850–856.
155. Wall, J. D.; Krumholz, L. R. *Annu. Rev. Microbiol.* **2006**, *60*, 149–166.

156. Guiral, M.; Leroy, G.; Bianco, P.; Gallice, P.; Guigliarelli, B.; Bruschi, M.; Nitschke, W.; - Giudici-Orticoni, M. T. *Biochim. Biophys. Acta* **2005**, *1723*, 45–54.
157. Higuchi, Y.; Kusunoki, M.; Matsuura, Y.; Yasuoka, N.; Kakudo, M. *J. Mol. Biol.* **1984**, *172*, 109–139.
158. Matias, P. M.; Frazão, C.; Morais, J.; Coll, M.; Carrondo, M. A. *J. Mol. Biol.* **1993**, *234*, 680–699.
159. Morimoto, Y.; Tani, T.; Okumura, H.; Higuchi, Y.; Yasuoka, N. *J. Biochem.* **1991**, *110*, 532–540.
160. Czjzek, M.; Payan, F.; Guerlesquin, F.; Bruschi, M.; Haser, R. *J. Mol. Biol.* **1994**, *243*, 653–667.
161. Nørager, S.; Legrand, P.; Pieulle, L.; Hatchikian, C.; Roth, M. *J. Mol. Biol.* **1999**, *290*, 881–902.
162. Simões, P.; Matias, P. M.; Morais, J.; Wilson, K.; Dauter, Z.; Carrondo, M. A. *Inorg. Chim. Acta* **1998**, *273*, 213–224.
163. Bento, I.; Teixeira, V. H.; Baptista, A. M.; Soares, C. M.; Matias, P. M.; Carrondo, M. A. *J. Biol. Chem.* **2003**, *278*, 36455–36469.
164. Einsle, O.; Foerster, S.; Mann, K.; Fritz, G.; Messerschmidt, A.; Kroneck, P. M. *Eur. J. Biochem.* **2001**, *268*, 3028–3035.
165. Pattarkine, M. V.; Tanner, J. J.; Bottoms, C. A.; Lee, Y.-H.; Wall, J. D. *J. Mol. Biol.* **2006**, *358*, 1314–1327.
166. Matias, P. M.; Morais, J.; Coelho, R.; Carrondo, M. A.; Wilson, K.; Dauter, Z.; Sieker, L. *Protein Sci.* **1996**, *5*, 1342–1354.
167. Ozawa, K.; Takayama, Y.; Yasukawa, F.; Ohmura, T.; Cusanovich, M. A.; Tomimoto, Y.; Ogata, H.; Higuchi, Y.; Akutsu, H. *Biophys. J.* **2003**, *85*, 3367–3374.
168. Takayama, Y.; Taketa-Sato, M.; Komori, H.; Morita, K.; Kang, S.-J.; Higuchi, Y.; Akutsu, H. *Bull. Chem. Soc. Jpn.* **2011**, *84*, 1096–1101.
169. Yahata, N.; Ozawa, K.; Tomimoto, Y.; Morita, K.; Komori, H.; Ogata, H.; Higuchi, Y.; Akutsu, H. *Biophysics* **2006**, *2*, 45–56.
170. Takayama, Y.; Werbeck, N. D.; Komori, H.; Morita, K.; Ozawa, K.; Higuchi, Y.; Akutsu, H. *Biochemistry* **2008**, *47*, 9405–9415.
171. Emsley, P.; Lohkamp, B.; Scott, W. G.; Cowtan, K. *Acta Crystallogr. D* **2010**, *66*, 486–501.
172. Krissinel, E.; Henrick, K. *Acta Crystallogr. D* **2004**, *D60*, 2256–2268.
173. Sanner, M. F.; Olson, A. J.; Spehner, J. C. *Biopolymers* **1996**, *38*, 305–320.
174. Dolinsky, T. J.; Nielsen, J. E.; McCammon, J. A.; Baker, N. A. *Nucl. Acids Res.* **2004**, *32*, W665–667.
175. MacKerell, A. D.; Bashford, D.; Bellott; Dunbrack, R. L.; Evanseck, J. D.; Field, M. J.; Fischer, S.; Gao, J.; Guo, H.; Ha, S.; Joseph-McCarthy, D.; Kuchnir, L.; Kuczera, K.; Lau, F. T. K.; Mattos, C.; Michnick, S.; Ngo, T.; Nguyen, D. T.; Prodhom, B.; Reiher, W. E.; Roux, B.; Schlenkrich, M.; Smith, J. C.; Stote, R.; Straub, J.; Watanabe, M.; Wiorkiewicz-Kuczera, J.; Yin, D.; Karplus, M. *J. Phys. Chem. B* **1998**, *102*, 3586–3616.
176. Bashford, D. In *Lecture Notes in Computer Science*; Ishikawa, I., Oldehoeft, R. R., Reinders, J. V. W., Tholburn, M., Eds.; Springer: Berlin, **1997**; Vol. 1343, pp. 233–240.
177. Louro, R. O.; Catarino, T.; Salgueiro, C. A.; LeGall, J.; Xavier, A. V. *J. Biol. Inorg. Chem.* **1996**, *1*, 34–38.
178. Bento, I.; Matias, P. M.; Baptista, A. M.; da Costa, P. N.; van Dongen, W. M.; Saraiva, L. M.; Schneider, T. R.; Soares, C. M.; Carrondo, M. A. *Proteins* **2004**, *54*, 135–152.

179. Matias, P. M.; Soares, C. M.; Saraiva, L. M.; Coelho, R.; Morais, J.; Le Gall, J.; Carrondo, M. A. *J. Biol. Inorg. Chem.* **2001**, *6*, 63–81.
180. Bruschi, M.; Le Gall, J.; Hatchikian, C. E.; Dubordieu, M. *Bull. Soc. Fr. Physiol. Veg.* **1969**, *15*, 381–390.
181. Bruschi, M.; Hatchikian, C. E.; Golovleva, L. A.; Gall, J. L. *J. Bacteriol.* **1977**, *129*, 30–38.
182. Czjzek, M.; Guerlesquin, F.; Bruschi, M.; Haser, R. *Structure* **1996**, *4*, 395–404.
183. Aubert, C.; Giudici-Orticoni, M. T.; Czjzek, M.; Haser, R.; Bruschi, M.; Dolla, A. *Biochemistry* **1998**, *37*, 2120–2130.
184. Aragão, D.; Frazao, C.; Sieker, L.; Sheldrick, G. M.; LeGall, J.; Carrondo, M. A. *Acta Crystallogr. D* **2003**, *59*, 644–653.
185. Saraiva, L. M.; da Costa, P. N.; Conte, C.; Xavier, A. V.; LeGall, J. *Biochim. Biophys. Acta* **2001**, *1520*, 63–70.
186. Matias, P. M.; Coelho, R.; Pereira, I. A.; Coelho, A. V.; Thompson, A. W.; Sieker, L. C.; Gall, J. L.; Carrondo, M. A. *Structure* **1999**, *7*, 119–130.
187. Saraiva, L. M.; da Costa, P. N.; LeGall, J. *Biochem. Bioph. Res. Co.* **1999**, *262*, 629–634.
188. Matias, P. M.; Saraiva, L. M.; Soares, C. M.; Coelho, A. V.; LeGall, J.; Carrondo, M. A. *J. Biol. Inorg. Chem.* **1999**, *4*, 478–494.
189. Umhau, S.; Fritz, G.; Diederichs, K.; Breed, J.; Welte, W.; Kroneck, P. M. *Biochemistry* **2001**, *40*, 1308–1316.
190. Fritz, G.; Griesshaber, D.; Seth, O.; Kroneck, P. M. *Biochemistry* **2001**, *40*, 1317–1324.
191. Paquete, C. M.; Reis, C.; Louro, R. O.; Xavier, A. V.; Catarino, T.; Turner, D. L. *Ann. Magn. Reson.* **2005**, *4*, 100–104.
192. Reis, C.; Louro, R. O.; Pacheco, I.; Catarino, T.; Turner, D. L.; Xavier, A. V. *Inorg. Chim. Acta* **2002**, *339*, 248–252.
193. Higuchi, Y.; Inaka, K.; Yasuoka, N.; Yagi, T. *B. B. A. — Protein Struct. M.* **1987**, *911*, 341–348.
194. Pollock, W. B.; Loutfi, M.; Bruschi, M.; Rapp-Giles, B. J.; Wall, J. D.; Voordouw, G. *J. Bacteriol.* **1991**, *173*, 220–228.
195. Rossi, M.; Pollock, W. B. R.; Reij, M. W.; Keon, R. G.; Fu, R.; Voordouw, G. *J. Bacteriol.* **1993**, *175*, 4699–4711.
196. Ogata, M.; Kiuchi, N.; Yagi, T. *Biochimie* **1993**, *75*, 977–983.
197. Chen, L.; Pereira, M. M.; Teixeira, M.; Xavier, A. V.; Le Gall, J. *FEBS Lett.* **1994**, *347*, 295–299.
198. Verhagen, M. F.; Pierik, A. J.; Wolbert, R. B.; Mallee, L. F.; Voorhorst, W. G.; Hagen, W. R. *Eur. J. Biochem.* **1994**, *225*, 311–319.
199. Pereira, I. A. C.; LeGall, J.; Xavier, A. V.; Teixeira, M. *J. Biol. Inorg. Chem.* **1997**, *2*, 23–31.
200. Czjzek, M.; ElAntak, L.; Zamboni, V.; Morelli, X.; Dolla, A.; Guerlesquin, F.; Bruschi, M. *Structure* **2002**, *10*, 1677–1686.
201. Matias, P. M.; Coelho, A. V.; Valente, F. M.; Plácido, D.; LeGall, J.; Xavier, A. V.; Pereira, I. A.; Carrondo, M. A. *J. Biol. Chem.* **2002**, *277*, 47907–47916.
202. Sato, M.; Shibata, N.; Morimoto, Y.; Takayama, Y.; Ozawa, K.; Akutsu, H.; Higuchi, Y.; Yasuoka, N. *J. Synchrotron Radiat.* **2004**, *11*, 113–116.
203. Czjzek, M.; Arnoux, P.; Haser, R.; Shepard, W. *Acta Crystallogr. D* **2001**, *57*, 670–678.
204. Shibata, N.; Suto, K.; Ichimura, E.; Yoshimura, K.; Muneo, K.; Tomigami, S.; Morimoto, Y.; Ogata, M.; Yagi, T.; Higuchi, Y.; Yasuoka, N. *Protein Pept. Lett.* **2004**, *11*, 93–96.
205. Santos-Silva, T.; Dias, J. M.; Dolla, A.; Durand, M. C.; Goncalves, L. L.; Lampreia, J.; Moura, I.; Romão, M. J. *J. Mol. Biol.* **2007**, *370*, 659–673.
206. Marshall, R. D. *Annu. Rev. Biochem.* **1972**, *41*, 673–702.

207. Weidel, W.; Pelzer, H. *Adv. Enzymol. Relat. Areas Mol. Biol.* **1964**, *26*, 193–232.
208. Hussain, H.; Grove, J.; Griffiths, L.; Busby, S.; Cole, J. *Mol. Microbiol.* **1994**, *12*, 153–163.
209. Simon, J. *FEMS Microbiol. Rev.* **2002**, *26*, 285–309.
210. Einsle, O. *Methods Enzymol.* **2011**, *496*, 399–422.
211. Liu, M. C.; Peck, H. D., Jr. *J. Biol. Chem.* **1981**, *256*, 13159–13164.
212. Costa, C.; Moura, J. J.; Moura, I.; Liu, M. Y.; Peck, H. D., Jr.; LeGall, J.; Wang, Y. N.; Huynh, B. H. *J. Biol. Chem.* **1990**, *265*, 14382–14388.
213. Costa, C.; Moura, J. J.; Moura, I.; Wang, Y.; Huynh, B. H. *J. Biol. Chem.* **1996**, *271*, 23191–23196.
214. Pereira, I. C.; Abreu, I. A.; Xavier, A. V.; LeGall, J.; Teixeira, M. *Biochem. Bioph. Res. Co.* **1996**, *224*, 611–618.
215. Schumacher, W.; Hole, U.; Kroneck, M. H. *Biochem. Bioph. Res. Co.* **1994**, *205*, 911–916.
216. Cunha, C. A.; Macieira, S.; Dias, J. M.; Almeida, G.; Gonçalves, L. L.; Costa, C.; Lampreia, J.; Huber, R.; Moura, J. J.; Moura, I.; Romão, M. J. *J. Biol. Chem.* **2003**, *278*, 17455–17465.
217. Simon, J.; Gross, R.; Einsle, O.; Kroneck, P. M.; Kroger, A.; Klimmek, O. *Mol. Microbiol.* **2000**, *35*, 686–696.
218. Almeida, M. G.; Macieira, S.; Goncalves, L. L.; Huber, R.; Cunha, C. A.; Romão, M. J.; Costa, C.; Lampreia, J.; Moura, J. J.; Moura, I. *Eur. J. Biochem.* **2003**, *270*, 3904–3915.
219. Einsle, O. In *Handbook of Metalloproteins*; Messerschmidt, A., Huber, R., Poulos, T., Wieghardt, K., Eds.; John Wiley & Sons: Chichester, **2006**; Vol. 1, pp. 440–453.
220. Clarke, T. A.; Mills, P. C.; Poock, S. R.; Butt, J. N.; Cheesman, M. R.; Cole, J. A.; Hinton, J. C.; Hemmings, A. M.; Kemp, G.; Soderberg, C. A.; Spiro, S.; Van Wonderen, J.; Richardson, D. J. *Methods Enzymol.* **2008**, *437*, 63–77.
221. Mitchell, G. J.; Jones, J. G.; Cole, J. A. *Arch. Microbiol.* **1986**, *144*, 35–40.
222. Pereira, I. A.; LeGall, J.; Xavier, A. V.; Teixeira, M. *Biochim. Biophys. Acta* **2000**, *1481*, 119–130.
223. Greene, E. A.; Hubert, C.; Nemati, M.; Jenneman, G. E.; Voordouw, G. *Environ. Microbiol.* **2003**, *5*, 607–617.
224. Haveman, S. A.; Greene, E. A.; Stilwell, C. P.; Voordouw, J. K.; Voordouw, G. *J. Bacteriol.* **2004**, *186*, 7944–7950.
225. He, Q.; Huang, K. H.; He, Z.; Alm, E. J.; Fields, M. W.; Hazen, T. C.; Arkin, A. P.; Wall, J. D.; Zhou, J. *Appl. Environ. Microbiol.* **2006**, *72*, 4370–4381.
226. Lukat, P.; Rudolf, M.; Stach, P.; Messerschmidt, A.; Kroneck, P. M.; Simon, J.; Einsle, O. *Biochemistry* **2008**, *47*, 2080–2086.
227. Einsle, O.; Messerschmidt, A.; Stach, P.; Bourenkov, G. P.; Bartunik, H. D.; Huber, R.; Kroneck, P. M. *Nature* **1999**, *400*, 476–480.
228. Rodrigues, M. L.; Oliveira, T. F.; Pereira, I. A.; Archer, M. *EMBO J.* **2006**, *25*, 5951–5960.
229. Rodrigues, M. L.; Scott, K. A.; Sansom, M. S.; Pereira, I. A.; Archer, M. *J. Mol. Biol.* **2008**, *381*, 341–350.
230. Eaves, D. J.; Grove, J.; Staudenmann, W.; James, P.; Poole, R. K.; White, S. A.; Griffiths, I.; Cole, J. A. *Molecular Microbiology* **1998**, *28*, 205–216.
231. Einsle, O.; Messerschmidt, A.; Huber, R.; Kroneck, P. M.; Neese, F. *J. Am. Chem. Soc.* **2002**, *124*, 11737–11745.
232. Murgida, D. H.; Martins, G.; Rodrigues, L.; Cunha, F. M.; Matos, D.; Hildebrandt, P.; Pereira, I. A. C.; Todorovic, S. *J. Phys. Chem. B* **2010**, *114*, 5563–5566.
233. Roldan, M. D.; Sears, H. J.; Cheesman, M. R.; Ferguson, S. J.; Thomson, A. J.; Berks, B. C.; Richardson, D. J. *J. Biol. Chem.* **1998**, *273*, 28785–28790.

234. Rodrigues, M. L.; Pereira, I. A. C.; Archer, M. In *Handbook of Metalloproteins*; Messerschmidt, A., Ed.; John Wiley & Sons: Chichester, 2008; Vol. 4 & 5, p 89–102.
235. Gross, R.; Eichler, R.; Simon, J. *Biochem. J.* **2005**, *390*, 689–693.
236. Simon, J.; Pisa, R.; Stein, T.; Eichler, R.; Klimmek, O.; Gross, R. *Eur. J. Biochem.* **2001**, *268*, 5776–5782.
237. Iverson, T. M.; Arciero, D. M.; Hsu, B. T.; Logan, M. S. P.; Hooper, A. B.; Rees, D. C. *Nature Struct. Biol.* **1998**, *5*, 1005–1012.
238. Mowat, C. G.; Rothery, E.; Miles, C. S.; McIver, L.; Doherty, M. K.; Drewette, K.; Taylor, P.; Walkinshaw, M. D.; Chapman, S. K.; Reid, G. A. *Nat. Struct. Mol. Biol.* **2004**, *11*, 1023–1024.
239. Lee, J. P.; Peck, H. D. *Biochem. Bioph. Res. Co.* **1971**, *45*, 583–589.
240. Moura, I.; LeGall, J.; Lino, A. R.; Peck, H. D.; Fauque, G.; Xavier, A. V.; DerVartanian, D. V.; Moura, J. J. G.; Huynh, B. H. *J. Am. Chem. Soc.* **1988**, *110*, 1075–1082.
241. Crane, B. R.; Getzoff, E. D. *Curr. Opin. Struct. Biol.* **1996**, *6*, 744–756.
242. Dhillon, A.; Goswami, S.; Riley, M.; Teske, A.; Sogin, M. *Astrobiology* **2005**, *5*, 18–29.
243. Loy, A.; Duller, S.; Wagner, M. In *Microbial Sulfur Metabolism*; Dahl, C., Friedrich, C., Eds.; Springer: Heidelberg, **2007**, pp. 46–59.
244. Dahl, C.; Kredich, N. M.; Deutzmann, R.; Truper, H. G. *J. Gen. Microbiol.* **1993**, *139*, 1817–1828.
245. Hipp, W. M.; Pott, A. S.; Thum-Schmitz, N.; Faath, I.; Dahl, C.; Truper, H. G. *Microbiology* **1997**, *143*, 2891–2902.
246. Molitor, M.; Dahl, C.; Molitor, I.; Schafer, U.; Speich, N.; Huber, R.; Deutzmann, R.; Truper, H. G. *Microbiology* **1998**, *144*, 529–541.
247. Wagner, M.; Roger, A. J.; Flax, J. L.; Brusseau, G. A.; Stahl, D. A. *J. Bacteriol.* **1998**, *180*, 2975–2982.
248. Lui, S. M.; Soriano, A.; Cowan, J. A. *Biochem. J.* **1994**, *304*, 441–447.
249. Marritt, S. J.; Hagen, W. F. *Eur. J. Biochem.* **1996**, *238*, 724–727.
250. Peck, H. D., Jr.; LeGall, J. *Philos. Trans. R. Soc. Lond. B Biol. Sci.* **1982**, *298*, 443–466.
251. Chen, C. J.; Hsieh, Y. C.; Liu, M. Y.; Wang, V. C. C.; Chiang, Y. L.; Liu, E. H.; Wu, W. G.; Chan, S. I. *Mol. Microbiol.* **2010**, *78*, 1101–1116.
252. Pierik, A. J.; Duyvis, M. G.; van Helvoort, J. M.; Wolbert, R. B.; Hagen, W. R. *Eur. J. Biochem.* **1992**, *205*, 111–115.
253. Cort, J. R.; Mariappan, S. V.; Kim, C. Y.; Park, M. S.; Peat, T. S.; Waldo, G. S.; Terwilliger, T. C.; Kennedy, M. A. *Eur. J. Biochem.* **2001**, *268*, 5842–5850.
254. Dahl, C.; Engels, S.; Pott-Sperling, A. S.; Schulte, A.; Sander, J.; Lubbe, Y.; Deuster, O.; Brune, D. C. *J. Bacteriol.* **2005**, *187*, 1392–1404.
255. Mander, G. J.; Weiss, M. S.; Hedderich, R.; Kahnt, J.; Ermler, U.; Warkentin, E. *FEBS Lett.* **2005**, *579*, 4600–4604.
256. Pires, R. H.; Venceslau, S. S.; Morais, F.; Teixeira, M.; Xavier, A. V.; Pereira, I. A. *Biochemistry* **2006**, *45*, 249–262.
257. Cort, J. R.; Selan, U.; Schulte, A.; Grimm, F.; Kennedy, M. A.; Dahl, C. *J. Mol. Biol.* **2008**, *382*, 692–707.
258. Ostrowski, J.; Wu, J. Y.; Rueger, D. C.; Miller, B. E.; Siegel, L. M.; Kredich, N. M. *J. Biol. Chem.* **1989**, *264*, 15726–15737.
259. Christner, J. A.; Munck, E.; Janick, P. A.; Siegel, L. M. *J. Biol. Chem.* **1983**, *258*, 11147–11156.
260. Crane, B. R.; Siegel, L. M.; Getzoff, E. D. *Science* **1995**, *270*, 59–67.
261. Ikeuchi, Y.; Shigi, N.; Kato, J.; Nishimura, A.; Suzuki, T. *Mol. Cell* **2006**, *21*, 97–108.
262. Numata, T.; Fukai, S.; Ikeuchi, Y.; Suzuki, T.; Nureki, O. *Structure* **2006**, *14*, 357–366.

263. Pereira, I. A. C. In *Microbial Sulfur Metabolism*; Friedrich, C., Dahl, C., Eds.; Springer-Verlag: Heidelberg, **2008**, pp. 24–35.
264. Unpublished.
265. Pires, R. H.; Lourenço, A. I.; Morais, F.; Teixeira, M.; Xavier, A. V.; Saraiva, L. M.; Pereira, I. A. *Biochim. Biophys. Acta* **2003**, *1605*, 67–82.
266. Kaster, A. K.; Moll, J.; Parey, K.; Thauer, R. K. *Proc. Natl. Acad. Sci. USA.* **2011**, *108*, 2981–2986.
267. Thauer, R. K.; Kaster, A. K.; Seedorf, H.; Buckel, W.; Hedderich, R. *Nat. Rev. Microbiol.* **2008**, *6*, 579–591.
268. Zane, G. M.; Yen, H. C.; Wall, J. D. *Appl. Environ. Microbiol.* **2010**, *76*, 5500–5509.
269. Junier, P.; Junier, T.; Podell, S.; Sims, D. R.; Detter, J. C.; Lykidis, A.; Han, C. S.; Wigginton, N. S.; Gaasterland, T.; Bernier-Latmani, R. *Environ. Microbiol.* **2010**, *12*, 2738–2754.
270. Pott, A. S.; Dahl, C. *Microbiology* **1998**, *144*, 1881–1894.
271. Frigaard, N. U.; Dahl, C. *Adv. Microb. Physiol.* **2009**, *54*, 103–200.
272. Mander, G. J.; Duin, E. C.; Linder, D.; Stetter, K. O.; Hedderich, R. *Eur. J. Biochem.* **2002**, *269*, 1895–1904.
273. Grein, F.; Pereira, I. A. C.; Dahl, C. *J. Bacteriol.* **2010**, *192*, 6369–6377.
274. Hedderich, R.; Hamann, N.; Bennati, M. *Biol. Chem.* **2005**, *386*, 961–970.
275. Cheesman, M. R.; Little, P. J.; Berks, B. C. *Biochemistry* **2001**, *40*, 10562–10569.
276. Kappler, U.; Aguey-Zinsou, K. F.; Hanson, G. R.; Bernhardt, P. V.; McEwan, A. G. *J. Biol. Chem.* **2004**, *279*, 6252–6260.
277. Alric, J.; Tsukatani, Y.; Yoshida, M.; Matsuura, K.; Shimada, K.; Hienerwadel, R.; Schoepp-Cothenet, B.; Nitschke, W.; Nagashima, K. V.; Vermeglio, A. *J. Biol. Chem.* **2004**, *279*, 26090–26097.
278. Mander, G. J.; Pierik, A. J.; Huber, H.; Hedderich, R. *Eur. J. Biochem.* **2004**, *271*, 1106–1116.
279. Madadi-Kahkesh, S.; Duin, E. C.; Heim, S.; Albracht, S. P.; Johnson, M. K.; Hedderich, R. *Eur. J. Biochem.* **2001**, *268*, 2566–2577.
280. Dolla, A.; Pohorelic, B. K. J.; Voordouw, J. K.; Voordouw, G. *Arch. Microbiol.* **2000**, *174*, 143–151.
281. Keon, R. G.; Fu, R.; Voordouw, G. *Arch. Microbiol.* **1997**, *167*, 376–383.
282. Caffrey, S. A.; Park, H. S.; Voordouw, J. K.; He, Z.; Zhou, J.; Voordouw, G. *J. Bacteriol.* **2007**, *189*, 6159–6167.
283. Pereira, P. M.; He, Q.; Valente, F. M. A.; Xavier, A. V.; Zhou, J. Z.; Pereira, I. A. C.; Louro, R. O. *Anton. Leeuw. Int. J. G.* **2008**, *93*, 347–362.
284. Caffrey, S. M.; Park, H. S.; Been, J.; Gordon, P.; Sensen, C. W.; Voordouw, G. *Appl. Environ. Microbiol.* **2008**, *74*, 2404–2413.
285. Park, H. S.; Lin, S.; Voordouw, G. *Anton. Leeuw. Int. J. G.* **2008**, *93*, 79–85.
286. Walker, C. B.; He, Z.; Yang, Z. K.; Ringbauer, J. A., Jr.; He, Q.; Zhou, J.; Voordouw, G.; Wall, J. D.; Arkin, A. P.; Hazen, T. C.; Stolyar, S.; Stahl, D. A. *J. Bacteriol.* **2009**, *191*, 5793–5801.
287. Magro, V.; Pieulle, L.; Forget, N.; Guigliarelli, B.; Petillot, Y.; Hatchikian, E. C. *Biochim. Biophys. Acta* **1997**, *1342*, 149–163.
288. Teixeira, V. H.; Baptista, A. M.; Soares, C. M. *Biophys. J.* **2004**, *86*, 2773–2785.
289. Keller, K. L.; Wall, J. D. *Front. Microbiol.* **2011**, *2*, 135.
290. Pereira, I. A. C.; Haveman, S. A.; Voordouw, G. In *Sulphate-Reducing Bacteria: Environmental and Engineered Systems*; Barton, L. L., Allan Hamilton, W. A., Eds.; Cambridge University Press: Cambridge, **2007**, pp. 215–240.

291. Coelho, A. V.; Matias, P. M.; Sieker, L. C.; Morais, J.; Carrondo, M. A.; Lampreia, J.; Costa, C.; Moura, J. J. G.; Moura, I.; Le Gall, J. *Acta Crystallogr. D* **1996**, *52*, 1202–1208.
292. Venceslau, S. S.; Lino, R. R.; Pereira, I. A. C. *J. Biol. Chem.* **2010**, *285*, 22774–22783.
293. Rothery, R. A.; Workun, G. J.; Weiner, J. H. *Biochim. Biophys. Acta* **2008**, *1778*, 1897–1929.
294. Refojo, P. N.; Sousa, F. L.; Teixeira, M.; Pereira, M. M. *B. B. A. - Bioenergetics* **2010**, *1797*, 1869–1876.
295. Pereira, M. M.; Carita, J. N.; Teixeira, M. *Biochemistry* **1999**, *38*, 1268–1275.
296. Yanyushin, M. F.; del Rosario, M. C.; Brune, D. C.; Blankenship, R. E. *Biochemistry* **2005**, *44*, 10037–10045.
297. Venceslau, S. S.; Matos, D.; Pereira, I. A. C. *FEBS Lett.* **2011**, *585*, 2177–2181.
298. Li, X.; Luo, Q.; Wofford, N. Q.; Keller, K. L.; McInerney, M. J.; Wall, J. D.; Krumholz, L. R. *J. Bacteriol.* **2009**, *191*, 2675–2682.
299. Borisov, V. B.; Gennis, R. B.; Hemp, J.; Verkhovsky, M. I. *Biochim. Biophys. Acta* **2011**, *1807*, 1398–1413.
300. Pereira, M. M.; Santana, M.; Teixeira, M. *Biochim. Biophys. Acta* **2001**, *1505*, 185–208.
301. Sousa, F. L.; Alves, R. J.; Pereira-Leal, J. B.; Teixeira, M.; Pereira, M. M. *PLoS One* **2011**, *6*, e19117.
302. Pereira, M. M.; Santana, M.; Soares, C. M.; Mendes, J.; Carita, J. N.; Fernandes, A. S.; Saraste, M.; Carrondo, M. A.; Teixeira, M. *Biochim. Biophys. Acta* **1999**, *1413*, 1–13.
303. Pereira, M. M.; Verkhovskaya, M. L.; Teixeira, M.; Verkhovsky, M. I. *Biochemistry* **2000**, *39*, 6336–6340.
304. Srinivasan, V.; Rajendran, C.; Sousa, F. L.; Melo, A. M.; Saraiva, L. M.; Pereira, M. M.; Santana, M.; Teixeira, M.; Michel, H. *J. Mol. Biol.* **2005**, *345*, 1047–1057.
305. Buschmann, S.; Warkentin, E.; Xie, H.; Langer, J. D.; Ermler, U.; Michel, H. *Science* **2010**, *329*, 327–330.
306. Hagerhall, C.; Hederstedt, L. *FEBS Lett.* **1996**, *389*, 25–31.
307. Lancaster, C. R.; Simon, J. *Biochim. Biophys. Acta* **2002**, *1553*, 84–101.
308. Lemos, R. S.; Fernandes, A. S.; Pereira, M. M.; Gomes, C. M.; Teixeira, M. *Biochim. Biophys. Acta* **2002**, *1553*, 158–170.
309. Lancaster, C. R. In *Handbook of Metalloproteins*; Messerschmidt, A., Huber, R., Poulos, T., Wieghardt, K., Eds.; John Wiley & Sons: Chichester, **2006**; Vol. 1, pp. 440–453.
310. Mileni, M.; Haas, A. H.; Mantele, W.; Simon, J.; Lancaster, C. R. *Biochemistry* **2005**, *44*, 16718–16728.
311. Zaunmuller, T.; Kelly, D. J.; Glockner, F. O.; Unden, G. *Microbiology* **2006**, *152*, 2443–2453.